1989

Frost susceptibility of concrete in near-saturated states

Kian Sin Soo
Iowa State University

Order Number 9014958

Frost susceptibility of concrete in near-saturated states

Soo, Kian Sin, Ph.D.

Iowa State University, 1989

U·M·I
300 N. Zeeb Rd.
Ann Arbor, MI 48106

Frost susceptibility of concrete in near-saturated states

by

Kian Sin Soo

A Dissertation Submitted to the

Graduate Faculty in Partial Fulfillment of the

Requirements for the Degree of

DOCTOR OF PHILOSOPHY

Department: Civil and Construction Engineering
Co-majors: Civil Engineering Materials
Geotechnical Engineering

Approved:

Signature was redacted for privacy.

In Charge of Major Work

Signature was redacted for privacy.

For the Major Department

Signature was redacted for privacy.

For the Graduate College

Iowa State University
Ames, Iowa
1989

TABLE OF CONTENTS

INTRODUCTION

One of the primary modes of failure of concrete structures such as pavements is durability failure caused by frost action in temperate climates. During the past four decades, a considerable amount of excellent research has been done to elucidate the mechanism of frost damage, and various methods have been proposed to evaluate the frost resistance of concrete.

That frost damage to concrete is related to its pore structure is well known. Since 1940s, air entrainment has been used to affect the pore structure of concrete to protect it from frost damage. Although air entrainment has proved effective, it has not prevented frost damage in some cases. Among the proposed mechanisms of frost action on concrete, the hypothesis put forward by Powers [52] is the most widely accepted. Powers' model has been very successful in explaining the role of entrained air. According to his hypothesis, the failure of concrete during freezing is mainly due to hydraulic pressure. As water freezes, the volume increase upon freezing causes water to be expelled from the frozen pores to nearby empty pores, and the resistance to this flow results in the generation of hydraulic pressure. Entrained air is therefore incorporated into concrete to relieve this destructive pressure. Based on his hypothesis, Powers introduced the spacing factor to characterize frost resistance of concrete.

Although Powers' model is useful, it can not explain the abruptness of the drop in frost resistance of concrete as the saturation level increases to near-saturated states. It is believed that concrete will be subjected to far greater stresses in near-saturated states because of the extrusion of ice to the

exterior of concrete. Therefore, the question is whether air entrainment minimizes the frost damage by reducing the internal stresses as in Powers' model or by protecting concrete from critical saturation. If the latter is the case, then rather than correlate frost resistance to air voids characteristics, a more rational approach would be to correlate the frost resistance to the reluctance of the concrete to become saturated.

A new model was therefore proposed to provide a basic understanding of the freezing mechanism of pore water in concrete in near-saturated states [15]. The model, also known as the two-stage model, is based on the plastic ice theory of capillary freezing and melting of pore water. According to this theory, ice forms a continuous plastic mass in a porous medium as a non-wetting phase adjacent to capillary water, and the capillary freezing and melting occurs by virtue of movement of the ice/water interface along the capillary pore in one direction or another [20].

Extensive research in recent years has resulted in the introduction of various methods for evaluating the frost resistance of aggregate and concrete. Some of these methods are based on testing the aggregate or the concrete in a laboratory simulated freeze-thaw environment. Other methods are based on measuring the physical properties such as porosity, pore size distribution, absorption and length change, and correlating them with known performance. The ASTM recommended standard test method, designation C-666 "Standard Test Method for Resistance of Concrete to Rapid Freezing and Thawing" [2], is considered to be the most widely accepted; however, it is tedious, time consuming, and labor intensive. This standard test method

represents extreme conditions of exposure which is not indicative of actual field conditions.

The objectives of this research are two-fold: (1) to provide a basic understanding of the freezing mechanism of pore water in concrete in near-saturated states; and (2) in the light of this understanding, to introduce a quick, simple, and economical method of predicting the frost resistance of concrete.

LITERATURE REVIEW

Freeze-Thaw Durability of Concrete

Durability of concrete is generally defined as the ability to resist deterioration under weathering action, chemical attack, abrasion, and any other process of deterioration [1]. A durable concrete is able to perform its function satisfactorily without damaging changes in form, structure, and integrity under a given service condition. Although man has been able to produce concrete of good quality, as evidenced by many concrete structures that stand tall and sound, problems still exist. For more than half a century, continued research on concrete durability has produced a tremendous amount of knowledge on the cause of durability failures, and the methods of preventing and detecting them. This trend still continues. At this point it is appropriate to review some of the important work done by various researchers on concrete in the area of freeze-thaw durability.

Perhaps the earliest study on the mechanism of frost action was done on building materials such as bricks and ceramic tiles. A review of this work was given by Butterworth [8]. He described the mechanism of formation and growth of ice lenses in these materials. Since then, various models have been proposed to explain the mechanism of frost action in porous materials; particularly in soil and concrete [9,10,19,52].

Collins [10] attributed the failure of concrete pavement to formation of ice lenses parallel to the cold surface. He noted the lamination of these ice lenses to be similar to those observed in soils during frost heave. Collins suggested that the mechanism of frost action in concrete may be similar to that which occurs in soils where the growth of ice lenses occurs

perpendicular to the outside surface. He postulated that if the expansive force caused by this growth of ice exceeds the tensile strength of concrete, it will cause delamination. Collins further developed a one surface freezing test to support his hypothesis. Rogers and Chojnacki [61] reported destruction of concrete water tanks due to ice lensing which supported Collins hypothesis.

Cady [9] described three major mechanisms of frost action in aggregate. They are the hydraulic pressure hypothesis, the ordered-water theory, and the dual mechanism theory.

Gordon [25] described four mechanisms which lead to the deterioration of aggregate and aggregate in concrete. They are elastic accommodation, the critical size of aggregate, the accretion of water from surrounding pastes, and the expulsion of water from aggregate into the surrounding paste. More detailed discussions of the above mechanisms can be found in the work cited in the references.

Hudec [29], based on 15 years of theoretical and laboratory-derived evidence, concluded that the primary cause of failure of aggregate in concrete is due to repeated wetting and drying rather than repeated freezing and thawing, since the fine pores in the fine grained aggregates and cement paste are too small to allow freezing to take place. He explained that the pore water in the small pores is under the influence of capillary and surface forces of the pore material and has a lower vapor pressure. This will prevent it from freezing, but will result in the difference in osmotic pressure, causing expansion. The osmotic potential is further increased in the presence of de-icing salt, whose cations are adsorbed and concentrated on the pore surface, causing greater expansion.

Perhaps the most widely accepted theory on the mechanism of frost action is the hydraulic pressure hypothesis proposed by Powers [52]. As will be shown later, this hypothesis forms the basis for the proposed model presented in this dissertation. Therefore, a separate section is devoted to the discussion of this hypothesis.

It generally is accepted that cement paste can be made immune to frost damage by incorporating entrained air. However, this would not completely avoid frost damage of concrete since the freezing phenomenon in aggregate must also be taken into consideration [1]. In view of this, research done on the freeze-thaw durability of concrete mainly concentrate on the methods of testing for frost resistance of aggregate and aggregate in concrete. Basically, there are two types of methods of evaluating frost resistance of aggregate and concrete: (1) methods based on direct testing of aggregate or aggregate in concrete in a given freeze-thaw environment; (2) methods based on measurements of some physical properties of concrete and aggregate such as porosity, pore size distribution, absorption, dilation, etc., and correlation with known field performance.

Laboratory tests on aggregate include absorption, specific gravity, pore structure, and soundness testing. The soundness test has been used to evaluate frost resistance of aggregates for many years. The ASTM standard for this test is designated C88-83 "Test Method for Soundness of Aggregates by Use of Sodium Sulfate or Magnesium Sulfate". Many investigators have found that the test results are generally not reproducible and do not correlate well with field performance, and thus are not suitable for prediction of field performance of aggregate in concrete subjected to freeze-thaw cycles

[36,47,63]. Schulze and Lange [63] presented a paper discussing various methods for determining the frost resistance of concrete aggregate. They concluded that methods that are used to determine the pore characteristics of aggregate are more important than the sulphate soundness test because volume stability depends mainly on pore volume, pore size, pore size distribution, and permeability.

Because aggregate is not the sole ingredient in concrete, it generally is accepted that incorporating aggregate into concrete before testing provides a more realistic indicator of durability. For testing aggregate in concrete, the specimen is subjected to a prescribed number of freeze-thaw cycles and testing environment. The extent of frost damage is then assessed by determining the change in the dynamic modulus of elasticity as a function of freeze-thaw cycles. A reduction in the modulus indicates deterioration of the concrete. The extent of damage can also be assessed by following the weight loss, by visual observation, or by pulse velocity measurements. The weight loss method is more indicative of external surface degradation, while dynamic modulus and pulse velocity measurements are more indicative of internal structure integrity. The current ASTM method requires the determination of a durability factor. The specimen is subjected to 300 freeze-thaw cycles or until the dynamic modulus drops to 60 percent of original value, whichever occurs first. The durability factor is defined as the product of the number of cycles at the end of the test and the percentage of original modulus retained divided by 300. Two procedures for evaluating the frost resistance of concrete are given by ASTM C-666 "Standard Test Method for Resistance of Concrete to Rapid Freezing and Thawing" [2]. These procedures differ mainly in the type of

freezing medium. Procedure A involves freezing in water and thawing in water, while procedure B involves freezing in air and thawing in water. ASTM does not offer criteria indicating what constitutes good or poor performance. This test mainly serves as a means for differentiating between good and bad aggregate in a relative sense. Thus, acceptance or rejection of an aggregate rests on criteria set by specifying agencies. The test procedures and results have been the subject of considerable research and discussion.

Although this test provides useful information on the durability of concrete, it has been strongly criticized for lack of consistent correlation with actual field performance. One of the most common criticisms is that this test represents more extreme conditions than those experienced under field conditions. It has been pointed out that in order to produce results quickly, the testing environments are more severe and thus more destructive than the field conditions. The major differences between laboratory testing and field exposure of concrete are the relatively young age of concrete at the start of the test, lack of drying periods, and the high rate of cooling in laboratory samples [25]. Also, the results depend on which procedure is used. Procedure A generally is found to be more severe than procedure B [34,67,76,83].

Sturrup et al. [67] indicated that procedure A does not differentiate between concretes of poor durability, such as those without air-entrainment, and those with poor quality aggregate. Procedure A can mainly be used to differentiate between concrete of poor and good aggregate but not concrete of marginal aggregate. Procedure B has poor reproducibility as well as difficulty in discriminating between air-entrained and non-air-entrained concrete having low water/cement ratios.

Wright and Gregory [83], in explaining the reason for the lesser severity of procedure B, suggested that the evaporation of water from the specimen surface before freezing mitigates damage by reducing the stresses developed near the surface when water freezes. They also investigated and compared the evaluation of the durability of concrete by dynamic modulus of elasticity and pulse velocity measurements and found them to be equally suitable.

In view of the problems associated with the standard ASTM test, it is not surprising that many researchers have attempted to correlate this standard laboratory accelerated freeze-thaw test results to actual field performance. Kennedy and Mather [32] attempted to find a correlation but were rather unsuccessful.

Powers [56] claimed that this standard freeze-thaw cycling test is too severe to be of any practical use mainly because no drying of the specimen is permitted, and the rate of freezing is many times higher than that which occurs in the field. Almost all concretes undergo some drying during the periods between freezing except those permanently submerged under water. The rate of freezing determines the rate at which ice forms in the pores, which in turn determines the rate at which water is being displaced. The faster the freezing, the higher the expected hydraulic pressure. Many aggregates which may otherwise prove to be durable in the field were rejected on the basis of this test. As a result, Powers conceived an alternate test, which was standardized by ASTM as "Standard Test Method for Critical Dilation of Concrete Specimens Subjected to Freezing", designation C-671 [3]. He proposed that specimen be conditioned to a moisture content expected in the field at the start of the freezing season, then immersed in water and periodically subjected

to freezing at the rate and frequency to be expected in the field. If the length change decreases linearly down to a temperature of 15 °F, the specimen is not critically saturated and therefore is immune to frost damage at that rate. If the length change deviates from a straight line in an expansive direction, the specimen is critically saturated and susceptible to frost damage. Figure 1 shows a typical length change and temperature plot for this test. In principle only one cycle need to be run; that is, at the end of freezing season.

Tremper and Spellman [69] of the California Division of Highways implemented this critical dilation test to evaluate aggregate for a major highway construction project. They placed concrete slabs of the same thickness as the prototype pavement at a project site and measured their moisture contents at the start of freezing season. Specimens conditioned to that moisture content were then subjected to dilation testing. Test results permitted the use of aggregates which otherwise would have been rejected if the repeated freeze-thaw tests had been used. Later performance of the prototype justified the usefulness of the test. However, this test still is not widely used; partly because the length of time required to run the test normally is longer than the usual repeated freezing and thawing test; and primarily because the initial field moisture content has to be known.

Many other researchers have attempted this one-cycle test with considerable success. MacInnis [45] proposed a one-cycle freezing test for the study of freeze-thaw durability of concrete. He considered the expansion and contraction of concrete during the freezing cycle to be an important indication regarding frost damage. He conducted tests on cement grouts, mortars, and concretes. He postulated that continuous expansion during

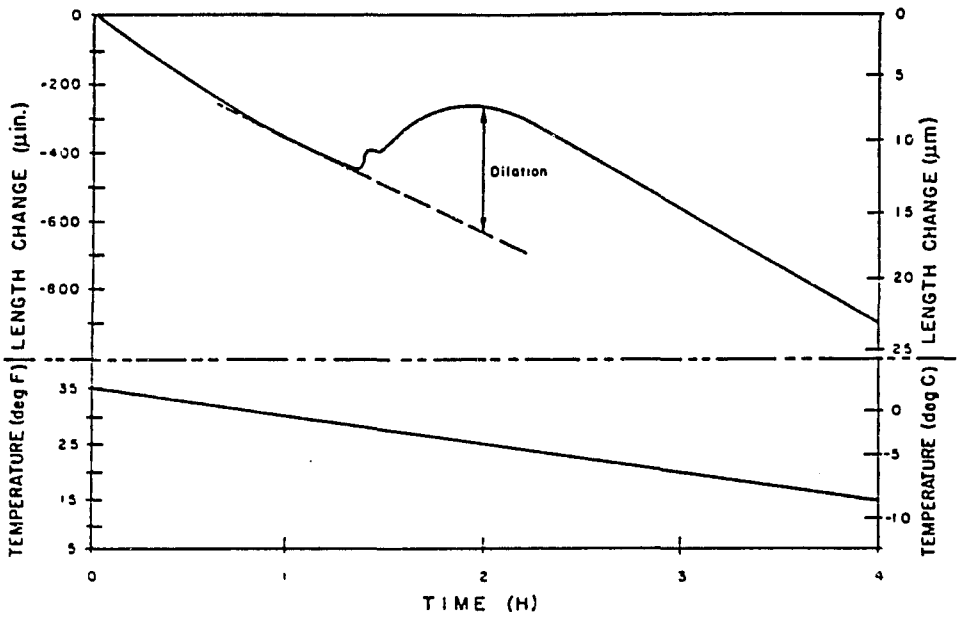

Figure 1. Typical length change and temperature plot for the critical dilation test [3]

freezing indicates frost susceptibility, while contraction indicates high resistance to freeze-thaw damage. However, he did not make any correlation between the results of one-cycle freezing test and the field performance of concrete.

By using a one-cycle test, Vuorinen [74] introduced a dilation factor and degree of saturation for evaluating the frost resistance of concrete. He found good correlation between the maximum dilation on first freezing and the residual expansion on subsequent thawing.

Faulkner and Walker [22] conducted a rapid one-cycle test for evaluating aggregate in concrete. They stated that a carefully measured length change during the first freezing period shows a "fingerprint" that can be successfully used for correlation with the durability factor that is obtained from the repeated freezing and thawing test. They used the slope of cumulative length change versus temperature and the length change versus time curves of the first freezing cycle near the freezing point of water as the "fingerprint". Experimental results indicated that the test was satisfactory for differentiating aggregate having a durability factor less than 30% and more than 50%, but unsatisfactory for intermediate percentages.

The physical properties of aggregate and concrete such as the porosity, pore size distribution, absorption, length change, etc. are important characteristics affecting their resistance to frost damage.

Larson and Cady [35] evaluated the frost susceptibility of aggregates by measuring their linear and volumetric particle expansions. The volumetric particle expansion was found to be an indicator of frost susceptibility.

Kaneuji [31] introduced an expected durability factor from his correlation between pore size distribution and freeze-thaw durability of coarse aggregates based on total porosity and median pore size obtained from mercury porosimetry measurements. The expected durability factor is given as

$$EDF = 0.579/PV + 6.12\ (MD) + 3.40$$

Where EDF = expected durability factor

PV = intruded volume of pores larger than 45 Å in diameter, cc/g

MD = median diameter of pores larger than 45 Å in diameter as measured by mercury porosimetry

Based on field performance of concretes showing varying degrees of durability failure, he concluded that the expected durability factors for non-durable, marginal, and durable aggregates were less than 40%, 40-50%, and more than 50%, respectively. Further investigations by Lindgren [42] on the pore characteristics of aggregates from 52 concrete cores from Indiana pavements demonstrated the usefulness of the proposed correlation.

Shakoor and Scholer [65] made a comparison of aggregate pore characteristics as measured by mercury porosimetry and the Iowa pore index test proposed by Myers and Dubberke [49] of the Iowa Department of Transportation. The apparatus for the Iowa pore index test is a modified version of a typical air pressuremeter with the replacement of the pressure chamber above the container by a 1" diameter plastic tube calibrated in millimeters. Approximately 9000 grams of oven-dried aggregate, graded

between 1/2" and 1 1/2", is placed in the container and covered with water to the zero mark in the plastic tube. The container is shaken to remove entrapped air, and a constant air pressure of 35 psi is applied through the top of the tube. The amount of water forced into the aggregate during the first minute represents the volume of macropores, and it is termed "primary load". The amount of water that is forced the next 14 minutes represents the volume of micropores, and it is termed "secondary load" or pore index. Shakoor and Scholer [65] reported strong correlation between the expected durability factor proposed by Kaneuji and the Iowa pore index test value. They further stated that the Iowa pore index test can be used as a reliable, less expensive, and quicker means for predicting aggregate durability and as an acceptance test for aggregate production than mercury porosimetry. Comparison between the expected durability factor and the pore index value of coarse aggregate indicates that unsound aggregates are characterized by high pore index values. Based on field performance data, a pore index of 50 ml was chosen to separate durable from nondurable aggregate.

The importance of aggregate pore characteristics to concrete durability has also been studied by Dolch [13], Lemish et al. [38], Lewis and Dolch [40], Sweet [68], Verbeck and Langren [73], and Walker and Hsieh [77].

Verbeck and Langren [73] showed the size of coarse aggregate to be an important factor in its frost resistance. They demonstrated that there is a critical size below which any given natural aggregate, unconfined by cement paste, can be frozen without damage. They observed that for a good quality aggregate, the critical size ranges upwards to a quarter of an inch.

Schuster and McLaughlin [64] found that cherts with high porosity were more susceptible to frost damage than those with low porosity.

Lewis and Dolch [40] stated that "harmful" pore sizes are those large enough to admit water but not large enough to permit easy drainage.

Sweet [68] stated that the volume of pores with a size smaller than 5 um appeared to be a critical index of field durability. He further noted that for limestone aggregates with good service record in concrete pavements, the volume of voids less than 5 um, expressed as the ratio of the total pore volume of the sample, was less than 0.06. For poor service record aggregates, this ratio was greater than 0.10. Later work by Schuster and McLaughlin [64] on cherts in concrete showed that their freeze-thaw durability was less dependent on the pore size content of 5 um or less.

Verbeck and Klieger [72] devised a calorimeter-strain apparatus for the study of the mechanism of frost action in concrete. This apparatus allows simultaneous determination of the amount of water actually frozen in concrete at a given temperature, and the resulting length change, which in turn allows the study of the influence of various factors such as air void characteristics, water/cement ratios, curing, and aggregates on frost resistance of concrete.

Levitt [39] developed a theory for the mechanism of fluid travelling through porous materials. He devised an apparatus for the initial surface absorption test and found the test to be sensitive to changes in the quality of concrete, and to correlate well with field and laboratory behavior. The initial surface absorption is defined as the rate of flow of water into concrete per unit area after a given time from the beginning of the test and at a constant head and water temperature. He suggested tentative limits for initial surface

absorption to protect concrete from frost damage, but stressed that more information is needed before any definite limits could be established.

Klieger [33] studied the effect of entrained air on durability of concrete with various sizes of aggregate. He reported that for air-dry concrete, the optimum air content can be achieved by providing a relatively constant air content in the mortar fraction regardless of its cement content, consistency, maximum size and type of aggregate. For maximum protection, the mortar air content appears to be in the range of 8% to 10%.

The Influence of Saturation

Perhaps two of the most important factors that influence the freeze-thaw durability of concrete are the relative ease with which it becomes saturated and the level in excess of critical saturation. The higher the rate of water intake, the faster the concrete attains critical saturation. Once a concrete reaches its critical degree of saturation, failure is inevitable. Thus, it may be postulated that any properties that influence these factors affect frost resistance.

Birger [7], in describing a model for the process of frost deterioration of concrete, stated that the time required to saturate the entrained air voids such that the concrete exceeds critical saturation is important to frost resistance mainly because the capillaries are usually saturated very quickly. However, this would not bring the paste above critical level of saturation. Frost damage therefore occurred only after certain entrained air voids were water-filled.

Verbeck and Langren [73] indicated that the durability of concrete made with different aggregates depends on the rate at which the aggregate becomes

critically saturated. They further stated that the time required for concrete to reach critical saturation is influenced by pore size and porosity of the aggregate as well as the thickness and permeability of mortar cover.

Walker and Hsieh [77] maintained that aggregates which exhibit good durability have a relatively low absorption. Aggregates with absorptions above 5% have a high potential for low durability.

Lemish et al. [38] stated that the abundance, size, shape, and continuity of pores determine the amount and rate of absorption, and the ease water can escape.

Hudec [30] reported that the durability of limestone rocks is a function of grain size, pore size, and rate of capillary absorption. He found the rate of absorption to be very fast initially and subsequently slower at later time. Rocks with high rates of absorption are less durable than rocks with low rates of absorption in terms of freezing action. Rocks of a fine-grained texture are more susceptible to frost damage than those which are coarse-grained, because the absorption is faster in the smaller pores in fine-grained rocks. Similarly, Myers and Dubberke [49] concluded that coarse aggregates with good service records are generally coarse-grained or extremely fine-grained in texture, and those with poor service records are usually fine-grained in texture.

Sweet [68] indicated that limestone aggregates with absorption and degree of saturation values greater than 3.9% and 86%, respectively, showed rapid deterioration when incorporated into concrete and subjected to freeze-thaw cycles. Those aggregates with an absorption value from 2-3% and a degree of saturation greater than 82% were intermediate, and those with

absorptions less than 2% and degree of saturation less than 80% were highly resistant.

It always has been assumed that a concrete exceeding its critical saturation level will experience such high destructive pressure that failure will be imminent. Then what is critical saturation? Various researchers have different ways of defining it. Since water expands about 9% upon freezing, a closed container 91.7% full of water will be completely filled upon freezing. Thus 91.7% can be considered as the critical saturation. However, freezing of water in a porous body is fundamentally different from freezing of bulk water in a container. Freezing of pore water depends on the pore size and structure, homogeneity, and rate of freezing.

MacInnis and Beaudoin [46] concluded that the critical degree of saturation of mortar mixes is approximately 90%. This critical saturation is defined based on length change pattern produced in a one-cycle freezing test. The critical saturation is defined as the saturation level below which no distinctive length change was observed. They studied the effect of the water/cement ratio and degree of saturation of air-entrained concrete on the expansion upon freezing, and found that no expansive tendencies occurred at water/cement ratios below 0.55 even at 100% saturation. However, at water/cement ratios above 0.60, expansion occurred when the saturation was above 90%. The higher the water/cement ratio, the higher the expansion.

Powers [55] stressed that it is impossible to establish a critical saturation value for an aggregate particle since the moisture content is not uniformly distributed in an aggregate at the time of freezing.

Fagerlund [21] conducted an extensive study on the significance of the critical degree of saturation. He stated that the critical degree of saturation is a material constant which adopts an individual value for each particular material. He further stated that proper use of the principle of critical saturation requires the knowledge of two properties: first, the moisture distribution in the structure; secondly, the critical saturation, which is a function of the material's properties, must be known at all parts of the structure. Based on the concepts presented, he defined frost resistance as the difference between critical and actual saturation. By using this definition, he claimed that all materials would be treated the same way, even though their properties such as densities, porosities, etc., were different. The frost resistance can then be expressed by single value which allows a rational choice of materials available.

Powers' Mechanism of Frost Damage

Some early attempts to explain the mechanism of frost damage were based on the fact that water expands about 9% upon freezing. Thus if water is frozen in a closed container filled above 91.7%, the expansive force may be sufficiently high to rupture the container. The freezing of pore water in porous materials was assumed to behave the same way as the freezing of water in a container. Based on this premise, the critical saturation of porous materials may be assumed to be 91.7%. Many experiments, as well as this research have proved otherwise; in fact, in many instances the critical saturation was found to be much below this level. This should be easily

recognized since the freezing of pore water is fundamentally different from the freezing of bulk water.

In 1945, Powers [52] proposed a hypothesis for the mechanism of frost action on concrete. The hypothesis is based on the premise that the destruction of concrete is mainly due to the generation of hydraulic pressure resulting from expansion of water upon freezing, instead of direct growth of bodies of ice crystals. When water freezes, the volume increase causes water to be displaced from the region of freezing, and the viscous resistance to flow of water through the concrete may generate hydraulic pressure large enough to rupture concrete. The magnitude of this stress depends on factors such as the rate of freezing, the degree of saturation, the permeability of concrete, and the paste properties.

The existence of ordinary bulk ice depends on the temperature and pressure of the prevailing environment. At normal atmospheric conditions, water freezes at 32 °F. At higher pressures, lower temperatures are required to freeze water. For instance, at 29,000 psi, a temperature below -4 °F is required to freeze water; or conversely, a pressure of 29,000 psi would be required to prevent the formation of ice at -4 °F. This essentially is the magnitude of pressure exerted on a closed cylinder piston if the piston is prevented from movement upon freezing [52].

The above gives an idea of the order of magnitude of internal stresses that a fully saturated, completely sealed concrete would be subjected to upon freezing. Powers pointed out that if a concrete is fully saturated, it would not be able to withstand the internal pressure, as evidenced by the failure of vacuum saturated specimens in low-temperature laboratory freeze-thaw

experiments. However, concrete does not ordinarily fail completely during the first cycle. This implies that it is not fully saturated, but has enough residual space to accommodate expansion upon freezing. However, in many instances concrete shows loss of resilience and abnormal expansion on repeated freeze-thaw cycles, even though the concrete not critically saturated. In other words, damage still occasionally occurs even if the concrete is below its critical degree of saturation. From these experimental observations, Powers proposed a working hypothesis to explain the mechanism of frost action in concrete. The hypothesis is as follows [52]:

If a surface of a concrete specimen is in contact with water for some time prior to the freezing and thawing cycle, the water content of the concrete at or near the surface probably is at or near total saturation, and may be slightly higher than the average water content of the specimen. If this surface is situated in such a way that heat transfer is towards the surrounding water, the sequence of events that takes place should be as follows: first, the water on the surface will freeze as the temperature is lowered, which seals off the surface; second, the water in the capillary spaces of the concrete nearest to the surface will freeze. As ice forms in these spaces, the still unfrozen water in the saturated region will be displaced towards the less saturated interior. Figure 2 may help in visualizing this. Figure 2 depicts the cross section of a part of the specimen. The surface in question is normal to the plane of the page at "aa". The saturated region near the surface is designated "A", whereas "B" is the region of lower water content. Ice will initially form outside at the surface. The inside of the specimen will remain unfrozen because freezing of pores occurs at subzero temperatures. Because of the

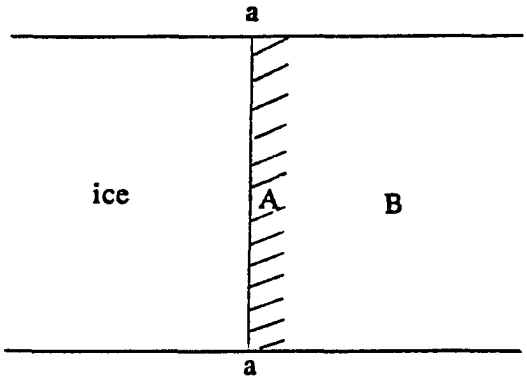

Figure 2. Cross section of a freezing specimen [52]

temperature gradient and higher water content in "A", freezing will first occur in region "A". When ice begins to form in region "A", the remaining unfrozen water will be displaced towards region "B". If water were free to move without any viscous resistance and the system is open-ended, there would be no hydraulic pressure generated. Since water is moving through a fine-textured, porous substance, the laws of hydraulic flow mandate that the force causing movement will result in corresponding viscous resistance, and hydraulic pressure gradients will be present during the flow of water. If the reaction against the viscous resistance of displacing water exceeds the tensile strength of concrete, failure is inevitable. The magnitude of this hydraulic pressure can be estimated based on the permeability of concrete.

Powers, in explaining the process of crumbling and spalling, stated that on repeated freezing and thawing region "A" would increase in thickness, depending on the amount of water absorbed. As the thickness of "A" increases, the resistance to displacement of water out of the freezing region towards the region of lower water content increases, since the path of flow also increases. If this saturated region "A" becomes sufficiently thick, the hydraulic pressure generated will exceed the strength of concrete, causing disintegration or spalling of some parts of region "A". The thickness of the region at which disintegration occurs is referred to as "the critical depth of saturation". This critical depth of saturation is somewhat arbitrary, since in actual situations there will be a gradual transition with a continuous moisture gradient between these two regions. One implication that can be derived from the above concept is that if a specimen were uniform in structure and not wholly saturated at the beginning, there would be no crumbling and spalling until a

certain amount of water had been absorbed such as to saturate the surface region to critical depth. The critical depth is different for different grades of concrete. This critical depth depends on factors such as the permeability of concrete, the rate of freezing, and the amount of water in region "A" in excess of critical saturation. At a given hydraulic pressure the average stress in the concrete depends on the proportion of solids in a unit cross sectional area.

If the critical depth of saturation of a specimen happens to be equal to or greater than half its thickness, disintegration should not take place until the entire specimen reaches critical saturation. Such a specimen should not exhibit any disintegration or crumbling during the process of acquiring water to reach critical saturation. Once it reaches critical saturation, it would take very few cycles for the concrete to disintegrate completely. This phenomenon has been observed in the laboratory [52].

The discussions up to this point are mainly based on the assumption that the submicroscopic pores in the partially desiccated paste are the only space available to accommodate the movement of water during freezing. Actually, concrete contains air-filled cavities that may or may not be connected directly to the exterior surface. These cavities are entrained air bubbles, accessible pores in the aggregate particles, and thin fissures under aggregate particles. These fissures are formed during the bleeding period. They are first water-filled, but may become partially or completely empty as hydration proceeds. All of these cavities are difficult to fill with water because liquid can not flow spontaneously from smaller to larger pores because of capillarity. Under normal conditions, a pressure exceeding one atmosphere is required to fill a cavity, and the pressure generated during freezing generally is sufficient to

force water into such pores. From the above discussion, one might be tempted to draw the conclusion that concrete will be protected if enough spaces are available to accommodate the expansion during freezing. Ordinary, concrete contains more than enough space to accommodate the expansion. In such a case, concrete would theoretically be protected from freeze-thaw damage indefinitely. This statement is clearly contrary to observed fact, leading to the hypothesis that the distance between the air voids or cavities rather than the total volume of air voids may be the controlling factor in frost susceptibility. Experience seems to indicate that if a concrete contains a large number of small, well distributed air cavities, its rate of deterioration is greatly reduced. This reduction can be accomplished by incorporating entrained air bubbles that serve as escape boundaries or relief valves for the displaced water. If they are closely and uniformly distributed, they limit the thickness of material through which displaced water must flow, thereby reducing the hydraulic pressure generated. However, in the event that concrete exceeds its critical level of saturation; for example, after prolonged soaking, there will not be enough empty spaces to accommodate all the excess water. As a result, some excess water will find its way to the exterior of specimen. Since the path of flow is greatly increased, there will be a proportional increase in hydraulic pressure, which is a potential source of frost damage.

The relative permeabilities of paste and aggregate also are important in determining frost damage. If the aggregate is impermeable relative to the paste, there should be an increase in hydraulic pressure in the region where the paste is saturated, because the aggregate block the most direct path of displaced water to the unsaturated region. Thus one would expect concrete

containing impermeable aggregate to fail along the aggregate surfaces under freeze-thaw action. Conversely, if concrete contains unsaturated aggregate that is more permeable than the paste, the aggregate should aid in alleviating the hydraulic pressure the same way cavities do until they become saturated. When they become saturated, water must flow to the surrounding paste during freezing. Otherwise the pressure which develops within the aggregate will be high enough to rupture both the aggregate and the surrounding paste. The magnitude of this pressure depends on the permeability of the paste that lies between the saturated aggregate and the unsaturated region.

Powers [52] stated that the frost resistance of concrete depends on its initial degree of saturation and rate of water absorption. One of the factors that governs the amount of water absorbed during thawing is the rate of thawing.

Subsequent studies by Powers and associates [53,54,58,59] led to the introduction of the air void spacing factor and the entrained air requirement of concrete.

As stated previously, entrained air is incorporated into concrete to protect it from destructive hydraulic pressure. The effectiveness of the entrained air depends on the void spacing factor, which is defined as the average maximum distance from any point in the paste to the edge of a void. Powers stated that the maximum permissible spacing is a function of paste properties, degree of saturation of the paste, and rate of cooling. He presented a theoretical calculation of the desired spacing factor based on experimental data from six different cement pastes, cooled at 20 °F per hour, and found the spacing factor to be in the range of 0.01 in. to 0.026 in. or more; depending on

the paste characteristics and void size. The spacing factor and the total volume of air can be determined by the linear transverse method. An actual maximum spacing factor for certain frost resistant concrete was estimated to be in the order of 0.01 in. or less using this method. This value is in close agreement with the theoretical spacing factor he presented. Powers also gave theoretical equations for the determination of the air requirements and the magnitude of hydraulic pressure. The amount of air required was found to be a function of paste content, specific surface of air voids, and maximum permissible spacing factor. The magnitude of hydraulic pressure generated depends on the permeability of the paste, spacing factor, degree of saturation, rate of cooling, viscosity of displaced water, and the amount of water frozen for each degree drop in temperature. Detailed discussions and derivations of these equations can be found in the cited references.

Pore Structure Analysis Methods

It is clear from previous discussions that many researchers recognize the important role pore structure plays on frost properties of porous materials. The influence of pore structure is considered as a significant factor influencing the freeze-thaw resistance of concrete. Powers and Helmuth [59] considered the size, shape, and pore size distribution as some of the most important factors controlling the magnitude of hydraulic pressure generated in concrete during freezing.

Various direct and indirect methods have been introduced in recent years for pore size distribution analysis. The most direct methods are scanning electron microscopy and transmission electron microscopy. These

methods are not routinely used because they are tedious, costly, and require special technique and skills. The most widely used indirect methods are mercury porosimetry and sorption isotherm. Mercury porosimetry was first proposed by Washburn [78] and subsequently developed by Ritter and Drake [60] and Winslow and Shapiro [82]. Sorption isotherm was first proposed by Wheeler and later developed by him [79a,b] and Cranston and Inkley [12]. Another useful method is phase transition porosimetry proposed by Eckrich et al. [14] and Enustun et al. [16]. All of these methods are commercially available. Mercury porosimetry has found application in the field of civil engineering materials, where it is considered to be the standard method for pore structure analysis. Phase transition porosimetry is still in its infancy stage and may become more popular because of the many advantages it offers and also because of the many problems associated with mercury porosimetry.

Mercury porosimetry theory

This method involves evacuation of pore air from an oven-dried sample by vacuum. Mercury is then forced into the pores of the sample at various increments of pressure. The theoretical principle behind this is that mercury, a non-wetting liquid, will only intrude into the pores of materials if the mercury is under pressure. As the pressure is gradually increased, the pore volume intruded by mercury is measured as a function of pressure. The Laplace equation is used to relate the pressure difference across the convex liquid meniscus to its mean radius of curvature. In the case of mercury, the pressure is given by

$$\Delta P = \frac{2\gamma_m}{r_m} \qquad (1)$$

Where γ_m and r_m are the surface tension and mean radius of curvature of the mercury meniscus, respectively.

As pressure is gradually increased, the mean radius of curvature becomes progressively smaller as mercury moves inward into the pores. When the pressure reaches a certain value, the geometry of pore opening can not tolerate the existence of the meniscus with r_m smaller than a minimum value, and mercury will invade the pore body. If mercury were a perfectly non-wetting liquid, r_m would give the characteristic pore neck size, r. However, the contact angle, θ, of mercury is always less than 180 degrees. Washburn [78] derived the relationship between r_m and r by considering the special case of a cylindrical pore opening. It is given by

$$r = - \frac{2\gamma_m \mathrm{Cos}\theta}{P} \qquad (2)$$

By knowing γ_m and θ, r can be obtained from the measured breakthrough pressure. In actual situations, there are assorted sizes of pore necks and intrusion will occur progressively as pressure increases. The intruded volume is monitored as a function of pressure, dV_p/dP, which then is converted to pore volume as a function of pore radius, dV_p/dr, using equation 2. The result is an integral form of the pore neck size distribution; derivative will give the pore neck size distribution.

If the pressure is gradually decreased, mercury starts extruding from the pores. The measured extruded pore volume, as a function of pressure, should give the pore body size distribution. However, due to problems associated with mercury entrapment and hysteresis, extrusion data do not allow a realistic pore body size distribution to be obtained.

Two theories have been suggested recently to explain hysteresis and mercury entrapment. The first, proposed by Hill [28], states that intrusion advances axially while extrusion occurs radially. He showed extrusion pressure to be equal to half of that required for intrusion into cylindrical pores. He also stated that in a porous system consisting of essentially cylindrical pores, if the neck radius is less than half the pore radius, mercury entrapment takes place. The second theory is based on Polanyi's pore potential theory and was suggested by Lowell and Shields [43]. This theory states that once a pore is intruded, mercury atoms fall into the potential field of capillary pore walls and acquire a lower free energy than that present during intrusion. Extrusion therefore is delayed and commences only at a lower pressure with a smaller contact angle than that of intrusion. According to this pore potential theory, entrapment occurs if the interfacial energy near a pore opening or constriction is equal to the pore potential.

In addition to entrapment and hysteresis, there are controversies regarding kinetic hysteresis due to hydraulic drag and the magnitude of contact angle that should be used. The contact angle depends on the nature of the matrix and must be determined independently for each individual material. This is further complicated by the difference in contact angle associated with an advancing and retreating meniscus [11]. Another problem

with this method is that if a void has an entrance or neck smaller than its body, the whole void volume will be incorrectly recorded as being the size of entrance. The pore size distribution is therefore weighted towards smaller pore sizes [13]. Another limitation of this method is the necessarily small size of sample that can be tested, which may not be representative of a sample that is heterogeneous in character.

Phase transition porosimetry theory

The plastic ice theory of capillary freezing and melting of pore water was first proposed by Everett [19] and Everett and Haynes [20]. Further investigations by Enustun et al. [17,18] confirmed the applicability of this theory. The mechanism is essentially similar to mercury intrusion and extrusion. The progress of capillary freezing occurs by virtual penetration of bulk ice, which corresponds to mercury intrusion; whereas the progress of melting, or virtual recession of bulk ice, corresponds to mercury extrusion provided that the contact angle is 180° [14]. The progress of phase changes can be followed by measuring the volume change of a completely saturated sample due to the freezing and melting of the pore water. Expansion takes place upon freezing because of the extrusion of ice from the freezing pores, while contraction occurs by admission of ice into the melting pores.

If it can be assumed that the pore geometry of a porous material consists of intersecting spheres or cylindrical capillaries with or without constrictions, the temperature t(°C) at which the solid-liquid phase transition of pore water takes place in a pore with effective radius, r(cm), is given by [14]

$$-t = \frac{2\gamma_o T_o}{(\rho\lambda r + 0.5T_o)} \qquad (3)$$

Where T_o = normal melting point of water in degrees Kelvin

λ = heat of fusion of ice per unit mass

ρ = density of water

γ_o = ice/water interfacial tension at 0 °C

The constant 0.5 is a dimensional constant for use with the C.G.S (centimeter, gram, second) units. The effective pore radius, r, corresponds respectively to the pore neck and the pore body radius during freezing and melting.

Consider a saturated sample placed in a mercury dilatometer at a controlled temperature t. As the temperature is gradually lowered and if there is no phase change, the mercury level in the dilatometer stem will decrease linearly with temperature with a slope "a". In the range of phase transition, the change in volume with respect to temperature, dV/dt, is related to the pore volume size distribution dV_p/dr by [14]

$$\frac{dV_p}{dr} = \left(a - \frac{dV}{dt}\right)\left(\frac{dt}{dr}\right)/\phi \qquad (4)$$

Where ϕ is the fractional change in volume of water upon freezing at temperature t. Taking the derivative of equation 3 and substituting into equation 4, the following equation is obtained

$$\frac{dV_p}{dr} = \left(a - \frac{dV}{dt}\right) \frac{\rho\lambda t^2}{2\gamma_o T_o \phi} \qquad (5)$$

By measuring the change in volume as a function of t, the pore size distribution curve can be obtained by evaluating equation 5 for dV_p/dr and plotting against the corresponding r values calculated from equation 3. This cooling curve gives the pore neck or constriction size distribution. On rewarming, the curve gives the pore body size distribution. The pore volume can be obtained by integrating equation 5 over the entire pore size range. The cooling data give the pore neck or constriction volumes, and the rewarming data gives the pore body volumes.

Pore surface area can also be calculated by using the rewarming data. In the case of cylindrical pores, this area is given by [14]

$$A = 2\int_{r_1}^{r_2} \frac{1}{r}\left(\frac{dV_p}{dr}\right) dr \qquad (6)$$

In the case of spherical pores, this area is given by

$$A = 3\int_{r_1}^{r_2} \frac{1}{r}\left(\frac{dV_p}{dr}\right) dr \qquad (7)$$

In the general case of irregularly shaped pores, it would be reasonable to replace the constant in front of the integral by 2.5.

Phase transition porosimetry is believed to be an important contribution to the field of civil engineering materials in terms of pore structure analysis because it is accurate and free from all the previous mentioned problems that confront mercury porosimetry. To further substantiate this statement, Table 1 presents the pore size range, porosity, and specific surface area of porous vycor glass obtained using various commonly known methods.

Table 1. The pore size range, porosity, and specific surface area of porous vycor glass obtained using various commonly known methods [14]

Method	Range of pore body radius, Å			Range of pore neck radius, Å			Porosity % by vol.	Specific surface, m^2/g
	Min.	Mode	Max.	Min.	Mode	Max.		
Phase Transition Porosimetry	17	42	75-100	12	21	40	25[a]-27[b]	135[c]
Mercury porosimetry	19	80	-	18	25	35	29[d]	-
Conductance	17	36	60	-	24	26	-	-
TEM	15	38[e]	85	-	-	-	-	-
Manufacturer's specification	10	-	100	-	-	-	28	150-200

[a]From rewarming data.

[b]From cooling data.

[c]Assuming spherical pores.

[d]From intrusion.

[e]After converting number-size dstribution to volume-size distribution.

PROPOSED HYPOTHESIS

As discussed in the introduction, although research on the mechanism of frost action is considered well established and successful in explaining the role of entrained air, it can not explain the abrupt drop in frost resistance of concrete in near-saturated states. A new model was therefore proposed to address this. This proposed model, also known as the two-stage model, is based on the plastic ice theory of capillary freezing and melting of pore water, discussed below.

Two mechanisms appear to operate during the freezing of pore water; namely, in situ nucleation and bulk-ice-initiated freezing. The first mechanism operates at low levels of saturation, i.e., below critical saturation, and was treated by Powers. The second controls freezing process at high levels of saturation, and it occurs when the excess volume of water expelled to the surface upon freezing begins to form bulk ice. The bulk ice/pore water boundary at the surface starts to form a convex ice front and moves inward through the pores. The mechanism of this freezing is similar to mercury intrusion. It is believed that the second stage of bulk-ice-initiated freezing will subject the concrete to far more intense dynamic stresses because of the extrusion of ice, and is responsible for the frost susceptibility of concrete in near-saturated states. Although Powers' model also considers dynamic stress as the main cause of frost damage in near-saturated states, it does not associate this stress with the extrusion of ice but rather with the extrusion of the excess volume of water as freezing occurs by in situ nucleation.

The operations of these two mechanisms are reflected in the volumetric expansion of concrete upon freezing as a function of the degree of saturation. The damage to concrete depends on the internal cyclic stresses developed during freezing and thawing because of the flow of water or ice.

Plastic Ice Theory

In order to fully comprehend the development of the two-stage model, a review of the plastic ice theory is warranted.

Two models have been advanced to explain the mechanism of capillary freezing and melting. They are crystalline ice and plastic ice models.

In the crystalline ice model, ice crystals are assumed to form in the capillaries. After ice crystals start to form in the capillaries, they grow as far as the capillary walls allow, and the remaining capillary space is occupied by unfrozen water. This model provides the relationship between the capillary melting point and the capillary size. Enustun et al. (17,18) investigated the validity of this model by electrical conductance measurements of a sample of porous glass saturated with dilute ammonium nitrate solution. They found that the melting point of pore water predicted by this model is inconsistent with the accepted value derived from a consideration of the ice/water interfacial tension and the capillary size. They further pointed out that in situ freezing is a rate process that is beyond the treatment of equilibrium thermodynamics. They therefore rejected this model in favor of the plastic ice model. Further investigations confirmed the validity of this model and subsequently led to the development of phase transition porosimetry discussed earlier.

The plastic ice model, first proposed by Everett [19], provides the relationship between the freezing temperature and the capillary pore opening, is based on equilibrium thermodynamic principles. The development of the theory is as follows [19,20]:

Consider two cylinders A and B, joined by a capillary tube and closed by pistons at both ends, as shown in Figure 3a. Let them be filled with water at pressure P. The temperature of water in B is then lowered below 0 °C and freezing is nucleated in B only. As the freezing progresses, the accompanying expansion upon freezing is taken by the movement of pistons. If the upper piston is fixed, then water will flow through the capillary tube into A and will displace the lower piston. If both pistons are not restrained from movement, when freezing is completed in B, further lowering of temperature will result in the formation of ice in either of two ways: (1) intrusion of ice crystals from B into the capillary tube; (2) continued growth of ice crystals over the lower face in B, followed by the migration of water from A to B. The latter will cause an upward movement of upper piston.

The Laplace equation gives the pressure difference across the ice/water meniscus as

$$P_i - P_w = \frac{2\gamma_{i,w}}{r_{i,w}} \qquad (8)$$

Where P_i and P_w are the pressure in the ice and water phase, respectively. $r_{i,w}$ is the radius of curvature of ice/water meniscus and $\gamma_{i,w}$ is the surface tension across the interface.

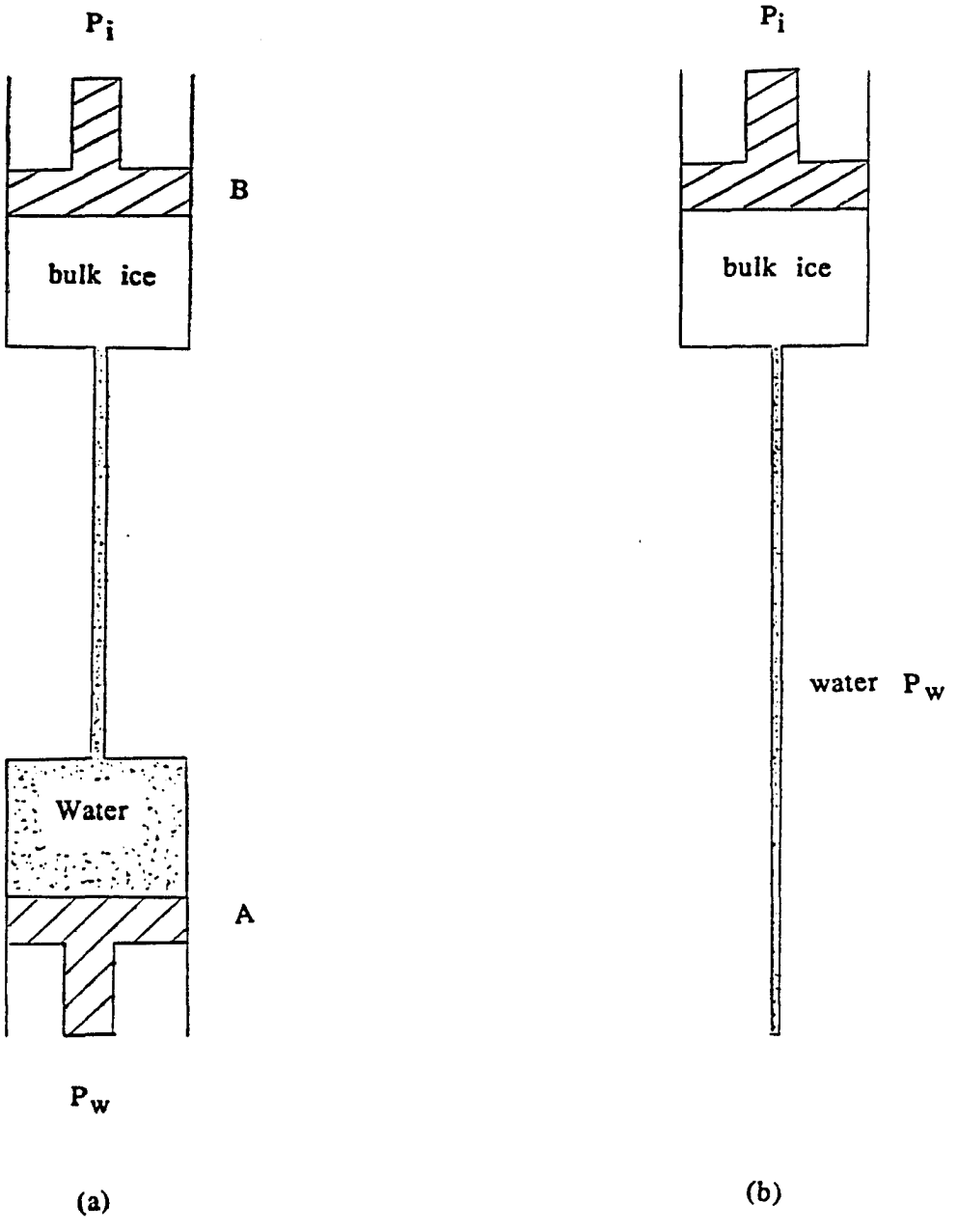

Figure 3. Schematic diagrams of capillary freezing and melting [19]

Provided that the pressures exerted by the pistons are equal at equilibrium, i.e., $P_i=P_w$, the ice/water interface will be a plane and there will be no tendency for ice to penetrate into the capillary. Figure 4 shows the equilibrium interface between ice and water. Growth of an ice crystal into the capillary would occur if the chemical potential of material in the capillary is higher than that of bulk ice. These essentially are the conditions that exist in weakly consolidated materials such as soil, where no pressure difference can be maintained. Once ice is formed, water is drawn from the surrounding unfrozen region to form a larger ice lens. Essentially, this is believed to be the mechanism behind frost heave because the chemical potential of liquid water is greater than that of bulk ice at temperature below 0 °C. Water will migrate from regions of high chemical potential to regions of low chemical potential. If P_i remains constant and the piston is not prevented from movement by friction in B, ice will continue to grow in B until all water is drawn from A.

The chemical potential of liquid water, u_w, at temperature, T(K), and pressure, P_w, is given by [18]

$$u_w(T,P_w) = u_w(T_o,P_o) - \int_{T_o}^{T} S_W \, dT + \int_{P_o}^{P_w} V_w \, dP \qquad (9)$$

Where T_o = melting point of water at K

P_o = atmospheric pressure

S_w = molar entropy of water

V_w = molar volume of water

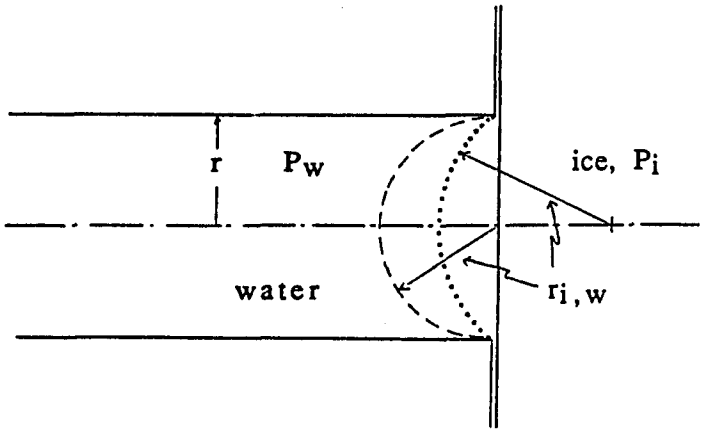

—————— $P_i = P_w$, $r_{i,w} = \infty$

..... $P_i - P_w < 2\gamma/r_{i,w}$, $r_{i,w} > r$

---------- $P_i - P_w = 2\gamma/r_{i,w}$, $r_{i,w} = r$

Figure 4. Equilibrium interface between ice and water [19]

Similarly, the chemical potential of bulk ice, u_i, at temperature, T(K), and pressure, P_i, can be given by

$$u_i(T,P_i) = u_i(T_o,P_o) - \int_{T_o}^{T} S_i\,dT + \int_{P_o}^{P_i} V_i\,dP \qquad (10)$$

Where S_i = molar entropy of ice

V_i = molar volume of ice

Consider a closed end capillary tube connected to a piston as shown in Figure 3b. Due to movement of piston, the pressure of ice will remain at atmospheric, P_o. As the temperature is gradually lowered, the transfer of water from the capillary tube to bulk ice lowers the pressure of water below atmospheric to $P_o - (2\gamma/r_{i,w})$. In accordance with the Laplace equation, the radius of curvature will increase. Since $u_i = u_w$ at equilibrium, if we assume that at the same temperature and pressure, any thermodynamic property of either phase is equal whether it is in bulk state or in the capillary, then by combining equations 8, 9, and 10, the following equation is obtained [18].

$$-\int_{T_o}^{T} S_i\,dT = -\int_{T_o}^{T} S_w\,dT + \int_{P_o}^{P_o-2\gamma/r_{i,w}} V_w\,dP \qquad (11)$$

If the pressure dependence of V_w is neglected, then equation 11 becomes

$$\frac{2\gamma V_w}{r_{i,w}} = \int_{T_o}^{T} (S_w - S_i)\,dT \qquad (12)$$

From thermodynamic considerations [18]

$$S_w - S_i = \frac{L}{T_o} + \int_{T_o}^{T} \frac{C_{pw} - C_{pi}}{T} dT \qquad (13)$$

Where L = normal molar heat of fusion for ice

C_{pw}, C_{pi} = molar heat capacities at constant pressure of water and ice, respectively

From equations 12 and 13, we obtain

$$\frac{2\gamma V_w}{r_{i,w}} = \frac{L}{T_o}(T_o - T) + \int_{T_o}^{T}\int_{T_o}^{T} \frac{C_{pw} - C_{pi}}{T} dT\, dT \qquad (14)$$

The double integral term is small and can be neglected [17]. Since the density of water is the molecular weight per molar volume and the heat of fusion of ice per unit mass is the molar heat of fusion divided by the molecular weight, equation 14 is further reduced to [18]

$$r_{i,w} = \frac{2\gamma T_o}{\rho_w \lambda (T_o - T)} \qquad (15)$$

Where ρ_w = density of water at temperature T

λ = normal heat of fusion of ice per unit mass

Equation 15 provides the relationship between equilibrium temperature T and the radius of curvature of ice/water interface, $r_{i,w}$, in a capillary. Freezing of

ice in the capillary will occur if the radius of curvature is equal to the pore opening.

Proposed Two-Stage Model

As stated earlier, the Powers' model of frost damage is valid as long as the concrete is below critical saturation. However, in near-saturated states, i.e., above critical saturation, greater stresses than those predicted by Powers are believed to develop within the structure because of the extrusion of ice during second stage bulk-ice-initiated freezing.

The development of the two-stage model, proposed by Enustun and Bergeson [15], is as follows: Consider the pore structure of concrete as an assembly of some globular macropores (pore cavities) on a background of freezable capillary pores and nonfreezable micropores (gel pores) interconnected as a network. The mechanism of freezing and thawing of pore water in such a structure is discussed by using a simplified model. Although this model is far from representing the actual complicated conditions in the field, it illustrates the mechanistic cause of frost damage as well as the role of the presence of air in the pores, which will be discussed later. Some complications that arise in practice do not change the conclusions from a fundamental point of view. These complications are the presence of pores of assorted sizes, irregular interconnections, and supply of external water.

Consider a simple model of a solid sample containing a spherical cavity connected to the surface by tubular, freezable capillary pores as shown in Figure 5. Let the sample be saturated with water and covered with a thin film of excess water at its surface. As the sample is cooled below 0 °C, the excess

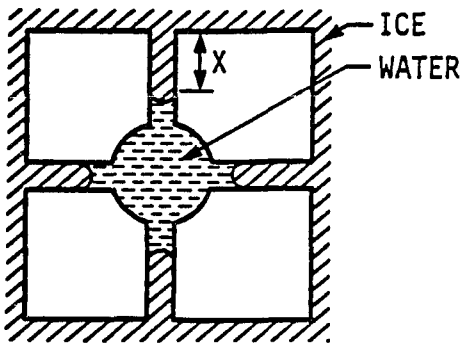

Figure 5. Schematic representation of bulk-ice-initiated freezing of pore [15]

water is converted to bulk ice but the pore water remains unfrozen. Only at temperatures far below 0 °C will it freeze.

By thermodynamic considerations, the temperature at which the freezing of a capillary pore occurs is related to the radius of its pore opening by

$$-t = \frac{2\gamma T_o}{\lambda \rho_w r_{i,w}} \tag{16}$$

in accordance to the plastic ice theory (refer to equation 15). The meaning of each variable was given in the preceding section. Neglecting the temperature dependence of γ and ρ_w, equation 16 can be written numerically as

$$t = -0.049/r \tag{17}$$

Here t is the temperature in °C and r is the pore radius in micrometers. The sample freezes from the surface, i.e., from the boundary of bulk ice/pore water at the surface, and bulk ice starts to form a convex ice front and moves inward.

During and upon freezing, the pore structure is subjected to static and dynamic stresses.

Under a given condition, there will be a pressure difference existing across the ice/water boundary. If the meniscus is within the capillary pores, then according to the Laplace equation this pressure difference is given by

$$\Delta P = 0.59/r \tag{18}$$

where ΔP is the excess pressure, in atmospheres, in the ice phase relative to the liquid phase or tension in the liquid phase relative to the ice phase. For a capillary pore radius of 0.01 micrometer, the pressure difference is about 60 atmospheres. Everett [19] attributed the frost damage to this static stress (such a pore freezes at about -5 °C according to equation 17).

Dynamic stresses develop as the ice meniscus virtually penetrates a capillary during the freezing process, because ice is extruded from the capillary in the opposite direction due to the volume increase that occurs upon freezing of water. The profile of stress developed inside a capillary along its length, x, under static and dynamic conditions at various stages of freezing and thawing is schematically shown in Figure 6. The full sloping lines represent the dynamic pressure in ice-occupied capillary space, and the horizontal lines represent the corresponding pressure in the liquid phase occupying the rest of the pore. The vertical lines indicate the pressure drop across the ice/water boundary.

As can be seen, a large pressure gradient develops along the ice path during freezing because of the extrusion of ice having very high viscosity. The magnitude of this pressure, which depends on the rate of freezing and the dimension of the ice path, is difficult to assess because of the lack of reliable data on viscosity of ice in literature.

When ice thaws, the process reverses and stresses become tensile. The magnitude of compressive and tensile stresses represented in this figure is based on the assumption that freezing and thawing proceed at the same rate. At a given stage, the absolute magnitude of the maximum thawing stress is larger than the freezing stress by an amount equal to static stress.

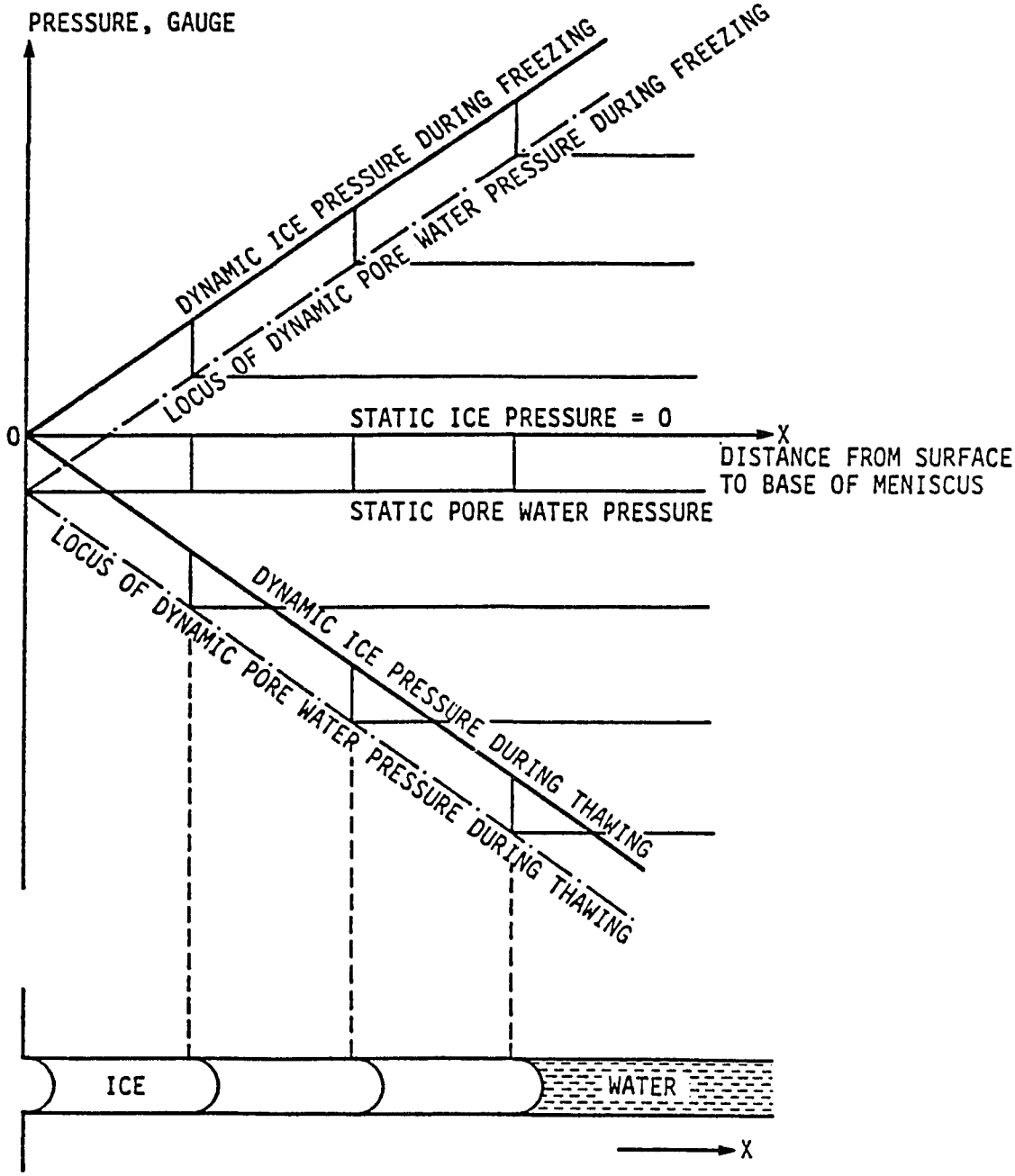

Figure 6. Static and dynamic stresses developed in a cylindrical capillary at various stages of freezing and thawing [15]

Obviously, the concrete is subjected to fatigue because of cyclic loading caused by freezing and thawing. This makes it more vulnerable to destruction.

When the ice meniscus reaches the macropore cavity during freezing, the dynamic compressive stress becomes particularly large because freezing of the cavity is thermodynamically spontaneous at low ambient temperature.

Powers also considered dynamic stress as the main cause of frost damage in concrete. However, he did not associate this stress with the extrusion of ice but rather with the extrusion of the excess volume of water from the freezing pores.

Accordingly, the protection of concrete from frost damage by entrained air is believed to be due to minimizing this dynamic stress by the presence of empty air pockets in close vicinity of the freezing pores. Powers et al. [59] also dealt with the migration of unfrozen pore water drawn by bulk ice ultimately formed in those large air voids.

What Powers et al. ignored is the possibility of bulk-ice-initiated freezing following in situ nucleated freezing, in spite of some air initially present in the pores. Bulk-ice-initiated freezing may occur when concrete is in near-saturated states, and it involves dramatically more intense dynamic stresses than those considered by Powers because of the extrusion of ice towards bulk ice as described earlier.

To distinguish the bulk-ice-initiated freezing mechanism from the mechanism dealt with by Powers, it must be noted that the pore structure illustrated in Figure 5 repeats itself many times in a surface-dry laboratory sample in the fashion shown in Figure 7. Figure 7a represents an increment of this structure in the interior of a sample far from saturation. Here the

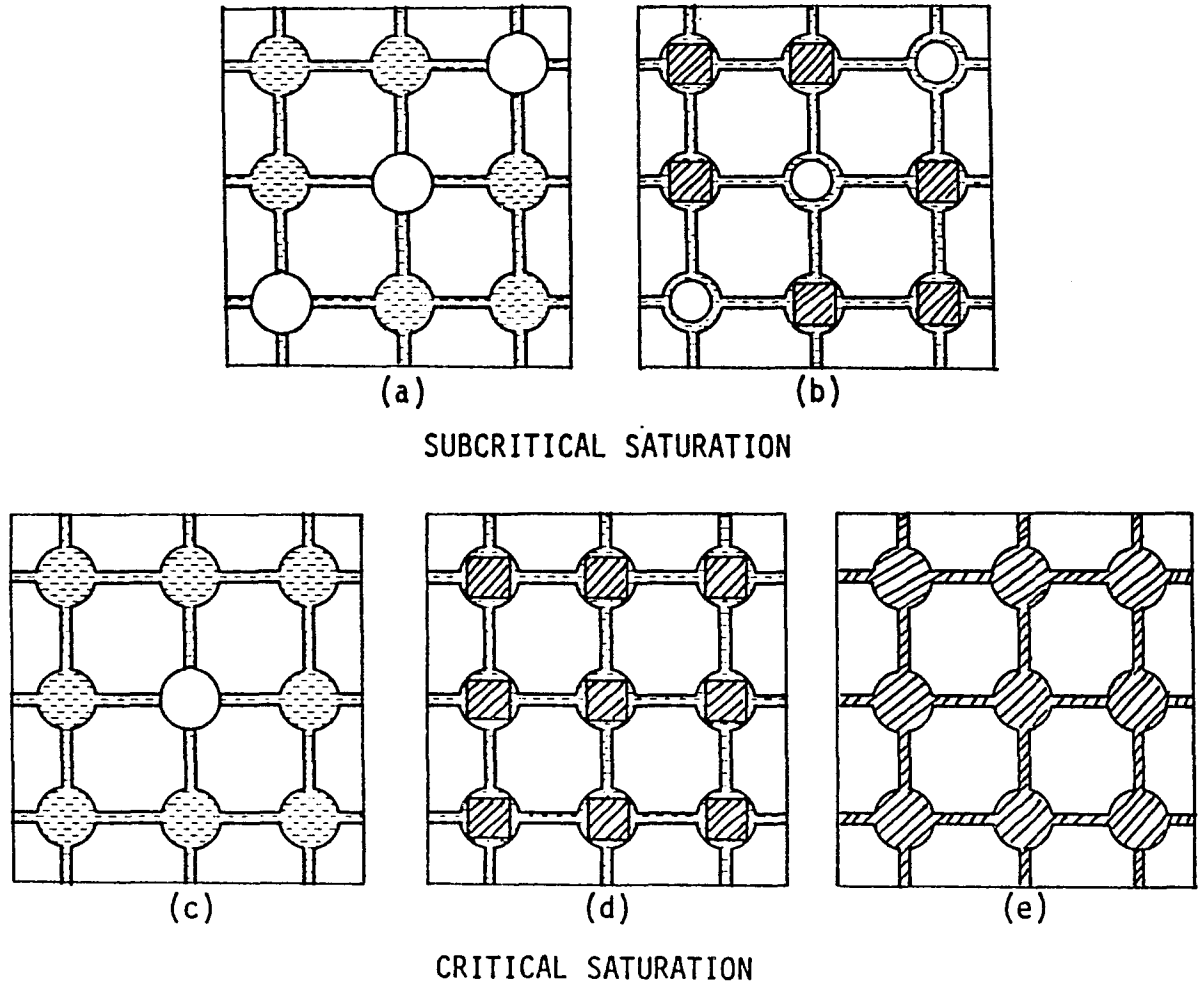

Figure 7. Schematic representation of the freezing mechanism of pore water as a function of saturation [15]

circular volumes are the pore cavities, and the tubular interconnections are freezable capillary pores. The rest of the volume contains gel pores filled with water which are not shown in the figure. The dashed areas represent water-occupied space, the blank circular areas represent air voids, and the cross-hatched areas represent ice.

When temperature drops below freezing, and if there is no bulk ice formed on the surface or in large pockets in the interior of the sample, freezing should depend only on in situ nucleation in water-filled pore cavities.

As ice is formed in these cavities, the excess volume of water brought about by expansion upon freezing is expelled into nearby air voids through unfrozen capillary pores and gel pores. This causes the air to be compressed, as shown in Figure 7b. This figure illustrates the situation in which the ice crystals are fully grown as far as their envelopes allow. Until this stage is reached, the structure is subjected to some dynamic stresses as considered and treated by Powers. In contrast to ice formed by bulk-ice-initiated freezing, there exists a considerable amount of unfrozen freezable water in the pore space in equilibrium with ice formed by in situ nucleation. If it is assumed that the compressed air does not find its way out of the sample at this stage, the sample should not exhibit any substantial volume change except a minute dilation due to internal stress [56]. However, if the saturation is increased above a critical level, as is shown in Figure 7c, the volume will change dramatically. The critical level is reached when upon freezing, the excess volume of water is just accommodated in the empty air voids and it freezes there (Figure 7d). Implicit in this argument is the assumption that the air in

these cavities will ultimately disappear as water freezes, through dissolution in the unfrozen pore water as a result of compression.

As saturation is increased by any amount above the critical level, the excess volume of water due to freezing is forced as far as the surface of the sample. There the excess water freezes to form bulk ice. This action should trigger the freezing of the rest of unfrozen freezable water in the entire pore structure as shown in Figure 7e. The final step should cause the sample to suffer far greater dynamic stresses than in the first step (in situ nucleated freezing) described earlier. It is believed that the second step is responsible for frost susceptibility of concrete in near-saturated states. This step also brings about an easily measurable volume increase because of the extrusion of some ice out of the pores to the sample surface.

At a given temperature, if ϕ is the fractional expansion of water upon freezing and f is the ratio of pore water frozen by in situ nucleation to that freezable by bulk-ice-initiated freezing, the critical degree of saturation, $X_c\%$, of freezable pore volume can be calculated from

$$X_c = 100/(1 + f\phi) \tag{19}$$

and the percent of volume change, $V_c\%$, on the basis of freezable volume from

$$V_c = 100(1- f)\phi \tag{20}$$

As the degree of saturation, X, increases from X_c to 100%, the percentage of volume change, V, varies linearly from V_c to 100ϕ.

Some experimental observations to support this model as well as an example of numerical application of these equations are now presented.

Two identical, completely saturated air-entrained samples of cement pastes cast in U-tubes were prepared, and their electrical conductance was measured as they were cooled step-wise to freezing [15]. Both were covered with bulk water. The first sample was totally immersed in a freezer bath to form bulk ice externally. The second sample was partially immersed to avoid formation of external bulk ice, and instead the sample was forced to freeze by in situ nucleation. The freezing points, as well as the extent of freezing, were monitored by the drops in conductance. It was observed that the initiation of freezing in the first sample depended on the formation of bulk ice on the surface either by seeding or spontaneous freezing. The second sample was observed to freeze at a temperature a small fraction of a degree below the spontaneous freezing point of the first sample. At -11 °C, bulk ice formed and triggered freezing of 66.5% of the total water content of the first sample, whereas in situ nucleation froze only 32.8% of that in the second sample. This means that only 49% of the pore water freezable by surface bulk-ice-initiated freezing froze when in situ nucleation freezing was forced. When the temperature was further lowered, freezing progressed in the first sample, whereas practically no further freezing was observed in the second sample.

These observations support the model as depicted in Figure 7d both in terms of the pore structure and the extent of freezing. Specifically; (a) freezable pores form a continuum in the entire matrix, and (b) freezable water only partly freezes in the absence of bulk ice. This partially frozen water

leaves the rest of the pore water unfrozen and does not behave as a plastic mass available to induce further freezing as considered by Everett [19,20].

The measurements made from the cement paste also allow us to assign a numerical value to the critical degree of saturation, X_c, and its corresponding volume change, V_c. If $f = 0.49$ and $\phi = 0.082$ at -11 °C, then using equations 19 and 20, the critical saturation and the volume change is 96% and 4.2%, respectively. The volume change versus saturation is shown in Figure 8.

Recent dilatometric measurements made with a mercury dilatometer on a mortar sample of low water/cement ratio appear to be compatible with this plot.

It was observed that no measurable volume change occurred on freezing down to -30 °C at a saturation of 90.5% in spite of some bulk ice on the surface; whereas at -11 °C and 100% saturation, the volume change was 8.2% relative to the total freezable pore volume.

It follows that in near-saturated states, the magnitude of volume change upon freezing, which is also an indication of the extent of bulk-ice-initiated freezing, should be a measure of the driving force of frost damage. If all variables are kept the same and saturation is increased, this model requires that concrete should become frost susceptible abruptly at critical saturation approaching 100%. This has indeed been observed experimentally as shown in Figure 9.

Powers' model also requires a threshold saturation level above which the excess water expelled from the freezing pores must travel through the unfrozen micropores all the way to the exterior surface of the sample, since there is no room to accommodate it in the interior. This is also a potential source of frost damage. But in this case the damage would be proportional to

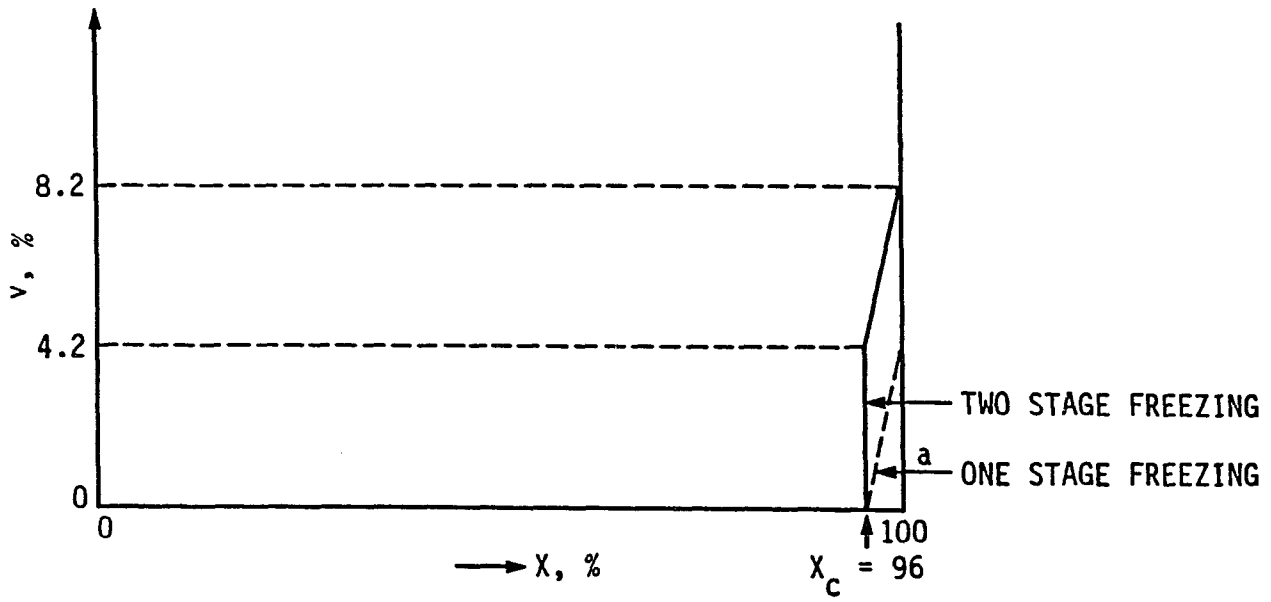

Figure 8. Expected change of volume of cement paste on freezing at -11 °C as a function of saturation and expressed on the basis of the pore volume freezable at -11 °C [15]

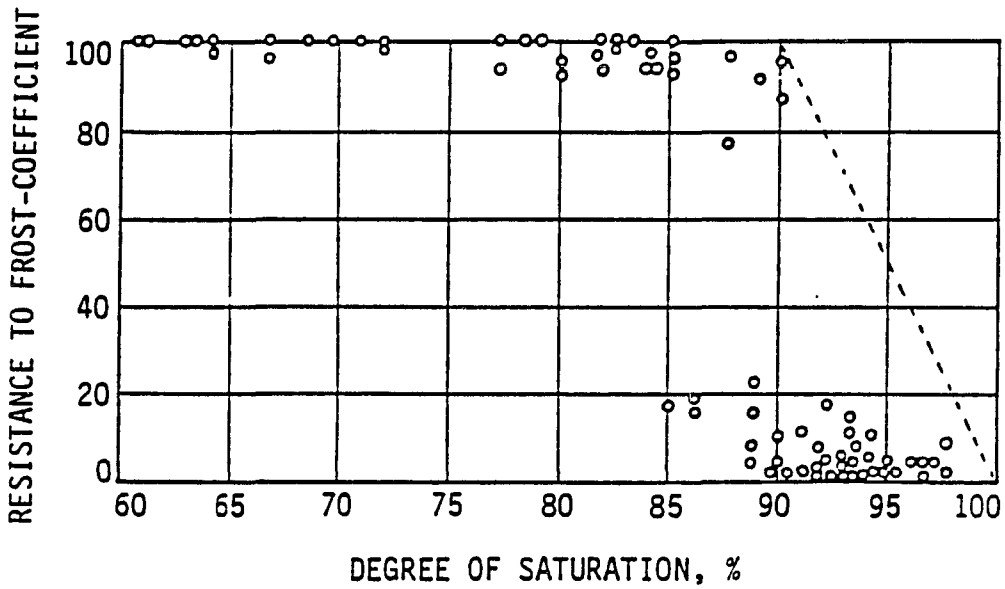

Figure 9. Influence of saturation of concrete on its resistance to frost [50]

the volume of excess water. For instance, if 90% were the critical saturation as implied by the plot in Figure 9, the experimental points at higher saturation would be expected to fall around the dashed line drawn in this figure according to Powers' model, but would not fall strikingly below it. In other words, Powers' model based on one-stage freezing can not explain the observed abruptness in frost resistance in near-saturated states, while the two-stage model described above does.

RESEARCH OBJECTIVES AND EXPERIMENTAL PROGRAMS

This dissertation research has three objectives. The first is to investigate the applicability of the proposed two-stage model. The second is to investigate the possibility of correlating the measured dilatometric volume increase upon freezing of a sample in near-saturated states to frost damage caused by freeze-thaw cycles. The third is to study the rate of water uptake of samples and to combine these data with the dilatometric data to predict the performance of concrete. The ultimate goal is that a quick, simple, economical and reliable laboratory testing method can be devised to predict the performance of concrete without resorting to the tedious and presumably less reliable standard freeze-thaw testing.

To accomplish the first objective, the work plan included dilatometric measurements with plain and air-entrained mortar and concrete samples with varying levels of saturation. For mortar samples, the water/cement ratios chosen were 0.43, 0.50, and 0.60, keeping all other compositional variables constant. For concrete samples, three different types of coarse aggregate were chosen, while keeping the other variables constant. The composition of the mortar fraction of these samples was chosen to be the same as the mortar samples with 0.43 water/cement ratio. The work plan also included plotting the dilatometric volume change versus levels of saturation for each sample and determining the critical saturation, which is defined as the saturation level above which a measurable dilatometric expansion is observed. If the plots are similar to that proposed, i.e., if the plots signify a sharp critical saturation point, then the model is verified. If the plots indicate a threshold

saturation rather than a sharp critical saturation, as was shown in Figure 8 by the dotted line, it means that freezing of pore water does not proceed beyond the first stage irrespective of level of saturation.

To accomplish the second objective, the research consisted of a systematic study of the frost damage on the samples at various saturation levels subjected to a number of freeze-thaw cycles, by a suitable method such as following the shift in their pore structure caused by such a cycling, and correlating these data with the dilatometric measurements mentioned above.

The third objective called for studying the rate of saturation of all samples in an immersed state, then combining these data with the dilatometric expansion data in a rational way, so that a frost susceptibility index can be assigned to each sample, and examining the variability of this index.

The research was divided into three phases:

1. Rate of water uptake experiments - samples were submerged in water and the amount of water absorbed were determined gravimetrically.

2. Dilatometric expansion experiments - samples were subjected to dilatometric measurements at various levels of saturation as they were frozen at -20 °C.

3. Pore structure and pore size distribution - Studies were based on earlier findings that the concrete showed a consistent and progressive shift in pore structure upon freezing and thawing in near-saturated states. It was considered that this shift might be used to measure frost damage. Therefore, samples were subjected to phase transition porosimetry to establish their pore structure and pore size distribution before and after being subjected to a

number of freeze-thaw cycles at selected subcritical and supercritical saturation levels.

The aggregates used in lab concrete samples were tested similarly as lab concrete and mortar samples to understand how predictable are the properties of concrete from the properties of mortar and aggregate.

MATERIALS AND EXPERIMENTAL PROCEDURES

Materials Preparation and Mix Design

Mortar

Six different batches of portland cement mortar mix were prepared and ten identical samples of each mix were molded in 1" diameter plastic vials, with the same cement/aggregate ratio in each batch. The first three mixes were plain (P) mortars at different water/cement ratios and the second three mixes were their air entrained (A) counterparts. The volumetric mix proportions for the plain and air-entrained samples are given in Appendix A. The portland cement used was Lehigh Type I. The fine aggregate was a sand obtained from Cordova quarry in eastern Iowa. Protex air entraining agent was used. Consolidation was done by rodding while the mortar was slowly poured into the plastic vials, and by tapping the side of the vial gently to eliminate any large entrapped air bubbles. Air content was determined using a volumetric method. Target air content was set at approximately 4%. Samples were cured in water at room temperature for 28 days before unmolding. After curing, samples were cut to a 1" height and air-dried until testing.

Laboratory concrete

Three types of coarse aggregate were used in this study to represent a range of aggregate physical and chemical characteristics. They were from the Garrison, Alden, and Lamont quarries. The Alden aggregate is a Mississippian Age, clean, coarse grained limestone with an open, well developed pore system. Iowa Department of Transportation (IDOT) durability factors for this aggregate are in the 90-98% range and it is expected to perform satisfactory for at least 20 years in concrete. The Lamont aggregate is

a Silurian Age, clean, coarse-grained dolomite with an open, well developed pore system. Durability factors for this aggregate are above 94% and it is also expected to perform satisfactory for at least 20 years in concrete. The Garrison aggregate is a highly porous dolomite containing disseminated pyrite. Durability factors for this aggregate are in the 80-90% range. It is classified by IDOT as Type II aggregate and is expected to perform satisfactory for 10-20 years. All aggregate sampling was from IDOT approved stockpiles of concrete aggregate from the respective sources. Fine aggregate used was a sand from Cordova. Type I cement (IDOT Blend R-11-Z) was used. For air-entrained concrete, Protex AES air entraining agent was used.

Coarse aggregates obtained were of 3/4 in. to 1 in. nominal size. To reduce them to different sizes, the aggregates were processed through a jaw crusher and separated by a Gilson mechanical screening unit on 3/8 in., #4, #8 and #10 sieve sizes. The individual size fractions of coarse aggregate were soaked in clean water for 24 hours and then stored in humidity room. Prior to use, excess water was drained. The different sizes of coarse aggregate were then brought to a saturated surface dry condition. Individual sizes of coarse aggregate were then proportioned to meet ASTM #8 grading of coarse aggregate for concrete, and prepared for batching. Fine aggregate was maintained in an air-dry condition. The amount of absorption of fine aggregate was taken into account when determining the amount of mixing water.

IDOT C-3 mix proportions were used for the concrete mix design, with the plastic air content targeted to be in the range of 6-9%. Air content was determined volumetrically using a Roll-A-Meter. In order to simulate field

mixing conditions, concrete mixing was done in a 1.5 cubic foot mixer. Mixes were "over-mortared" to account for drum adherence. All batches were mixed and cured according to ASTM C-192 "Making and Curing of Concrete Test Specimens in the Laboratory", with the exception that samples were first rodded and then consolidated on vibration table to achieve proper consolidation. The plastic concrete properties, volumetric mix proportions, and strength test (3"x3"x3 1/2" prisms) data are given in Appendix B. The strength test results are based on the average of three samples. After 90 days curing, one inch diameter cores were obtained from 3"x3"x16" prisms using a drill press mounted core barrel. They were then trimmed to approximately one inch height and ready for testing.

Aggregate

Quarry stone rock samples were obtained from the respective quarries. One inch diameter cores were obtained by using a drill press and core barrel. Cores were then trimmed to one inch height.

Apparatus and Experimental Procedures

Rate of water uptake experiments

Considering that the attainment of absolutely 100% saturation is extremely difficult and time consuming for practical purposes, the following conditions were set as a reference saturated state for each sample: samples were vacuum saturated by pumping out air for 15 minutes under a vacuum of 27 inches of mercury, they were then flooded with water for 10 minutes, stored in a water bath at room temperature for 3 days, and surface dried and weighed to determine their saturated weight. The samples were then dried in a

microwave oven for five minutes and reweighed to determine their dry weight. This method proved to be a convenient method of drying to a constant weight without losing any water of hydration.

Actual water uptake experiments were conducted by submerging the dry samples in a deionized water bath at room temperature and determining their weights, after surface drying with a paper towel at various time intervals. The percent water absorption was then expressed relative to the reference saturated state.

Dilatometric expansion experiments

Each sample was first vacuum-saturated with water as described above, and surface dried. The sample was then placed in the dilatometer cup. The dilatometer was assembled and filled with mercury through the inlet until the mercury reached the end of the stem. The dilatometer was then placed in a cryostat and maintained at +8 °C. When thermal equilibrium was established, the mercury level was reset and the test was initiated by turning control over to a computer. A schematic diagram of the mercury dilatometer is given in Figure 10.

The expansion measurement was fully computerized. The system consists of a mercury dilatometer made of stainless steel, a cryostat, an Apple IIe computer, two interfaces for temperature and volume measurements, and a plotter. The software; (a) controls the cryostat temperature, cooling the dilatometer containing the sample from +8 °C to -20 °C at a rate of 5 °C per hour, (b) collects volume and temperature data during cooling, and (c) extrapolates the initial volume data in the range of +8 °C to 0 °C, then to

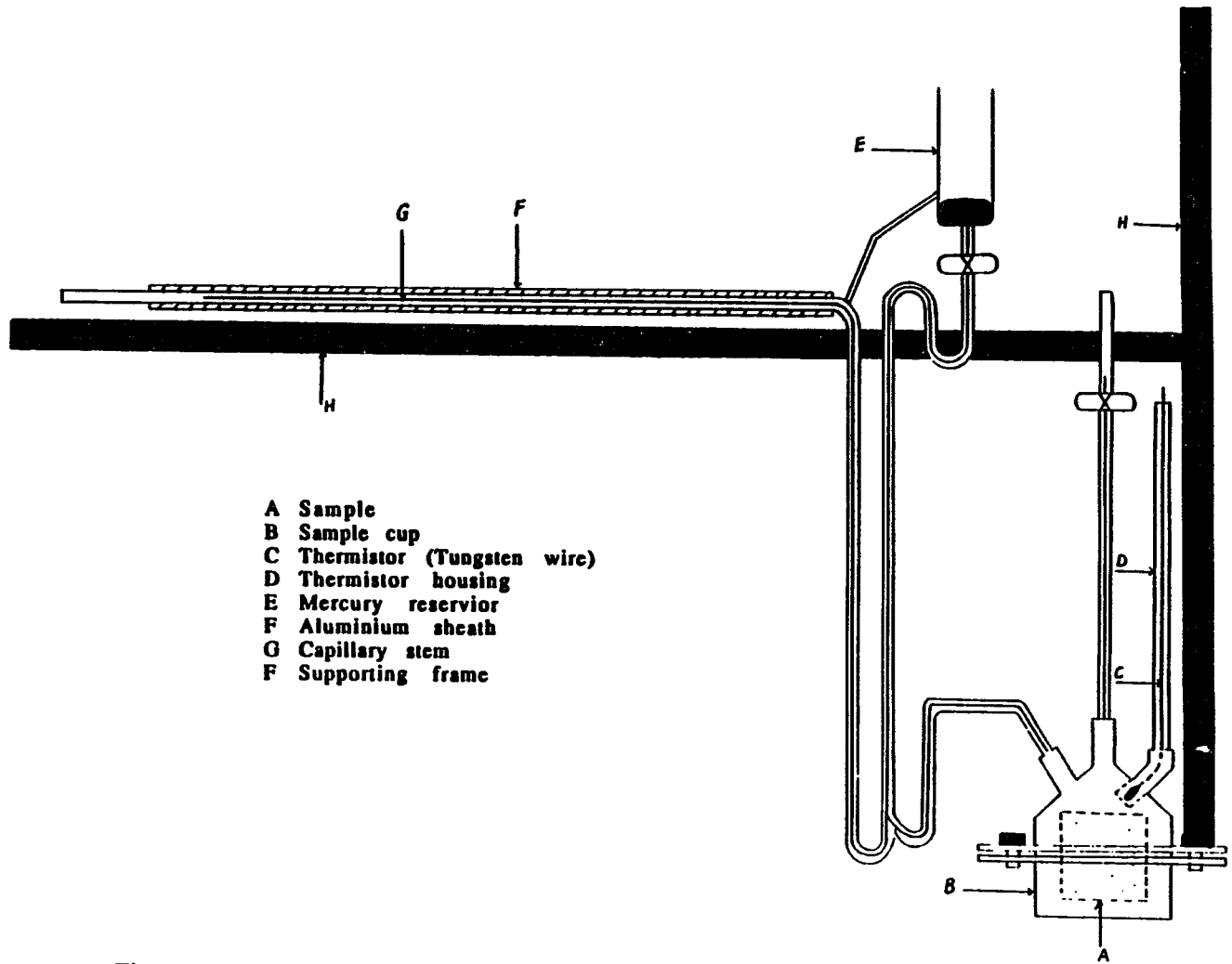

Figure 10. Mercury dilatometer

-20 °C, computes the difference between the collected volume data at -20 °C, and extrapolated value at the end of run. The temperature measuring interface utilizes the resistance of a thermistor inside the dilatometer, while the volume measuring interface uses the capacitance of the condenser consisting of a mercury thread in the dilatometer stem with an aluminum shield around it. Detailed discussions of the system and procedures are given by Eckrich et al. [14]. After each run, the percent of expansion was calculated and the sample was let to partially dry to a desired lower saturation for the next run. By reducing the level of saturation progressively, the change in volume of the sample was measured. The volume change upon freezing was plotted against saturation to determine critical saturation and to investigate the applicability of the proposed model.

Pore structure and pore size distribution

Before dilatometric expansion experiments, fully saturated samples were subjected to phase transition porosimetry to determine their pore structure and pore size distribution. The procedures for pore size distribution analysis are essentially similar to those described in the dilatometric expansion experiment. Because dissolved salts in cement mortar pore water also will act to depress the freezing point, blank samples of extracted pore water were tested and the effect found to be small, with a freezing point depression from this cause less than 1 °C. Analyses were done at zero cycle and also after samples had been subjected to 60 freeze-thaw cycles for mortar samples and 100 freeze-thaw cycles for concrete and aggregate samples at a selected subcritical and supercritical saturations. The subcritical and supercritical saturations used for mortar samples were 87% and 95%, respectively. For

concrete samples, the subcritical saturation was set at 70%, and the supercritical saturation was set at 90%. For aggregate samples, the subcritical saturation was set at 30%, and the supercritical saturation was set at 70%.

Freeze-thaw experiments

Samples were first vacuum saturated and then evaporated to arrive at the desired saturation by following their weight loss. Once they had reached the desired saturation, they were immersed in toluene in indivudual weighing bottle to prevent moisture variations. Samples were then immersed in the cryostat. Freeze-thaw cycles on the samples were then initiated with a cooling and warming rate of 15 °C per hour, between +8° and -20 °C.

RESULTS AND DISCUSSIONS

Followings are the results arranged and discussed according to the experiments conducted. The discussion on the applicability of the proposed model is given in the "Dilatometric Expansion" section.

Rate of Water Uptake

Figure 11 shows the progress of absorption for each mix of plain and air-entrained mortar samples at various water/cement ratios. The percent of absorption was determined based on the total pore volume, as explained in the experimental procedures. These data indicate that the plain samples acquire water at a higher rate than their air-entrained counterparts. For example, consider the mortar sample with a water/cement ratio of 0.60. It takes about 2 days for the plain sample to reach 90% saturation whereas it takes about 20 days for the air-entrained sample. These data indicate that incorporating entrained air bubbles much larger than the gel and capillary pores originally existing in the matrix may act to retard the saturation rate because it is more difficult to saturate larger air voids than smaller air voids by capillarity.

Figures 12 and 13 show the effect of water/cement ratio upon the rate of water absorption. It appears that the retarding effect of air-entrainment decreases as water/cement ratio increases. The reason may be that, at high water/cement ratios, segregation and bleeding takes place which increases the the size of capillary channels, thus increasing the permeability and the ease of water uptake. Although the capillary suction also decreases as capillary size increases, the former effect apparently predominates. For plain samples, no significant difference is observed as indicated on Figure 12.

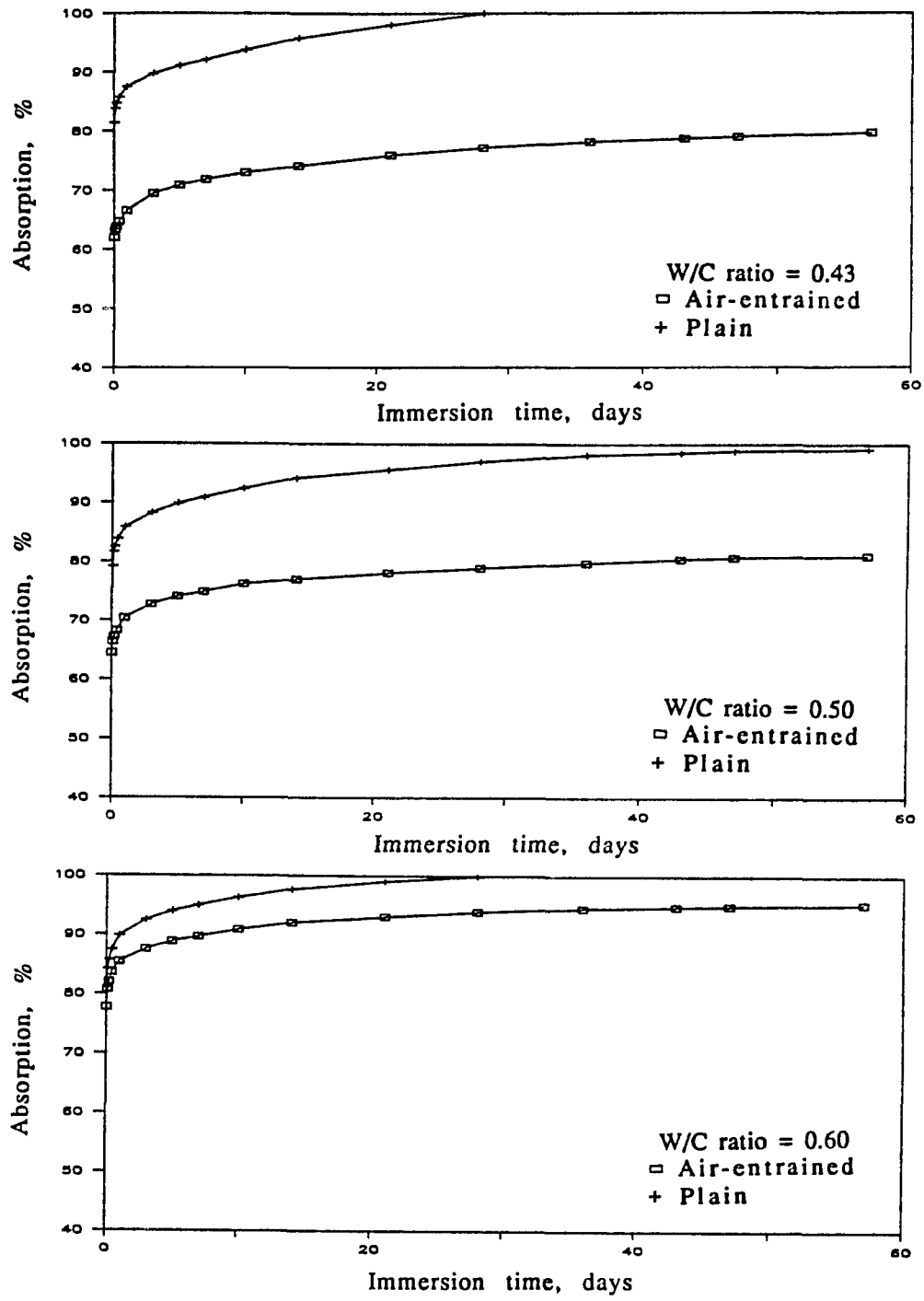

Figure 11. Plain and air-entrained mortar samples at 0.43, 0.50, and 0.60 water/cement ratios

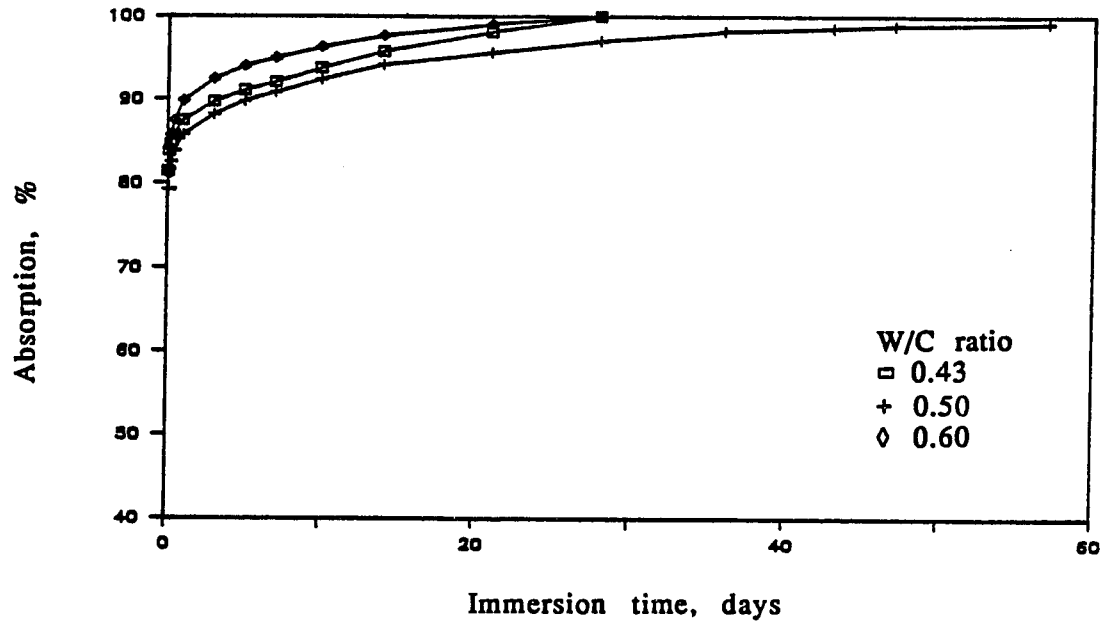

Figure 12. Plain mortar samples at 0.43, 0.50, and 0.60 water/cement ratios

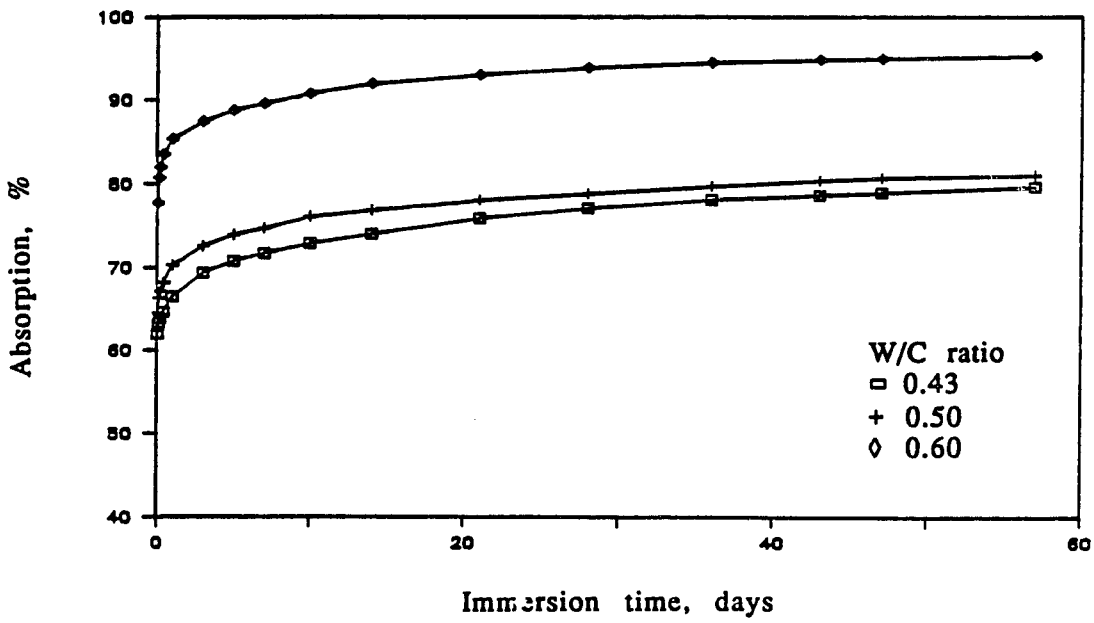

Figure 13. Air-entrained mortar samples at 0.43, 0.50, and 0.60 water/cement ratios

At this point it is appropriate to clarify the meaning of the rate of saturation that appears to be reduced by the presence of entrained air in concrete. Entrained air may or may not reduce the absolute rate of water absorption. What it reduces is the rate of saturation, relative to the total pore volume, simply by increasing the total pore volume. It must be noted that it is the relative saturation level that is crucial in problems related to frost susceptibility both in Powers' treatment and the proposed model.

Figure 14 shows the rate of absorption for plain and air-entrained concrete samples. The same trend that has been observed in mortar samples is observed here except that in general the rate is lower for plain samples. This may imply that coarse aggregate has an influence on the rate of absorption of plain samples. Since the rate of absorption of aggregate is considerably lower than the rate of plain mortar samples, it apparently helps to reduce the absorption rate. For air-entrained concrete, no significant change in the rate is observed, since the rate of absorption of aggregate is very close to the air-entrained mortar samples.

Figures 15 and 16 show the effect of different types of coarse aggregate on the rate of water uptake. It appears that the effect of different types of coarse aggregate on the rate of water uptake is minimal for both plain and air-entrained concrete.

Figure 17 shows the rate of absorption for the three different types of coarse aggregate that were incorporated in concrete as determined from blocks of quarry stone. The stone received from Lamont quarry appeared highly weathered and is not considered representative of the coarse aggregate used in the concrete. It is more porous and perhaps contains larger voids.

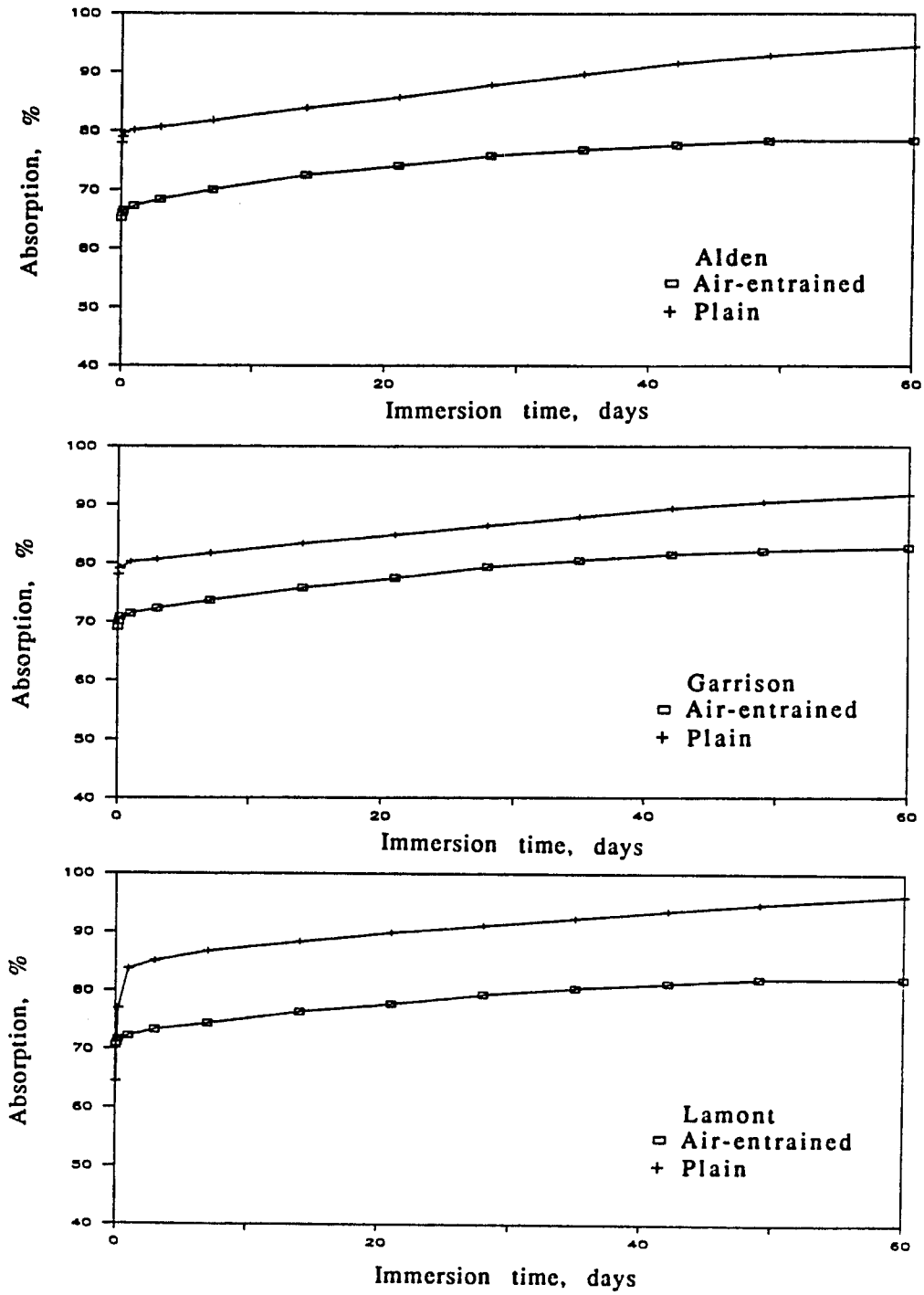

Figure 14. Plain and air-entrained concrete samples with Alden, Garrison, and Lamont aggregates at 0.43 water/cement ratio

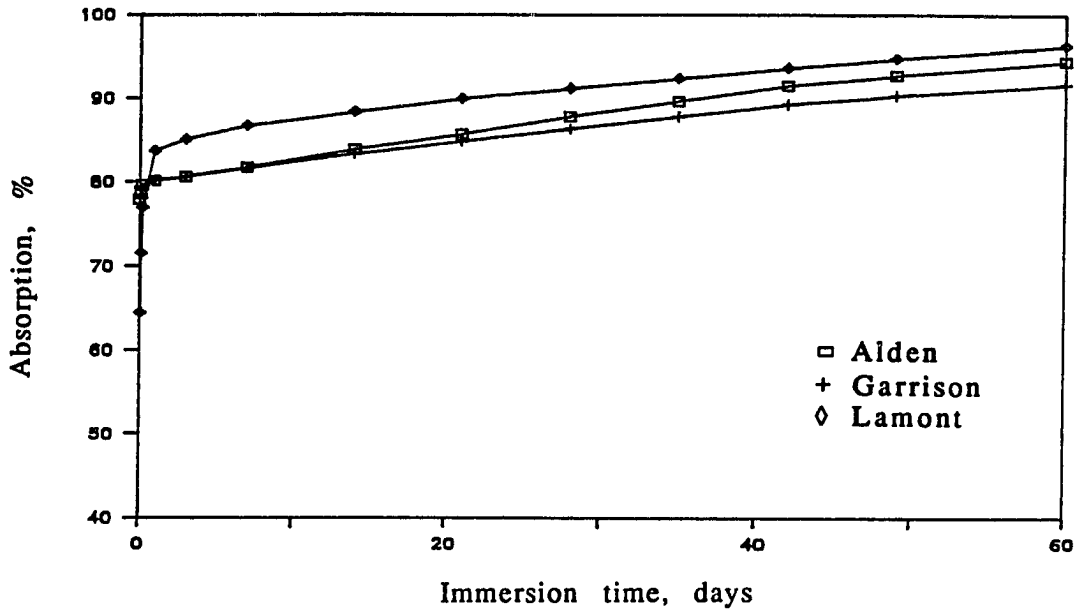

Figure 15. Plain concrete samples with Alden, Garrison, and Lamont aggregates at 0.43 water/cement ratio

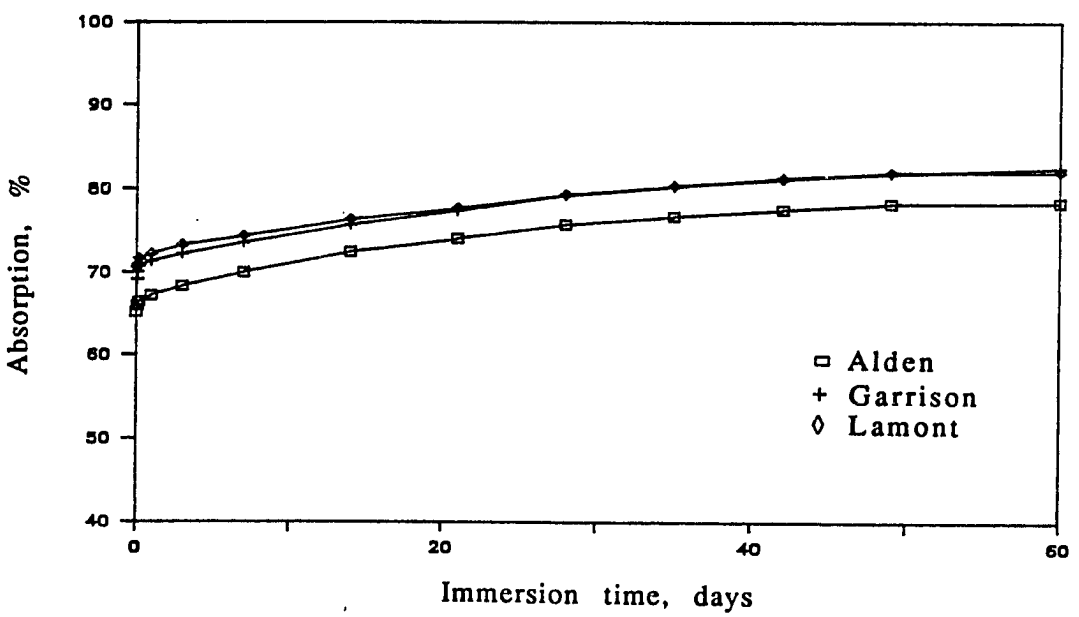

Figure 16. Air-entrained concrete samples with Alden, Garrison, and Lamont aggregates at 0.43 water/cement ratio

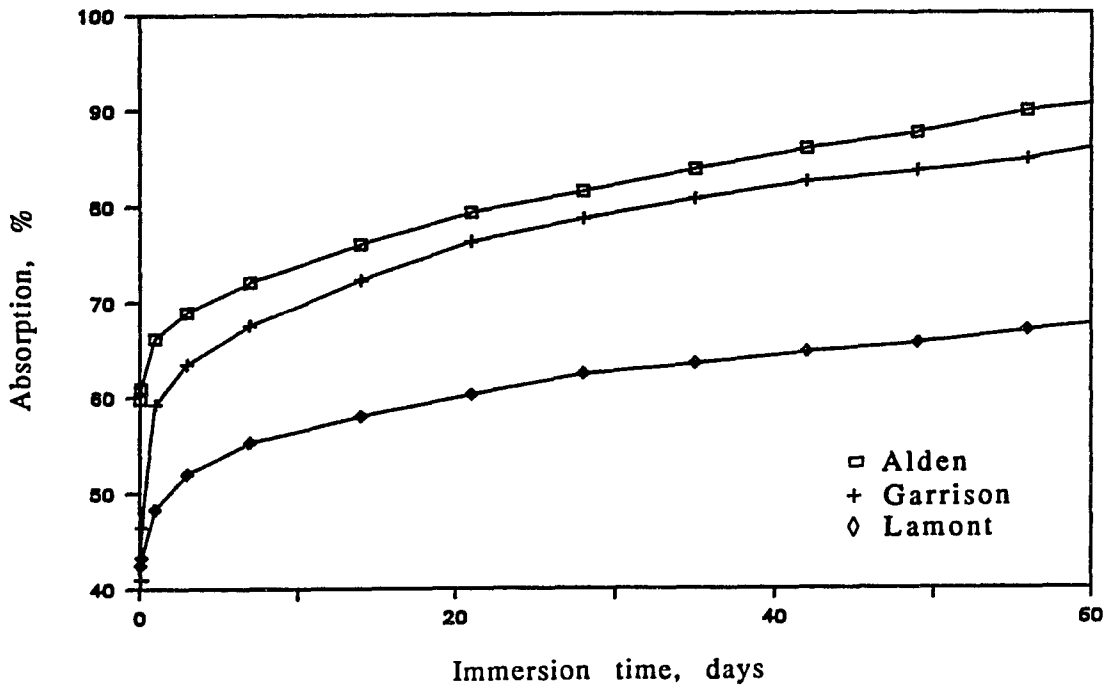

Figure 17. Alden, Garrison, and Lamont aggregates

As can be seen, Lamont aggregate has the lowest rate of absorption. Examination of the pore structure (Appendix E) of Lamont aggregate indicates that it contains a larger total pore volume and larger air voids than the Alden and Garrison aggregate. Alden and Garrison aggregate have a very similar pore structure, and they also seem to have the same rate of absorption.

Visual comparison of the rate of absorption of mortar, aggregate, and concrete samples seems to indicate that they have a proportional effect. That is, the rate of absorption of concrete is proportional to the rate of absorption of aggregate and mortar, independently. A relationship was derived to relate the rate of absorption of concrete as a function of the rate of absorption of mortar and aggregate. It was derived assuming that the rate of absorption of concrete is a linear combination of the rate of absorption of its mortar and aggregate components. Derivation of the relationship is given in Appendix C. It seems that the concept of proportional effect is not applicable in the case of absorption of concrete. As shown in Appendix C, the theoretical predicted values do not agree with the actual values. They are either lower or higher than predicted.

Dilatometric Expansion

The plots of dilatometric expansion versus level of saturation for mortar and concrete samples are given on Figures 18-23. The theoretical predicted relation for two of the samples (P43 & A60) are shown by the dashed lines on Figure 18. Typical dilatometric plots of volume change versus temperature to determine dilatometric expansion, on freezing at -20 °C, for one of the samples

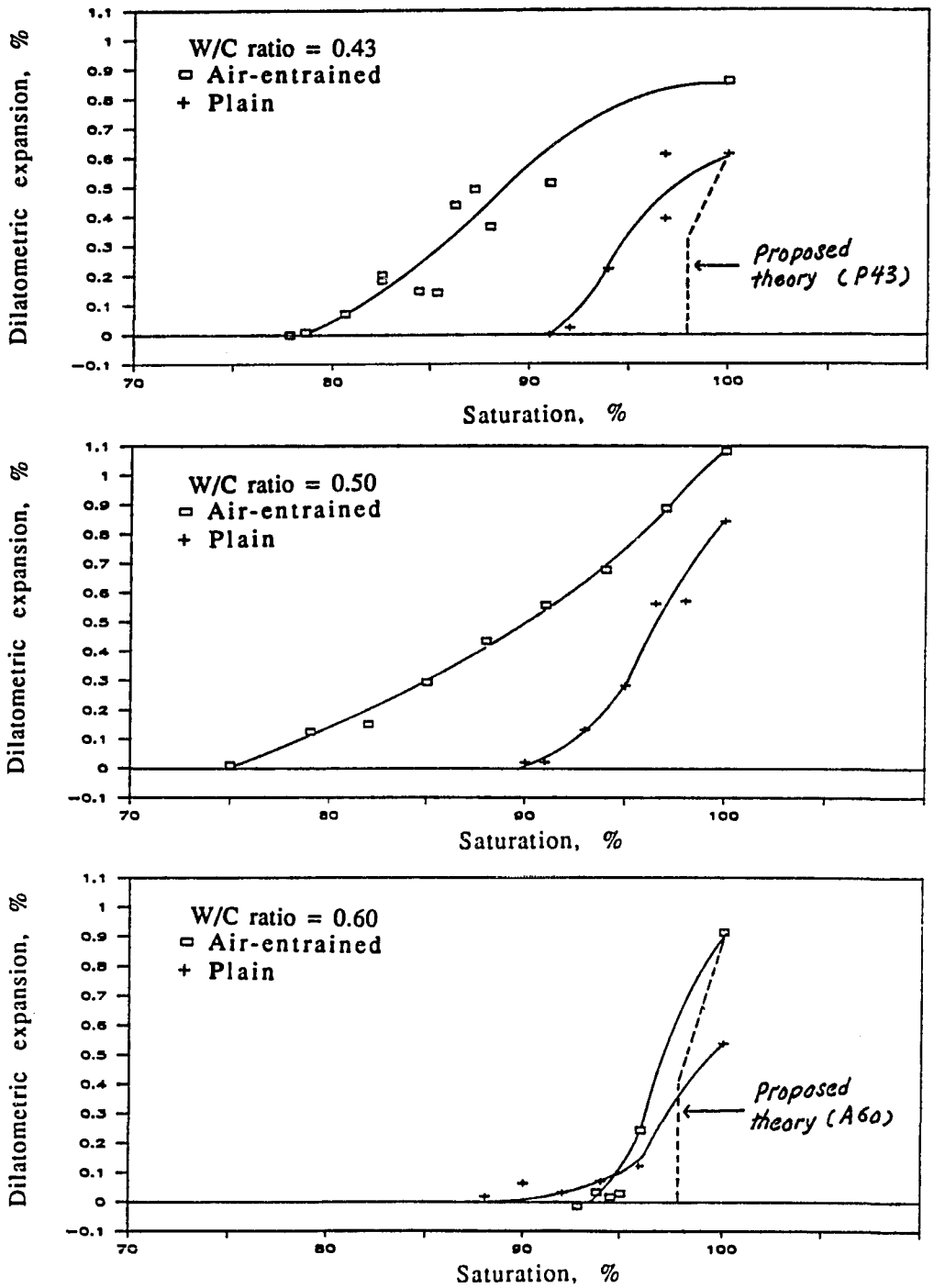

Figure 18. Plain and air-entrained mortar samples at 0.43, 0.50, and 0.60 water/cement ratios

are given in appendix D. It appears that the observed critical saturation levels are lower than predicted, and the expansions are higher on the whole. The trends of variations of expansion with saturation level for some of the samples resemble the theoretical trend but some do not. The deviations from the theory may be due to the air in the pores being more persistent than was assumed. That is, reduction in the volume of pore air through dissolution in pore water may not keep up with the rate of freezing. As a result, the excess volume of water formed upon freezing would be partly forced out to the exterior of the sample at high levels of saturation. This appears to be occurring in spite of the existence of "escape boundaries" within the sample. Also, considering that the theory was based on the observations from cement paste, the deviations could be due to the fine aggregate in mortar, and fine and coarse aggregates in the concrete samples.

The critical saturation of mortar ranges from 75% to 93% as indicated on Figure 18. Air-entrained samples generally have a lower critical saturation level and exhibit higher expansion than plain samples. The effect of water/cement ratio on the rate of absorption is shown on Figures 19 and 20. It appears that the mix with 0.50 water/cement ratio exhibits the highest expansion and lowest critical saturation level. This may indicate that there is an optimum water/cement ratio, below which the expansion is lower, and above which the critical saturation is higher.

Figures 21-23 show the plots of dilatometric expansion of concrete samples versus level of saturation. The trends of variations of expansion with saturation level for these concrete samples appear more closely resemble the proposed theoretical trend than the mortar samples. Generally, critical

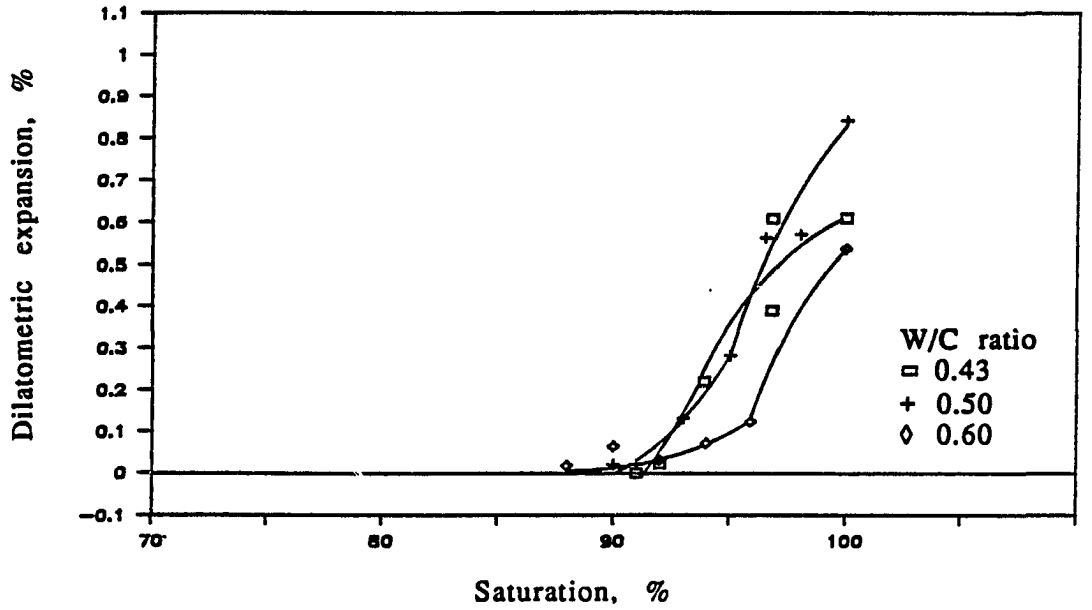

Figure 19. Plain mortar samples at 0.43, 0.50, and 0.60 water/cement ratios

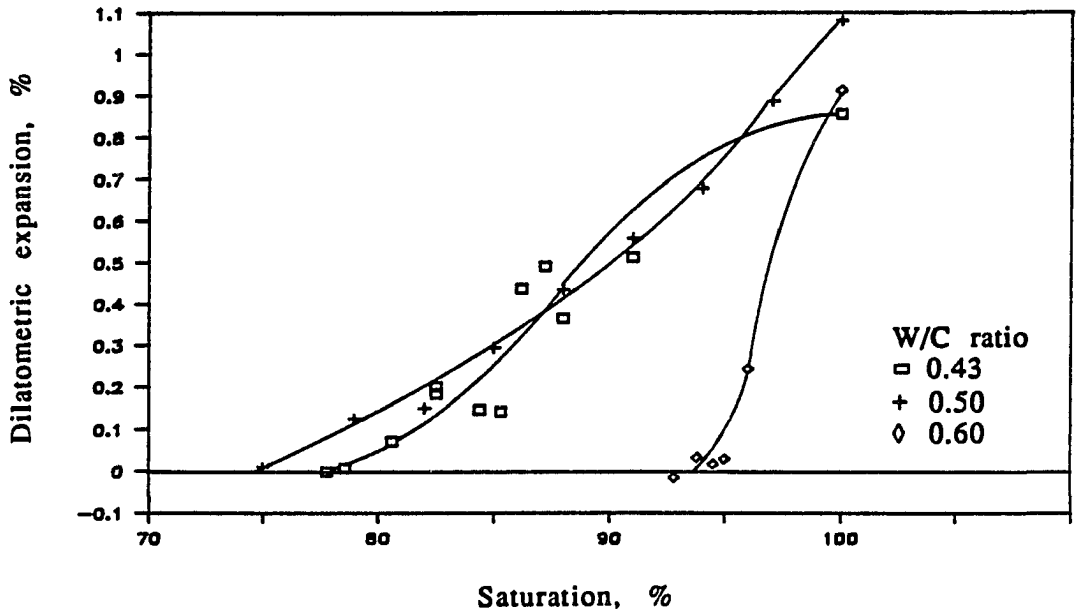

Figure 20. Air-entrained mortar samples at 0.43, 0.50, and 0.60 water/cement ratios

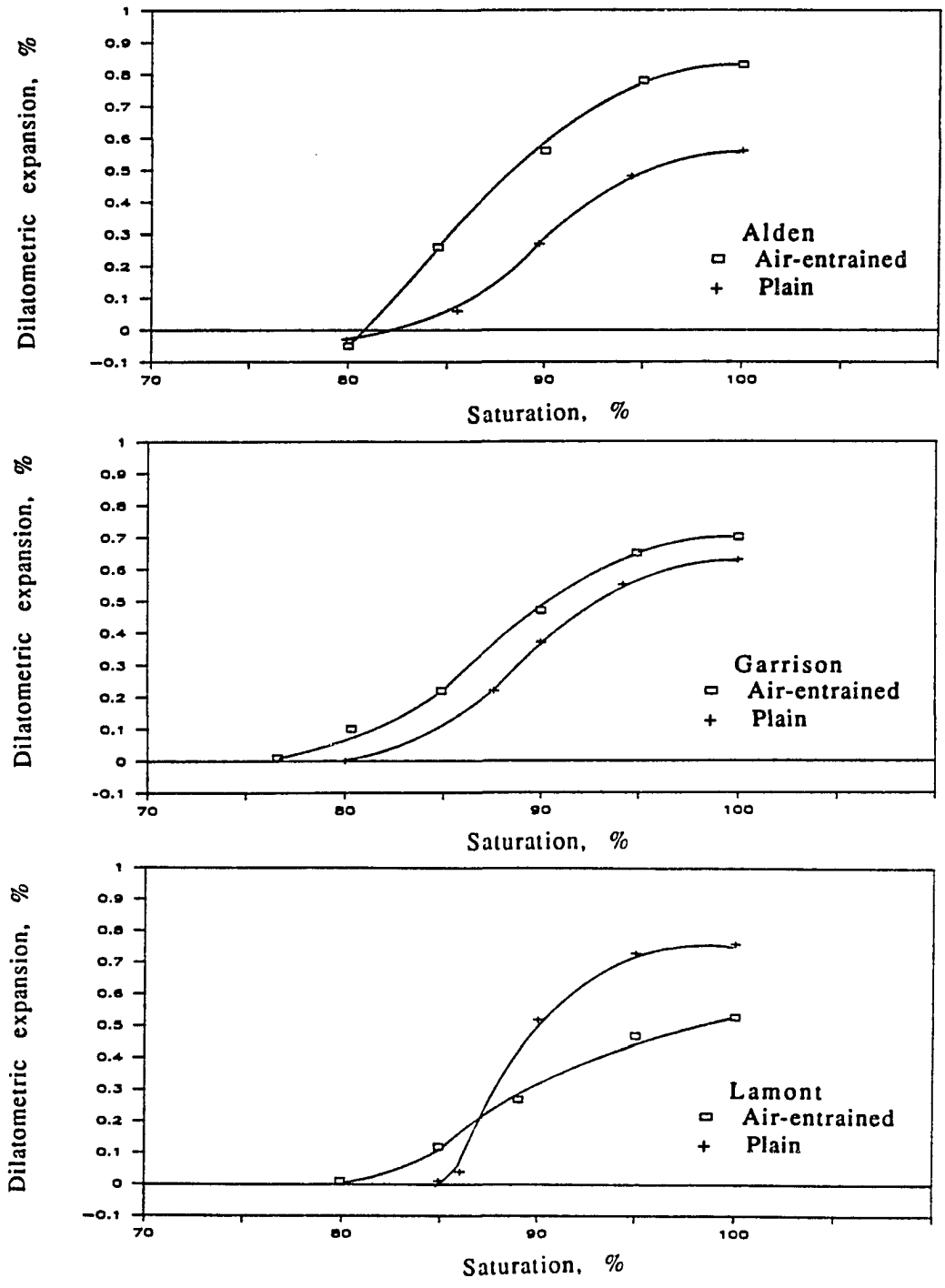

Figure 21. Plain and air-entrained concrete samples with Alden, Garrison, and Lamont aggregates at 0.43 water/cement ratio

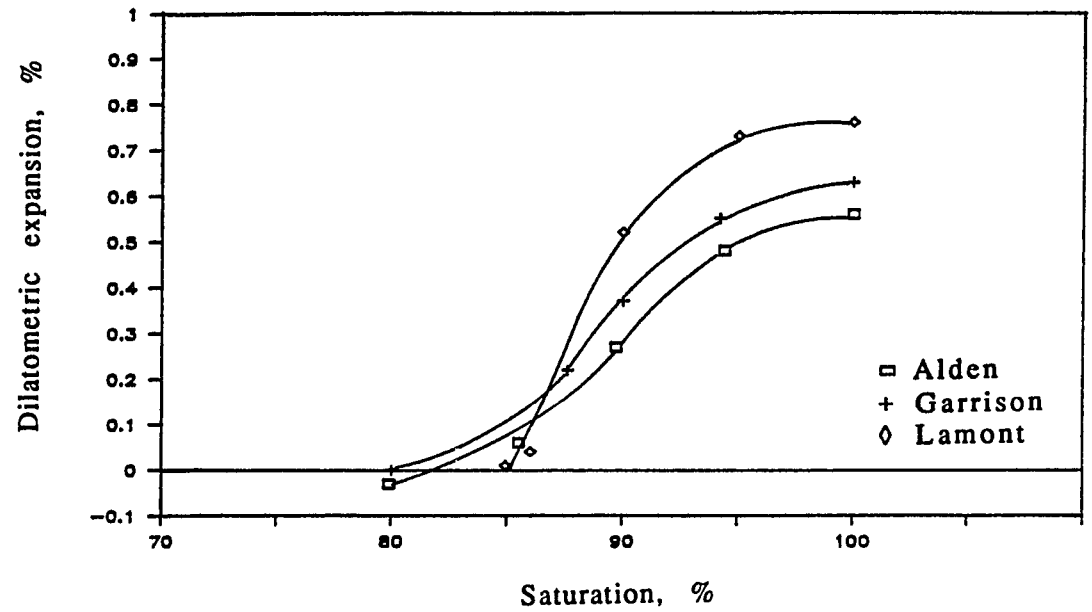

Figure 22. Plain concrete samples with Alden, Garrison, and Lamont aggregates at 0.43 water/cement ratio

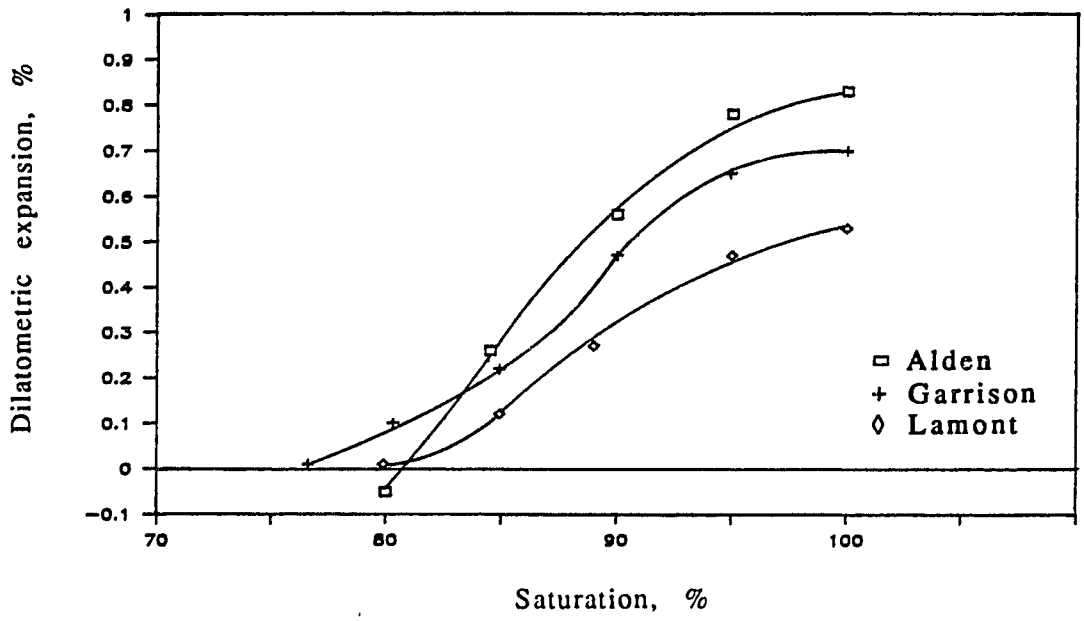

Figure 23. Air-entrained concrete samples with Alden, Garrison, and Lamont aggregates at 0.43 water/cement ratio

saturation is lower and expansion is higher in air-entrained versus plain samples except in the Lamont mix, where the expansion is lower for the air-entrained sample. The effect of different types of coarse aggregate on expansion and critical saturation is also obvious.

At this point it is appropriate to discuss the effect of sample size. Obviously, the smaller laboratory samples used in the above experiments are not quite representative of the actual field concrete. These samples represent more "severe" conditions since their total surface area, relative to the total volume of the sample, exposed to water and freezing temperature is larger.

The aggregates have a very low level of critical saturation as is shown on Figure 24. The Garrison aggregate exhibits the highest expansion and critical saturation level. The trends of variations of dilatometric expansion with level of saturation for these aggregates are different from the proposed model. This may indicate that the freezing mechanism of pore water in aggregate is different from that of concrete and mortar. This is probably due to the difference in their pore structure.

Pore Structure and Pore Size Distribution

Pore size distribution studies of mortar samples before and after they had been subjected to 60 freeze-thaw cycles show that there is a shift in pore structure (Figures 25-27).

Figure 25 shows the pore size distributions of the control sample obtained from phase transition porosimetry. Figure 26 shows the results of a duplicate sample subjected to freeze-thaw cycling at 87% (subcritical) saturation. Figure 27 shows the results of the control sample after freeze-thaw

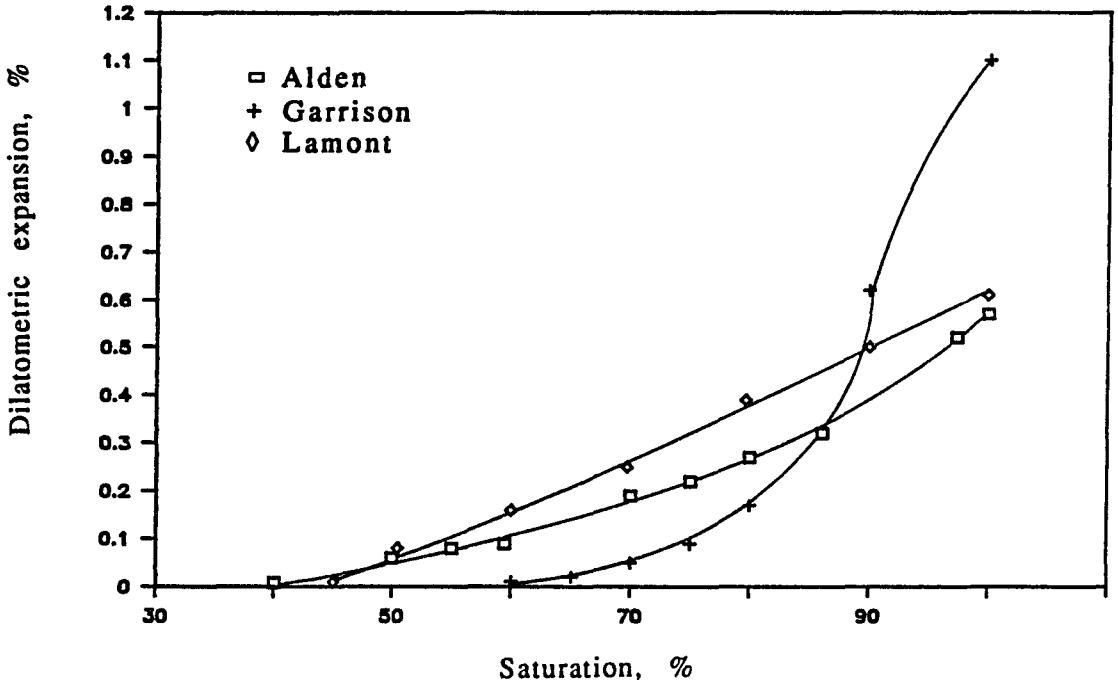

Figure 24. Alden, Garrison, and Lamont aggregates

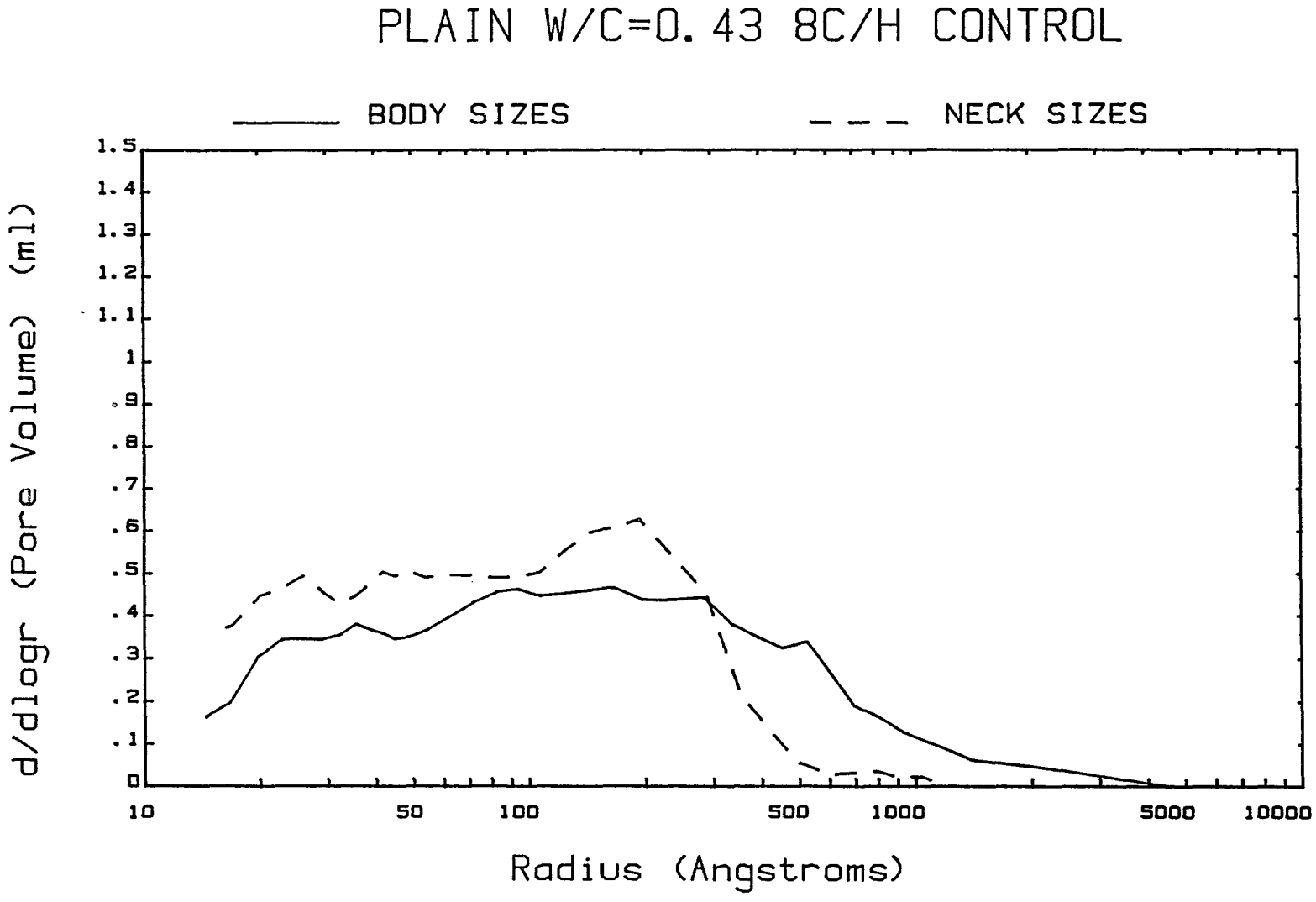

Figure 25. Pore size distribution of a control air-entrained mortar sample at 0.43 water/cement ratio

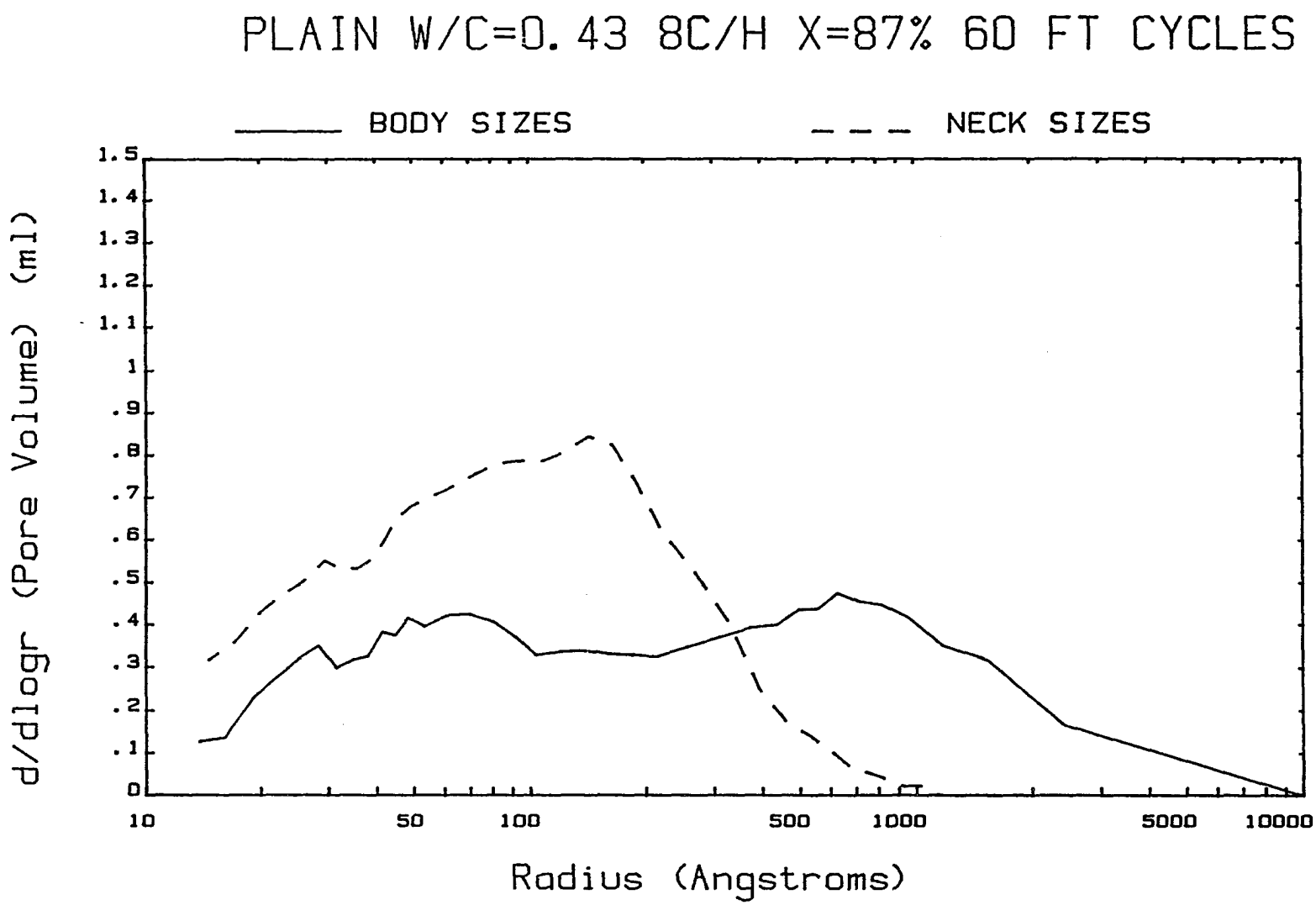

Figure 26. Pore size distribution of an air-entrained mortar control sample at 0.43 water/cement ratio after 60 freeze-thaw cycles at 87% saturation

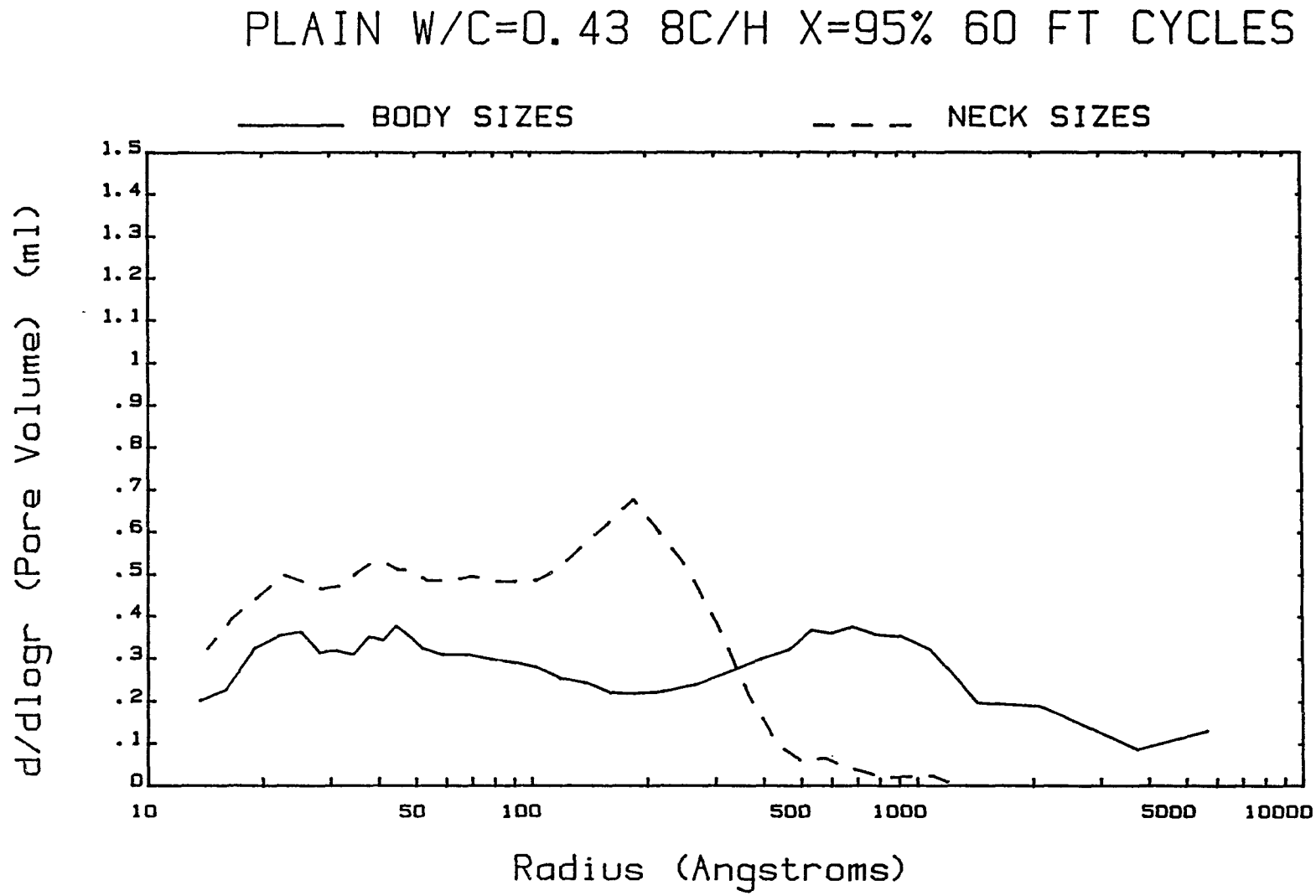

Figure 27. Pore size distribution of the air-entrained mortar sample at 0.43 water/cement ratio after 60 freeze-thaw cycles at 95% saturation

cycling at 95% (supercritical) saturation. Comparing these data, one can conclude, for mortar of this compositions that:

(a). Pore neck sizes do not appear to be an indicator of frost damage, because they do not exhibit a detectable change after freezing and thawing.

(b). On the other hand, pore bodies go through a consistent change upon cycling. The pore body peak shown on Figure 25 at about 150 A radius undergoes a significant change after freeze-thaw cycling at 95% saturation, and exhibits a bimodal distribution with a new tall peak at about 700 A, as shown on Figure 27. At 87% saturation, the change is similar.

The second observation appeared to be promising in the use of the pore body size shift as a measure of frost damage. However, after review of all pore size distribution curves, obtained with the original and cycled plain and air-entrained mortar samples of various water/cement ratios at 87% and 95% saturations (Appendix E), it was observed that this observation was inconsistent: Each different sample exhibited its own characteristic shift in different regions of the pore size range. It was concluded that it was not possible to use any specific shift to measure the extent of frost damage on all samples as a comparative measure. Nor did the shift in median pore sizes work for this purpose. Therefore, this method of assessing frost damage was abandoned in favor of another method which is based on the permanent expansion of samples upon freezing and thawing, as explained in the next section.

Permanent Expansion upon Freezing and Thawing

After samples had been subjected to freeze-thaw cycling, their permanent expansion (volumetric) was measured by mercury displacement. The permanent expansion was obtained after the samples had been subjected to 60 freeze-thaw cycles for mortar samples and 100 freeze-thaw cycles for concrete samples. Percent expansion is then expressed based on their initial volume. Results are given in Table 2. All samples exhibit permanent expansion after freeze-thaw cycling. However, samples with saturation above critical levels (supercritical) show more significant expansion.

Reasonably good correlations were obtained between the dilatometric expansion and permanent expansion for mortar and concrete samples as shown on Figure 28. It is interesting to observe that the regression line in both cases has a finite intercept. It is 3% for mortar and 1% for concrete samples. This signifies that at zero dilatometric expansion, i.e., below critical saturations, the samples suffer some frost damage apparently through the mechanism considered by Powers. However, especially in concretes, the magnitude of this residual damage is almost insignificant. This indicates that significant frost damage is primarily caused by bulk-ice-induced freezing at supercritical saturations, as put forward in the proposed model.

Prediction of Performance

From the rate of absorption and dilatometric expansion data, relationships were established between dilatometric expansion and immersion time as shown on Figures 29 and 30. These relationships were obtained by combining the dilatometric expansion versus saturation and the rate of

Table 2. Permanent expansion of mortar and concrete samples at various saturation levels after being subjected to 60 and 100 freeze-thaw cycles, respectively

Sample	W/C ratio (%)	Type	Coarse agg.	Saturation, %		Expansion, %	
				actual	critical	dilatometric	permanent
Mortar	0.43	Plain	-	87	91	0	2.73
Mortar	0.43	Plain	-	95	91	0.36	4.44
Mortar	0.43	Air	-	87	78	0.40	6.23
Mortar	0.43	Air	-	95	78	0.81	5.01
Mortar	0.50	Plain	-	87	90	0	2.64
Mortar	0.50	Plain	-	95	90	0.28	4.98
Mortar	0.50	Air	-	87	75	0.37	5.64
Mortar	0.50	Air	-	95	75	0.76	6.22
Mortar	0.60	Plain	-	87	88	0	2.87
Mortar	0.60	Plain	-	95	88	0.10	3.62
Mortar	0.60	Air	-	87	93	0	2.87
Mortar	0.60	Air	-	95	93	0.11	7.13
Concrete	0.43	Plain	Alden	70	80	0	1.71
Concrete	0.43	Plain	Alden	90	80	0.29	4.33
Concrete	0.43	Air	Alden	70	81	0	0.58
Concrete	0.43	Air	Alden	90	81	0.56	4.98
Concrete	0.43	Plain	Garrison	70	80	0	1.44
Concrete	0.43	Plain	Garrison	90	80	0.37	4.47
Concrete	0.43	Air	Garrison	70	76	0	0.46
Concrete	0.43	Air	Garrison	90	76	0.47	4.92
Concrete	0.43	Plain	Lamont	70	85	0	0.55
Concrete	0.43	Plain	Lamont	90	85	0.52	3.85
Concrete	0.43	Air	Lamont	70	80	0	0.31
Concrete	0.43	Air	Lamont	90	80	0.33	4.39

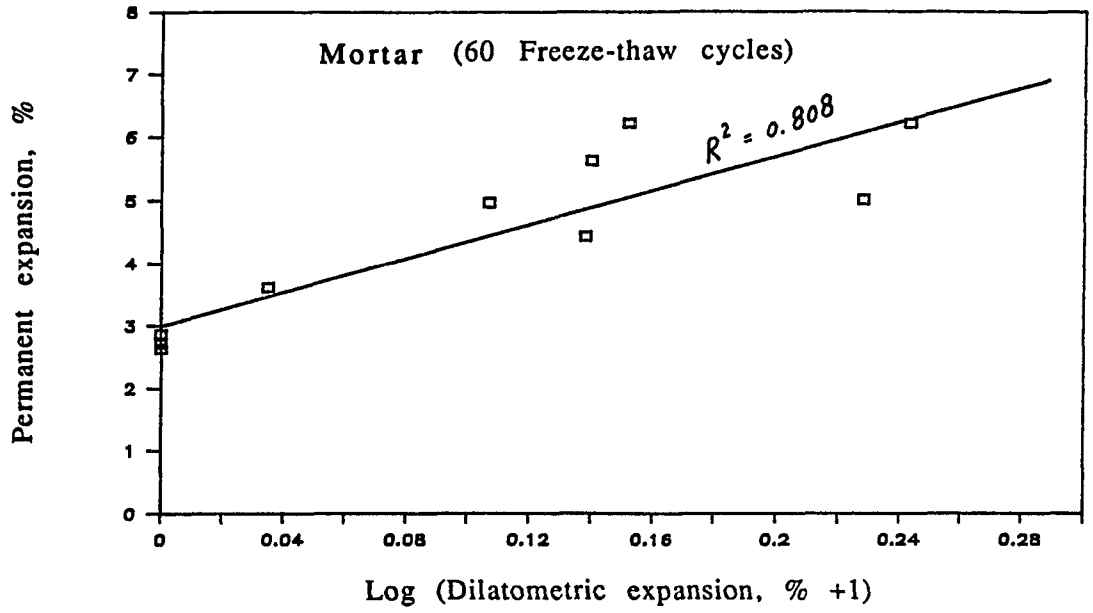

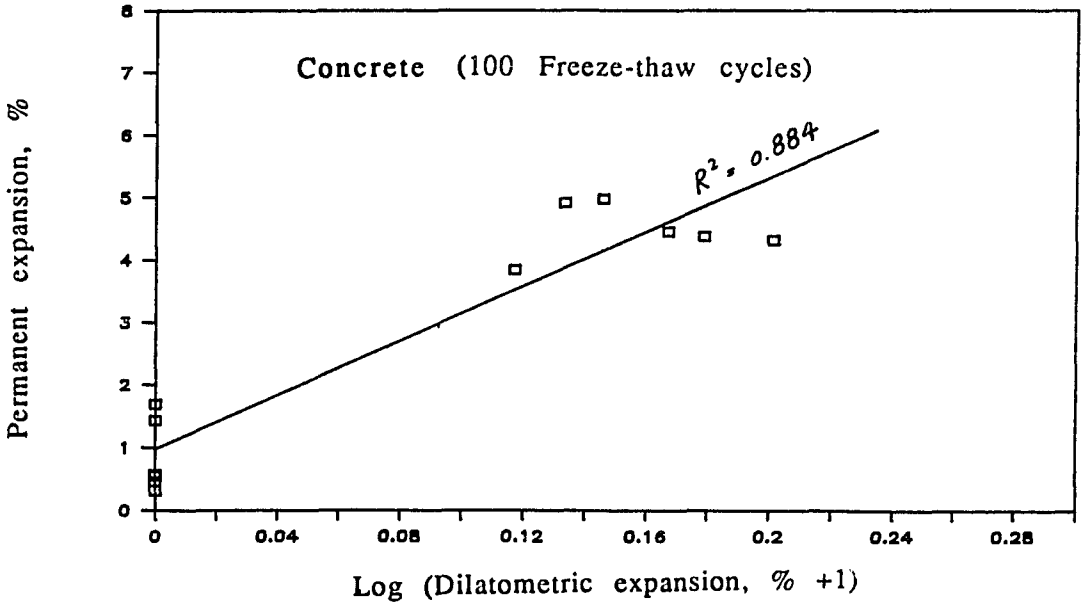

Figure 28. Correlation between dilatometric and permanent expansions of mortar and concrete samples

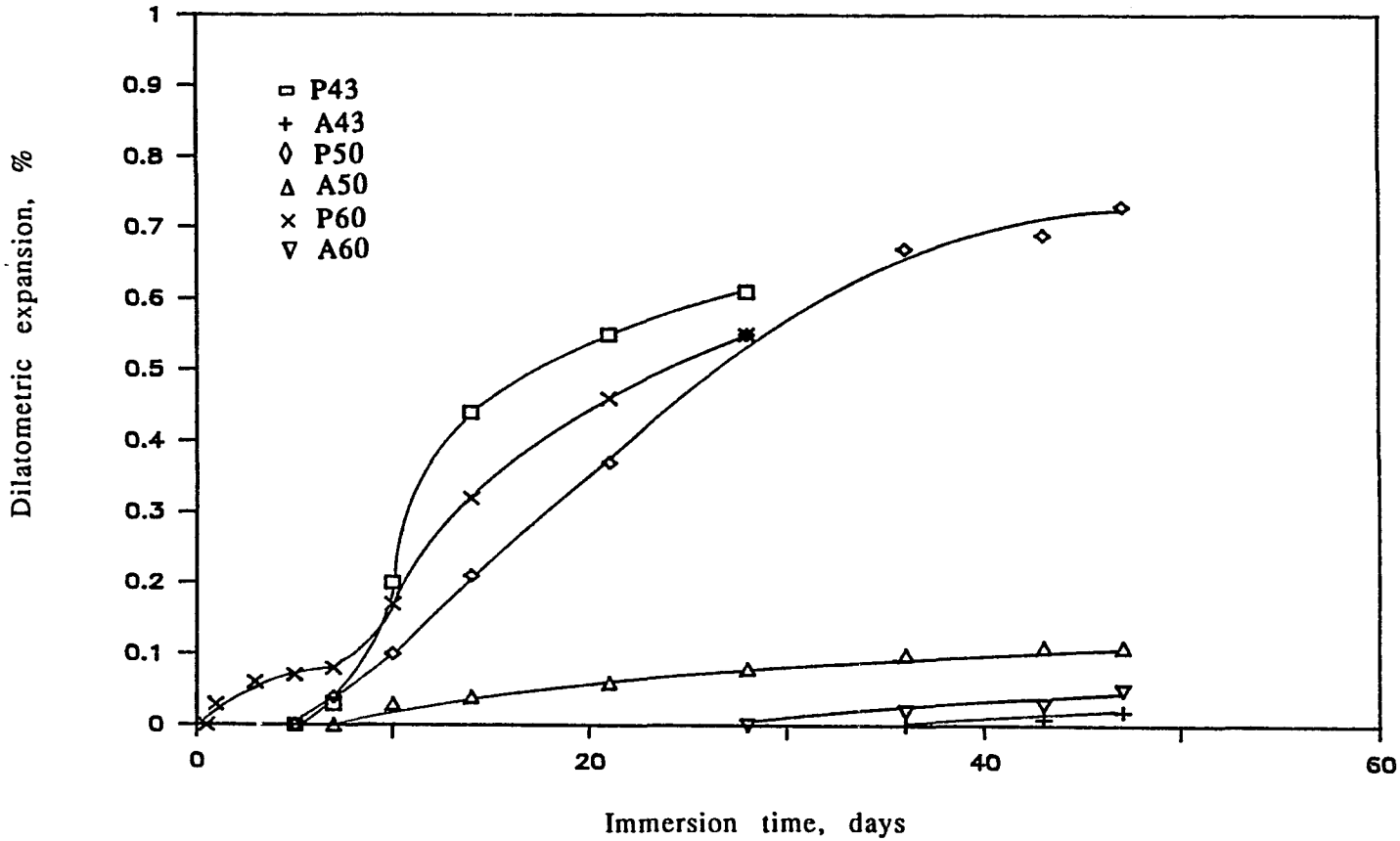

Figure 29. Relationship between dilatometric expansion and immersion time of mortar samples

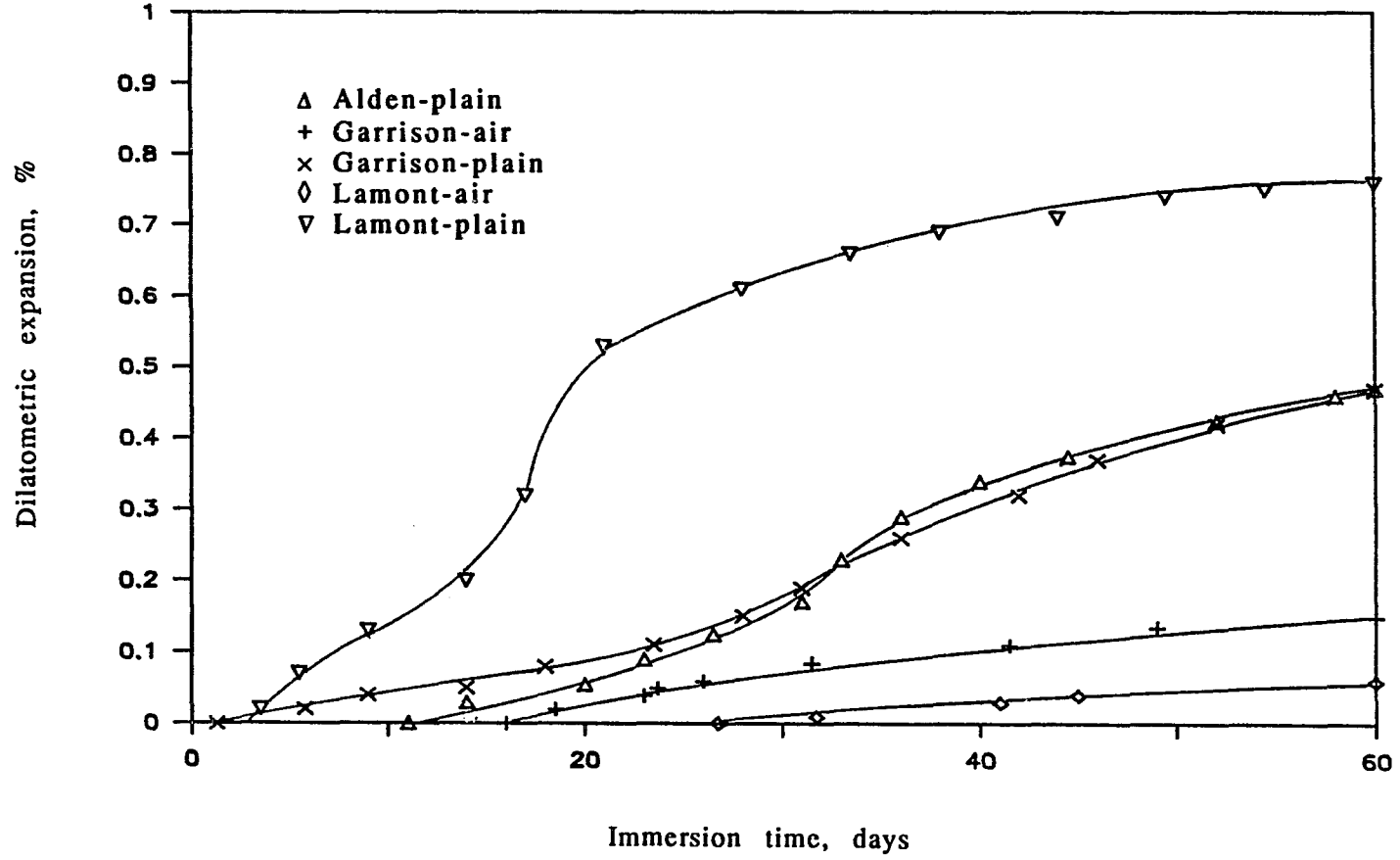

Figure 30. Relationship between dilatometric expansion and immersion time of concrete samples

absorption (saturation) versus immersion time data, taking advantage of the saturation as their common variable. Using the regression lines between dilatometric and permanent expansions presented earlier, relationships were also obtained between permanent expansion and immersion time. These relationships are shown on Figures 31 and 32 by the full curves. The dashed lines are the extrapolation of these curves (full) towards zero immersion time, i.e., below critical saturations. These extrapolations were made assuming that:

(a) the Powers' model is in operation in these regions, i.e., the damage is caused by in situ nucleated freezing, and is proportional to the amount of excess water displaced from the frozen pores in the interior of the sample, and

(b) the pore water which can freeze by this mechanism at -20 °C is only that is in excess of 56% saturation, as previously observed with a freezing sample of air-entrained cement paste by electrical conductance measurements [15].

It is noted that for the concrete samples, the air-entrained mix with Alden aggregate does not appear on Figures 30 and 32, since there is no dilatometric expansion at the length of immersion time considered. It can be seen that the permanent expansion of plain mortar and concrete samples is smaller at the early stage of immersion, since their saturation level is below the critical. Once the saturation reaches the critical level, the permanent expansion of plain samples increases substantially. This indicates that at saturation levels above the critical, bulk-ice-initiated freezing comes into play. As expected, at any stage of immersion, the permanent expansions of air-entrained mortar and concrete samples are significantly less and increase at a much slower rate than their plain counterparts. In general, the concrete

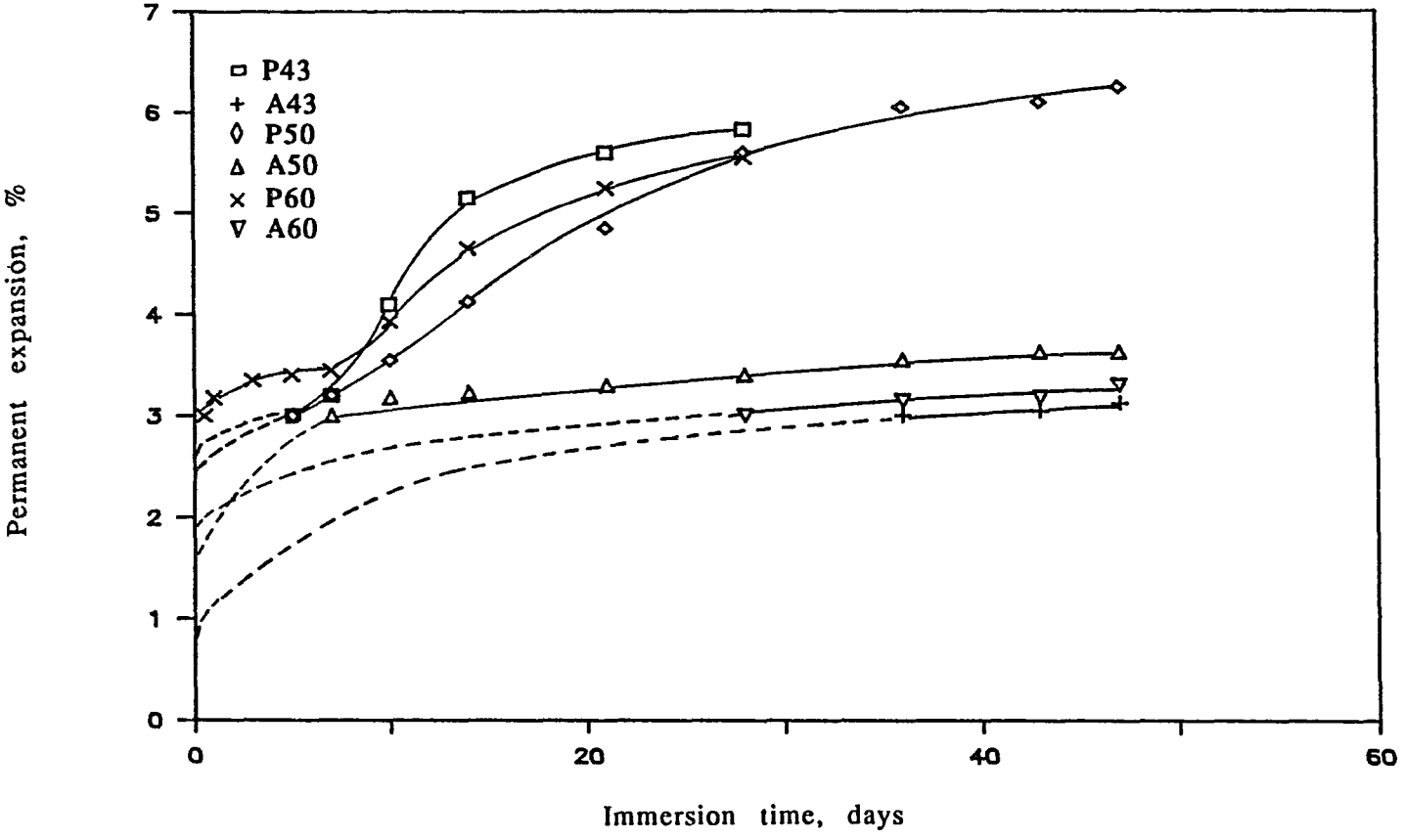

Figure 31. Relationship between permanent expansion and immersion time of mortar samples

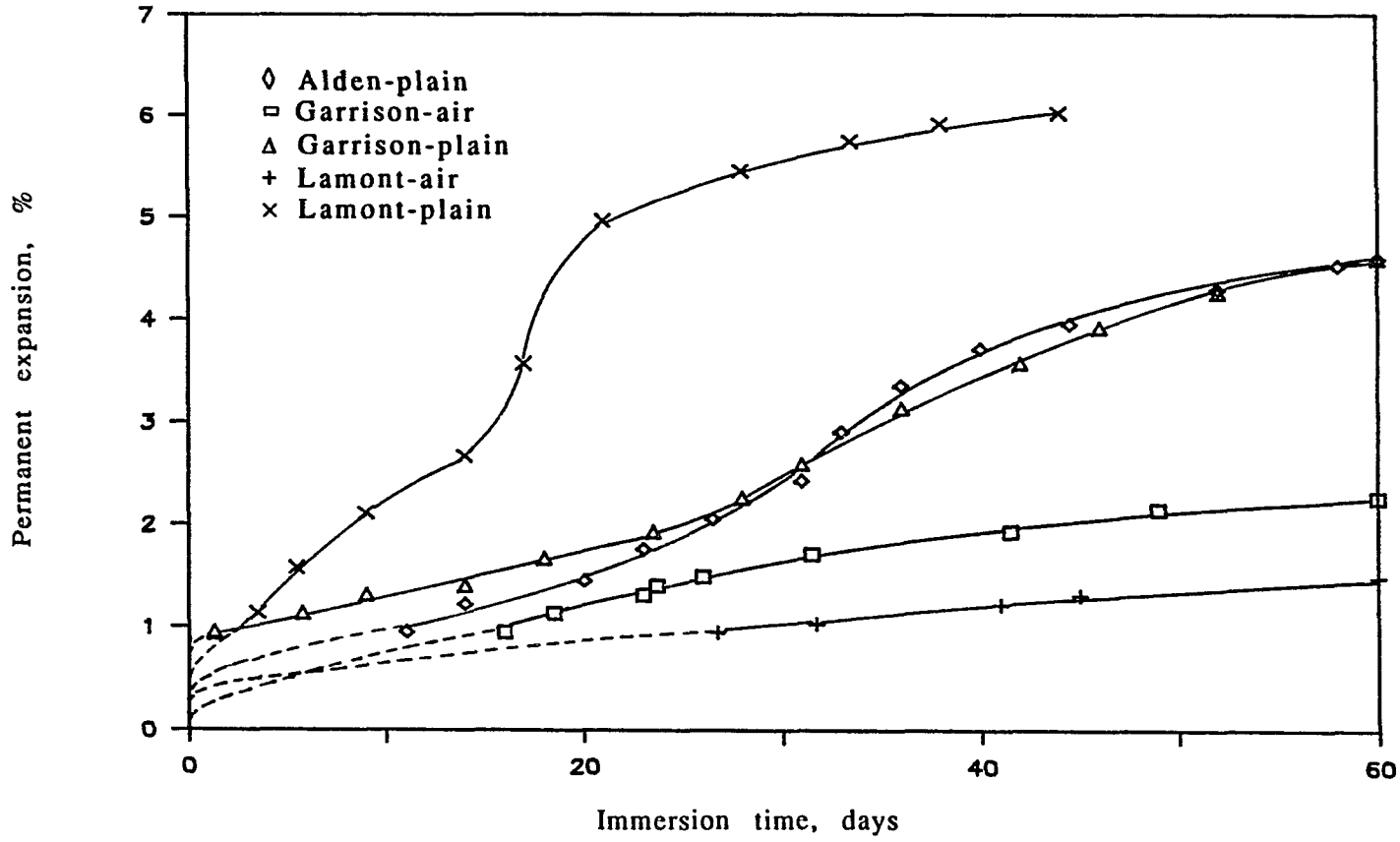

Figure 32. Relationship between permanent expansion and immersion time of concrete samples

samples suffer less damage than the mortar samples. The reason may be that the coarse aggregate in concrete is capable of elastic accommodation of the expansion.

At early stages of immersion, while plain samples begin to suffer significant frost damage due to rapid attainment of supercritical saturation, which results in the extrusion of ice during freezing, the air-entrained samples suffer only slight damages presumably through the Powers mechanism. However, upon prolonged immersion, air-entrained samples also exhibit some ice extrusion on freezing and subsequent damage, although they are still far from fully saturated state and, therefore, contain substantial amounts of air voids to act as "escape boundaries".

It follows from the results presented so far that the dilatometric expansion upon freezing is the primary cause of significant frost damage and that the attainment of supercritical saturation is its prerequisite. The probability that a given concrete in the field suffers frost damage is, therefore, proportional to the probability of occurrence of such a saturation state during the freezing season. On the other hand, the latter probability is obviously controlled by the rate of saturation and the availability of water. As expressed earlier, frost susceptibility can be evaluated by a suitable combination of dilatometric expansion and rate of saturation data.

The most direct and simplest approach appears to be measuring the dilatometric expansion as a function of immersion time, rather than resorting to two different types of experiments and combining the data. The time-average of such dilatometric data, obtained by a set of measurements of a suitable duration, might serve as an index to compare various samples with

each other, regarding their frost susceptibility. This tentatively suggested time-average is determined by calculating the area under the dilatometric expansion versus immersion time curve for a specified duration from the beginning of the test. As an example, Table 3 gives the time-average of dilatometric expansion of concrete samples after 28 days of immersion.

Table 3 The time-average of dilatometric expansion of concrete samples after 28 days of immersion in water

Sample	Time-average	IDOT durability factor, %	Serviceability in years
Alden - air	0	90-98	>20
Alden - plain	1.13	-	-
Garrison - air	0.40	80-90	10-20
Garrison - plain	1.65	-	-
Lamont - air	0	>94	>20
Lamont - plain	6.54	-	-

CONCLUSIONS

The following conclusions can be made based on the experimental results obtained:

(1). For mortar samples, the trends of variations of expansion with saturation level for some of the samples resemble the theoretical trend but some do not. For concrete samples, the trends appear to more closely resemble the proposed theoretical trend than the mortar sample. The critical saturation levels are lower and the observed expansions are generally larger than expected, for both mortar and concrete samples. The deviations from theory may be due to air in the pores being more persistent than was assumed in the theory.

(2). Air-entrainment appears to simply reduce the rate of saturation relative to total pore volume.

(3). Pore structure analysis results are not consistent enough to be used for measurement of frost susceptibility.

(4). Permanent expansion of mortar and concrete samples, subjected to freeze-thaw cycles, seems to indicate that Powers' mechanism is operating at low levels of saturation (subcritical) and causing a mild damage, whereas at high levels of saturation (supercritical), the effect of bulk-ice-initiated freezing predominates and causes severe damage.

(5). A reasonably good correlation was obtained between dilatometric and permanent expansion data. It follows that dilatometric expansion can possibly be used as a measure of frost susceptibility, if its dependence on immersion time is considered.

(6). A frost susceptibility index is suggested. It can be determined by taking the time-average of dilatometric expansion. This time-average is determined by taking the area under the dilatometric expansion versus immersion time curve for a specified duration from the beginning of the test.

(7). A simple method is suggested to evaluate the frost susceptibility of concrete. This method consists of immersing a 1" diameter by 1" high concrete core in water, and monitoring its dilatometric expansion over a specified period of time and taking its time-average.

ACKNOWLEDGMENTS

I wish to express my sincere appreciation to my major professor, Dr. Kenneth Bergeson, for his invaluable guidance, encouragement, and assistance during this study. Thanks are also extended to my co-major professor, Dr. Richard Handy, for his suggestions and guidance.

To my committee members, Dr. John Pitt, Dr. Richard Groeneveld, and Dr. Dah-Yinn Lee, I would also like to express my thanks and appreciation.

To Dr. Enustun, thank you for everything. It was a real pleasure to work with you and to learn from your experience.

To the staffs of Materials and Environmental Research Laboratory, your help and cooperation is greatly appreciated.

To my parents, without whom I would not have gone this far in my education endeavor, I wish to express my greatest thanks and appreciation.

Finally, I like to thank my wife, Ling, for her encouragement, tolerance and support during the course of this study.

REFERENCES

1. ACI Committee 201. Guide to Durable Concrete. Proc. J. of American Concrete Institute, 74 (Dec. 1977), 573-609.

2. ASTM Designation C-666. "Standard Test Method for Resistance of Concrete to Rapid Freezing and Thawing." ASTM Annual Book of Standard, 04.02 (1985), 403-401.

3. ASTM Designation C-671. "Standard Test Method for Critical Dilation of Concrete Specimens Subjected to Freezing." ASTM Annual Book of Standard, 04.02 (1985), 420-425.

4. ASTM Designation C-682. "Standard Recommended Practice for Evaluation of Frost Resistance of Coarse Aggregates in Air-Entrained Concrete by Critical Dilation Procedures." ASTM Annual Book of Standard, 04.02 (1985), 429-434.

5. Axon, E. O., L. T. Murray and R. M. Rucker. "Laboratory Freeze-Thaw Tests Versus Outdoor Exposure Tests." Highway Research Board, 268 (1969).

6. Beaudoin, J. J. and C. MacInnis. "The Mechanism of Frost Damage in Hardened Cement Paste." Cement and Concrete Research, 4, No. 2 (1974), 139-147.

7. Birger, W. "Model Describing the Process of Frost Deterioration." Preliminary report B49-61. Proc. RILEM International Symp. on Durability of Concrete, Building Research Institute, Prague, 1969.

8. Butterworth, B. "The Frost Resistance of Bricks and Tiles - A Review." British Ceramic Society Trans., 1 (1964), 203.

9. Cady, P. D. "Mechanisms of Frost Action in Concrete Aggregates." J. of Materials, 4, No. 2 (June 1969), 294-311.

10. Collins, A. R. "The Destruction of Concrete by Frost." J. of Civil Engineers, 23, No. 1 (Nov. 1944), 29-41.

11. Conner, W. C., A. M. Lane and A. J. Hoffman. "Measurement of the Morphology of High Surface Area Solids: Hysteresis in Mercury Porosimetry." J. of Colloid and Interfacial Science, 100 (1984), 185-193.

12. Cranston, R. W. and F. A. Inkley. "The Determination of Pore Structure from Nitrogen Adsorption Isotherms." Advanced Catalysis and Related Subjects, 9 (1957), 143-154.

13. Dolch, W. L. "Porosity." Significance of Tests and Properties of Concrete and Concrete Making Materials. ASTM, STP 169A (1966), 443-461.

14. Eckrich, J., B. V. Enustun and T. Demirel. "Phase Transition Porosimetry." American Laboratory, 18, No. 3 (March 1986), 80-92.

15. Enustun, B. V. and K. L. Bergeson. "Frost Susceptibility of Concrete in Near-Saturated States." Proposal Submitted to NSF, 1988.

16. Enustun, B. V., J. Eckrich and T. Demirel. "Phase Transition Porosimetry." Proc. of International Symp. Workshop on Particulate and Multi-Phase Processes and the 16th Annual Meeting of Fine Particle Society, Miami Beach, Florida, April 1985

17. Enustun, B. V., H. S. Senturk and K. Kosal. "Freezing-Melting behavior of Capillary Water in Porous Materials." RILEM/ CIB Symp., Moisture Problems in Building, Helsinki Report 2-13 (1965).

18. Enustun, B. V., H. S. Senturk and O. Yordakul. "Capillary Freezing and Melting." J. of Colloid and Interfacial Science, 65 (1978), 509-516.

19. Everett, D. H. "The Thermodynamics of Frost Damage to Porous Solids." Transaction Faraday Society, 57 (1961), 1541-1551.

20. Everett, D. H. and J. M. Haynes. "Capillary Properties of Some Pore Model Systems with Special Reference to Frost Damage." RILEM, Bull. No. 27 (June 1965).

21. Fagerlund, G. "The Significance of Critical Degrees of Saturation at Freezing of Porous and Brittle Materials." In Durability of Concrete. American Concrete Institute, SP 47-2 (1975), 13-66.

22. Faulkner, T. and R. Walker. "Rapid One-Cycle Test for Evaluating Aggregate Performance When Exposed to Freezing and Thawing in Concrete." In Concrete Durability. Katharine and Bryant Mather International Conference, American Concrete Institute, SP 100-40 (1987), 705-722.

23. Fears, F. K. "Correlation between Concrete Durability and Air-Void Characteristics." Highway Research Board, Bull. 196 (1958), 17-24.

24. Gayner, R. D. and R. C. Meininger. "Investigation of Aggregate Durability in Concrete." Highway Research Record 196 (1967), 25-40.

25. Gordon, W. A. "Freezing and Thawing of Concrete - Mechanisms and Controls." American Concrete Institute Monograph No. 3 (1966), Detroit, Michigan.

26. Haynes, J. M. "Frost Action as a Capillary Effect." British Ceramic Society Trans., 63, No. 11 (1964), 697-703.

27. Helmuth, R. A. "Dimensional Changes of Hardened Portland Cement Pastes Caused by Temperature Changes." Proc. Highway Research Board, 40 (1961), 315-336.

28. Hill, R. D. "A Study of Pore Size Distribution." British Ceramic Society Trans., 59 (1960), 198-212.

29. Hudec, P. "Deterioration of Aggregates - the Underlying Causes." In Concrete Durability. Katharine and Bryant Mather International Conference. American Concrete Institute, SP 100-68 (1987), 1325-1342.

30. Hudec, P. "Durability of Rock as Function of Grain Size, Pore Size, and Rate of Capillary Absorption of Water." J. of Materials in Civil Engineering, 1, No. 1 (1989), 3-9.

31. Kaneuji, M. "Correlation between Pore Size Distribution and Freeze-Thaw Durability of Coarse Aggregate in Concrete." Joint Highway Research Project, FHWA/IN/JHRP-78/15 (Aug. 1978).

32. Kennedy, T. B. and K. Mather. "Correlation between Laboratory Accelerated Freezing and Thawing and Weathering at Treat Island, Maine." Proc. Journal of American Concrete Institute, No. 5 (Oct. 1951), 141-172.

33. Klieger, P. "Further Studies on the Effect of Entrained Air on Strength and Durability of Concrete with Various Sizes of Aggregates." Highway Research Board, Bull. No. 128 (1956), 1-19.

34. Lane, D. and R. Meininger. "Laboratory Evaluation of the Freezing and Thawing Durability of Marine Limestone Coarse Aggregate in Concrete." In Concrete Durability. Katharine and Bryant Mather International Conference. American Concrete Institute, SP 100-67 (1987), 1311-1323.

35. Larson, T. D. and P. D. Cady. "Identification of Frost Susceptible Particles in Concrete Aggregates." Highway Research Board, NCHRP Report No. 66 (1969).

36. Larson, T. D., A. Boettcher, P. D. Cady, M. Franzen and J. Reed. "Identification of Concrete Aggregates Exhibiting Frost Susceptibility - Interim Report." Highway Research Board, NCHRP Report No. 15 (1965).

37. Larson, T. D., P. D. Cady, M. Franzen and J. Reed. "A Critical Review of Literature Treating Methods of Identifying Aggregates Subjected to Destructive Volume Change When Frozen in Concrete and a Proposed Program of Research." Highway Research Board Special Report 80 (1964).

38. Lemish, J., E. Rush and C. L. Hiltrop. "Relationship of Physical Properties of Some Iowa Carbonate Aggregates to Durability of Concrete." Highway Research Board, Bull. 196 (1958), 1-16.

39. Levitt, M. "An Assessment of the Concrete Durability by the Initial Absorption Test." Preliminary Report A29-42. Proc. RILEM International Symp. on Durability of Concrete, Building Research Institute, Prague, 1969.

40. Lewis, W. D. and W. L. Dolch. "Porosity and Absorption." Significance of Tests and Properties of Concrete and Concrete Making Materials, ASTM Spec. Pub. No. 169 (1956).

41. Lewis, W. D., W. L. Dolch and K. B. Woods. "Porosity Determinations and the Significance of Pore Characteristics of Aggregates." Proc. ASTM, 53 (1953), 949-962

42. Lindgren, M. N. "The Prediction of Freeze-Thaw Durability of Coarse Aggregate in Concrete by Mercury Porosimetry." Joint Highway Research Project, FHWA/IN/JHRP-80/14 (Oct. 1989).

43. Lowell, S. and J. E. Shields. Powder Surface Area and Porosity. New York: Chapman and Hall, 1984.

44. Lyse, I. "Basic Questions, Principles and Methods of Testing and Determining of Concrete Durability under the Action of Frost." Final Report B5-14. Proc. RILEM International Symp. on Durability of Concrete, Building Research Institute, Prague, 1969.

45. MacInnis, C. "A One-Cycle Freezing Test for Concrete Durability." Preliminary Report B3-16. Proc. RILEM International Symp. on Durability of Concrete, Building Research Institute, Prague, 1969.

46. MacInnis, C. and J. J. Beaudoin. "Effect of Degree of Saturation on the Frost Resistance of Mortar Mixes." Proc. J. of American Concrete Institute, 65 (March 1968), 203-207.

47. Mielenz, R. C. "Petrographic Examination." Significance of Tests and Properties of Concrete and Concrete Making Materials, ASTM, STP 169B (1978), 539-572.

48. Munger, H. H. "The Influence of Durability of Aggregate upon the Durability of Resulting Concrete." Proc. ASTM, 42 (1942), 787-803.

49. Myers, V. J. and N. Dubberke. "Durability of Concrete and the Iowa Pore Index Test - Interim Report." Project HR-2022 (July 1981). Iowa Department of Transportation, Ames, Iowa.

50. Neville, A. M. Properties of Concrete. London: Pitman, 1981.

51. Philleo, R. E. "Freezing and Thawing Resistance of High Strength Concrete." Highway Research Board, NCHRP Report 20-5 (Jan. 1986).

52. Powers, T. C. "A Working Hypothesis for Further Studies of Frost Resistance of Concrete." Proc. J. of American Concrete Institute, 41 (Feb. 1945), 245-272.

53. Powers, T. C. "Void Spacing as a Basis for Producing Air-Entrained Concrete." Proc. J. of American Concrete Institute, 50 (May 1954), 741-760.

54. Powers, T. C. "The Air Requirement of Frost-Resistant Concrete." Proc. Highway Research Board, 29 (1949), 184-211.

55. Powers, T. C. "The Mechanism of Frost Action in Concrete." Stanton Walker Lecture No. 3. National Sand and Gravel Association, Silver Spring, Maryland, 1965.

56. Powers, T. C. "Basic Considerations Pertaining to Freezing and Thawing Tests." Proc. ASTM, 55 (1955), 1132-1154.

57. Powers, T. C. "Freezing Effects in Concrete." In Durability of Concrete. American Concrete Institute, SP 47-1 (1975), 1-12.

58. Powers, T. C., L. E. Copeland, J. C. Hayes and H. M. Mann. "Permeability of Portland Cement Paste." Proc. J. of American Concrete Institute, 51 (Nov. 1954), 285-298.

59. Powers, T. C. and R. A. Helmuth. "Theory of Volume Changes in Hardened Portland Cement Paste During Freezing." Proc. Highway Research Board, 32 (1953), 285-297.

60. Ritter, H. L. and L. C. Drake. "Pore-Size Distribution in Porous Materials; Pressure Porosimeter and Determinations of Complete Macropore-Size Distribution." Industry Engineering Chemical Analysis Edition 17 (1945), 782-786.

61. Rogers, C. and B. Chojnacki. "Destruction of Concrete Water Tanks in a Severe Climate Due to Ice Lensing." In Concrete Durability. Katharine and Bryant Mather International Conference, American Concrete Institute, SP 100-41 (1987), 723-739.

62. Sawan, J. "Cracking Due to Frost Action in Portland Cement Concrete Pavements - A Literature Survey." In Concrete Durability. Katharine and Bryant Mather International Conference, American Concrete Institute, SP 100-44 (1987), 781-803.

63. Schulze, W. and H. Lange. "Survey of Test Methods for the Determination of the Frost Resistance of Aggregates." Preliminary Report B63-78. Proc. RILEM International Symp. on Durability of Concrete, Building Research Institute, Prague, 1969.

64. Schuster, R. L. and J. F. McLaughlin. "A Study of Chert and Shale Gravel in Concrete." Highway Research Board, Bull. 305 (1961), 51-75.

65. Shakoor, A. and C. F. Scholer. "Comparison of Aggregate Pore Characteristics as Measured by Mercury Instrusion Porosimeter and Iowa Pore Index Tests." J. of American Concrete Institute, 82, No. 4 (July-Aug. 1985), 453-458.

66. Sridharan, A., A. G. Altshaeffl and S. Diamond. "Pore Size Distribution Studies." J. of Soil Mechanics and Foundation Division, 97, No. SM 5 (May 1971), 771-787.

67. Sturrup, V., R. Hooton, P. Mukherjee and T. Carmichael. "Evaluation and Prediction of Concrete Durability - Ontario Hydro's Experience." In Concrete Durability. Katharine and Bryant Mather International Conference, American Concrete Institute, SP 100-59 (1987), 1121-1154.

68. Sweet, H. S. "Research on Concrete Durability as Affected by Coarse Aggregate." Proc. ASTM, 48 (1948), 988-1016.

69. Tremper, B. and D. L. Spellman. "Test for Freeze-Thaw Durability of Concrete Aggregates." Highway Research Board, Bull. 305 (1961), 28-50.

70. U. S. Bureau of Reclamation. "Investigation Into the Effect of Water/Cement Ratio on the Freeze-Thaw Resistance of Non-air and Air-Entrained Concrete." Concrete Laboratory Report No. C-810 (1955), Denver, Colorado.

71. Valenta, O. "General Analysis of the Methods of Testing the Durability of Concrete." Preliminary Report A3-28. Proc. RILEM International Symp. on Durabiiity of Concrete, Building Research Institute, Prague, 1969.

72. Verbeck, G. J. and P. Klieger. "Calorimeter-Strain Apparatus for Study of Freezing and Thawing of Concrete." Highway Research Board, Bull. No. 176 (1958), 9-22.

73. Verbeck, G. J. and R. Langren. "Influence of Physical Characteristics of Aggregates on Frost Resistance of Concrete." Proc. ASTM, 60 (1960), 1063-1079.

74. Vuorinen, J. "On Use of Dilation Factor and Degree of Saturation in Testing Concrete for Frost Resistance." Nordisk Betong (Stockholm), No. 1 (1970), 37-64.

75. Walker, S. and D. L. Bloem. "Performance of Automatic Freezing-and-Thawing Apparatus for Testing Concrete." Proc. ASTM, 51 (1951), 1120-1135.

76. Walker, S. and D. L. Bloem. "Studies of Concrete Containing Entrained Air." Proc. J. of American Concrete Institute, 42 (June 1946), 629-639.

77. Walker, R. D. and T. Hsieh. "Relationship between Aggregates Pore Characteristics and Durability of Concrete Exposed to Freezing and Thawing." Highway Research Board, No. 226 (1968), 41-49.

78. Washburn, E. W. "Note on a Method of Determining the Distribution of Pore Sizes in a Porous Material." National Academy of Science, Proc. 7 (1921), 115-116.

79a. Wheeler, A. "Reaction Rates and Selectivity in Catalyst Pores." Advanced Catalysis and Related Subjects, 3 (1951), 249-327.

79b. Wheeler, A. "Reaction Rates and Selectivity in Catalyst Pores." Advanced Catalysis and Related Subjects, 2 (1955), 105-123.

80. Whiteside, T. M. and H. S. Sweet. "Effect of Mortar Saturation on Concrete Freezing and Thawing Tests." Proc. Highway Research Board, 30 (1950), 204-216.

81. Wills, M. H., H. A. Lepper, R. D. Gayner and S. Walker. "Volume Change as a Measure of Freezing and Thawing Resistance of Concrete Made with Different Aggregates." Proc. ASTM, 63 (1963), 946-965.

82. Winslow, N. M. and J. J. Shapiro. "An Instrument for the Measurement of Pore-Size Distribution by Mercury Penetration." ASTM Bull. TP49 (Feb. 1959), 39-44.

83. Wright, P. J. F. and J. M. Gregory. "An Investigation Into Methods of Carrying Out Accelerated Freezing and Thawing Tests on Concrete." Magazines of Concrete Research, (March 1955), 39-47.

APPENDIX A

ABSOLUTE VOLUME COMPOSITIONS OF MORTAR SAMPLES

	Sample Identification					
Component	P43	A43	P50	A50	P60	A60
Cement	0.194	0.194	0.186	0.186	0.175	0.175
Water	0.262	0.262	0.293	0.293	0.332	0.332
Fine aggregate	0.544	0.544	0.521	0.521	0.493	0.493
"Protex"	0	0.00049	0	0.00047	0	0.00044
Total	1.000	1.000	1.000	1.000	1.000	1.000
Water/cement ratio by weight	0.43	0.43	0.50	0.50	0.60	0.60

APPENDIX B

CONCRETE PROPERTIES AND MIX DESIGN

	Slump (in)	Air content (%)	Compressive strength 28-day (psi)	90-day
Alden agg.				
Plain	3	2.5	5290	7970
Air-entrained	4	6.5	4290	5420
Garrison agg.				
Plain	3	2.5	6180	7580
Air-entrained	4	6	4780	5930
Lamont agg.				
Plain	3	2.5	6420	6540
Air-entrained	3	6.8	4600	5990

IDOT C-3 Mix Proportion

Basic Absolute Volumes of Materials per Unit Volume of Concrete

Cement	Water	Entrained air	Fine aggregate	Coarse aggregate
0.114172	0.153840	0.06	0.301895	0.370093

APPENDIX C

DERIVATION OF THE RELATIONSHIP BETWEEN THE RATE OF SATURATION OF CONCRETE AS A FUNCTION OF THE RATE OF SATURATION OF AGGREGATE AND MORTAR COMPONENTS

	concrete	mortar	aggregate
Pore volume	V_c	V_m	V_a
Volume fractions	v_c	v_m	v_a
Water content at time, t	w_c	w_m	w_a
% Saturation at time, t	X_c	X_m	X_a

$$w_c = v_m w_m + v_a w_a \qquad \text{(assumption)}$$

$$X_c = (w_c/V_c) \times 100$$

$$X_m = (w_m/V_m) \times 100$$

$$X_a = (w_a/V_a) \times 100$$

$$X_c V_c = v_m X_m V_m + v_a X_a V_a$$

$$X_c = 1/V_c(v_m V_m X_m + v_a V_a X_a)$$

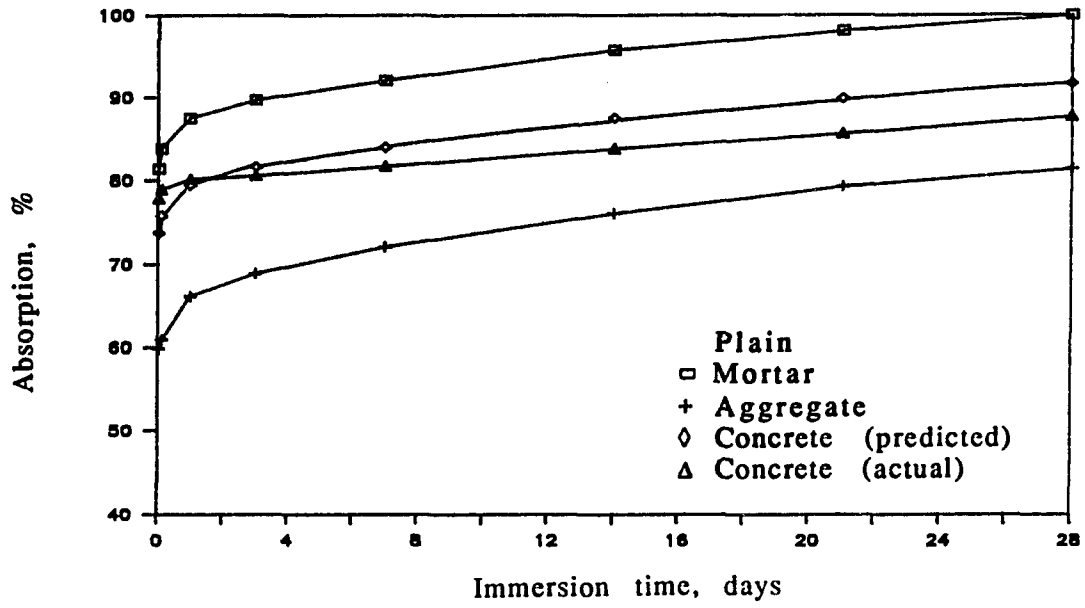

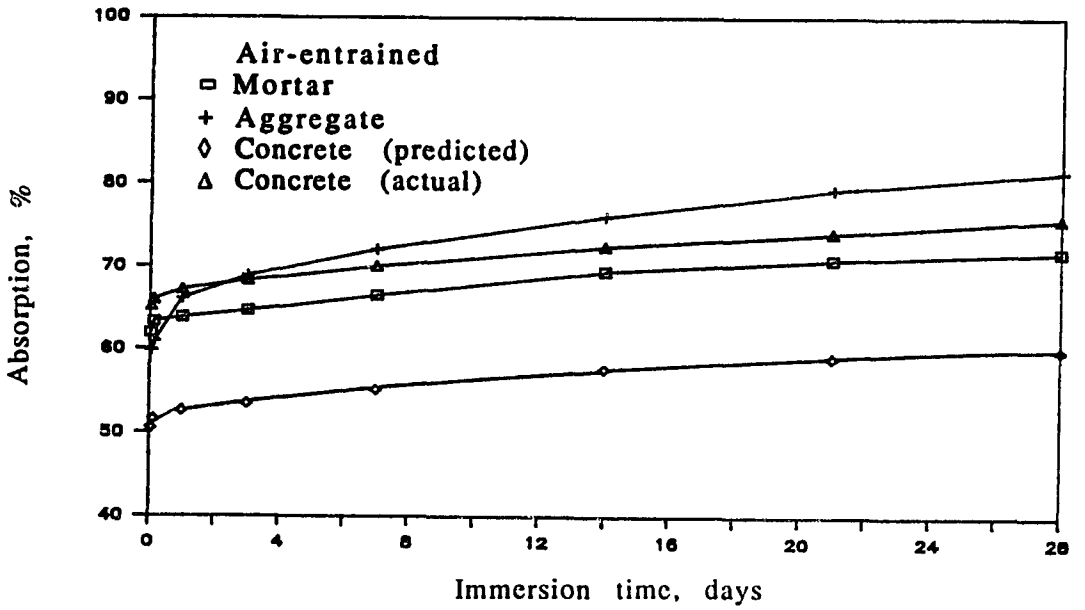

Theoretical prediction of the rate of saturation of concrete with Alden aggregate as a function of the rate of saturation of mortar and aggregate components

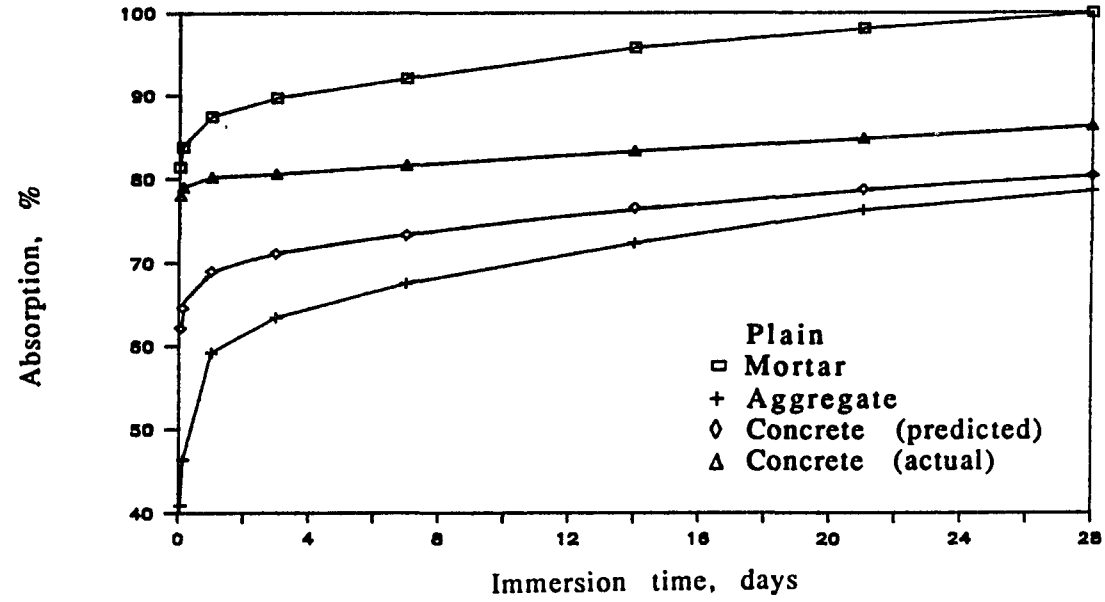

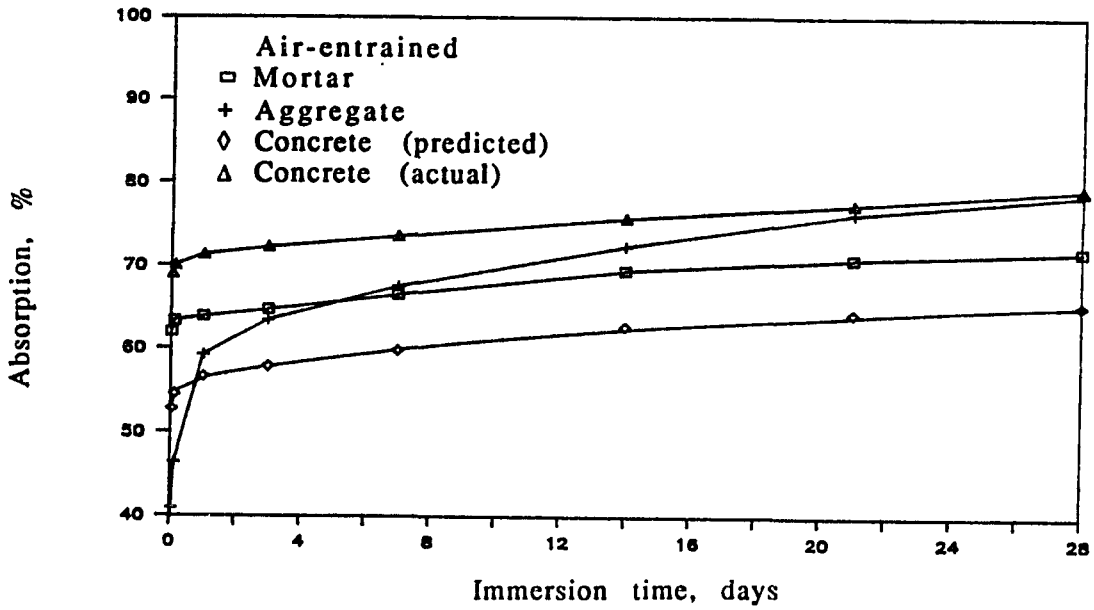

Theoretical prediction of the rate of saturation of concrete with Garrison aggregate as a function of the rate of saturation of mortar and aggregate components

APPENDIX D

TYPICAL DILATOMETRIC EXPANSION VERSUS TEMPERATURE PLOTS AT -20 °C

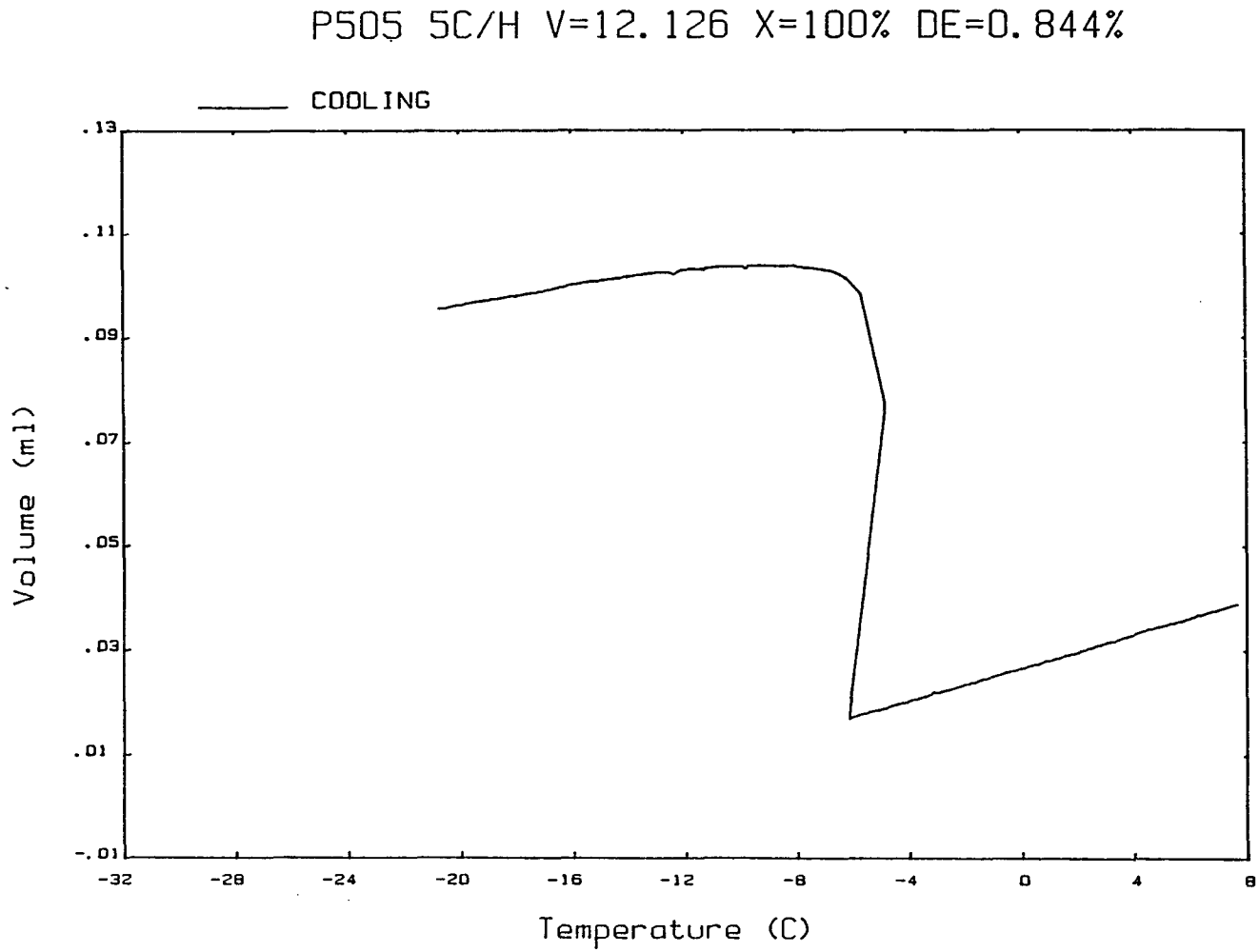
P505 5C/H V=12.126 X=100% DE=0.844%
COOLING
.13
.11
.09
.07
.05
.03
.01
-.01
Volume (ml)
-32
-28
-24
-20
-16
-12
-8
-4
0
4
8
Temperature (C)

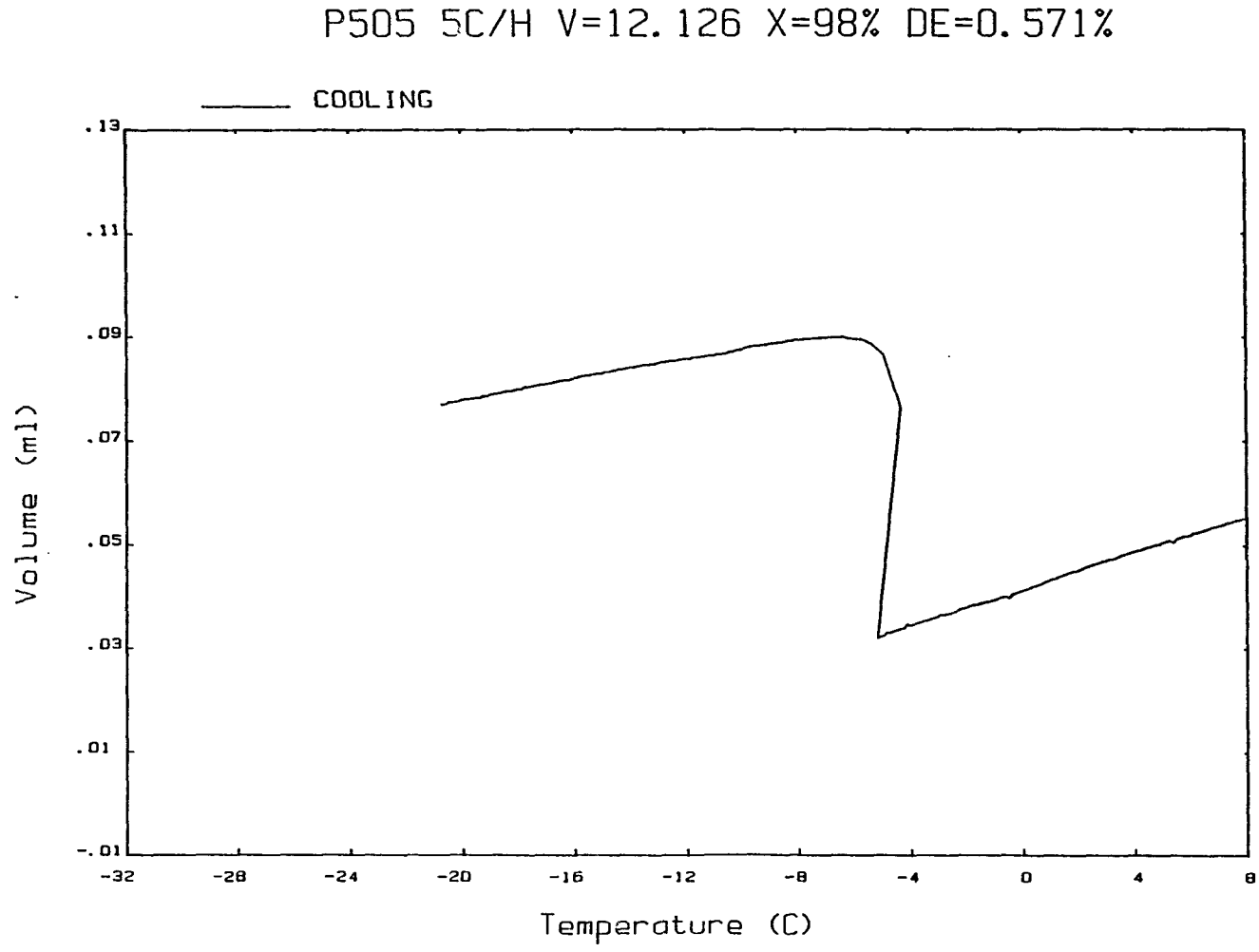
P505 5C/H V=12.126 X=98% DE=0.571%
COOLING
.13
.11
.09
.07
.05
.03
.01
-.01
Volume (ml)
-32
-28
-24
-20
-16
-12
-8
-4
0
4
8
Temperature (C)

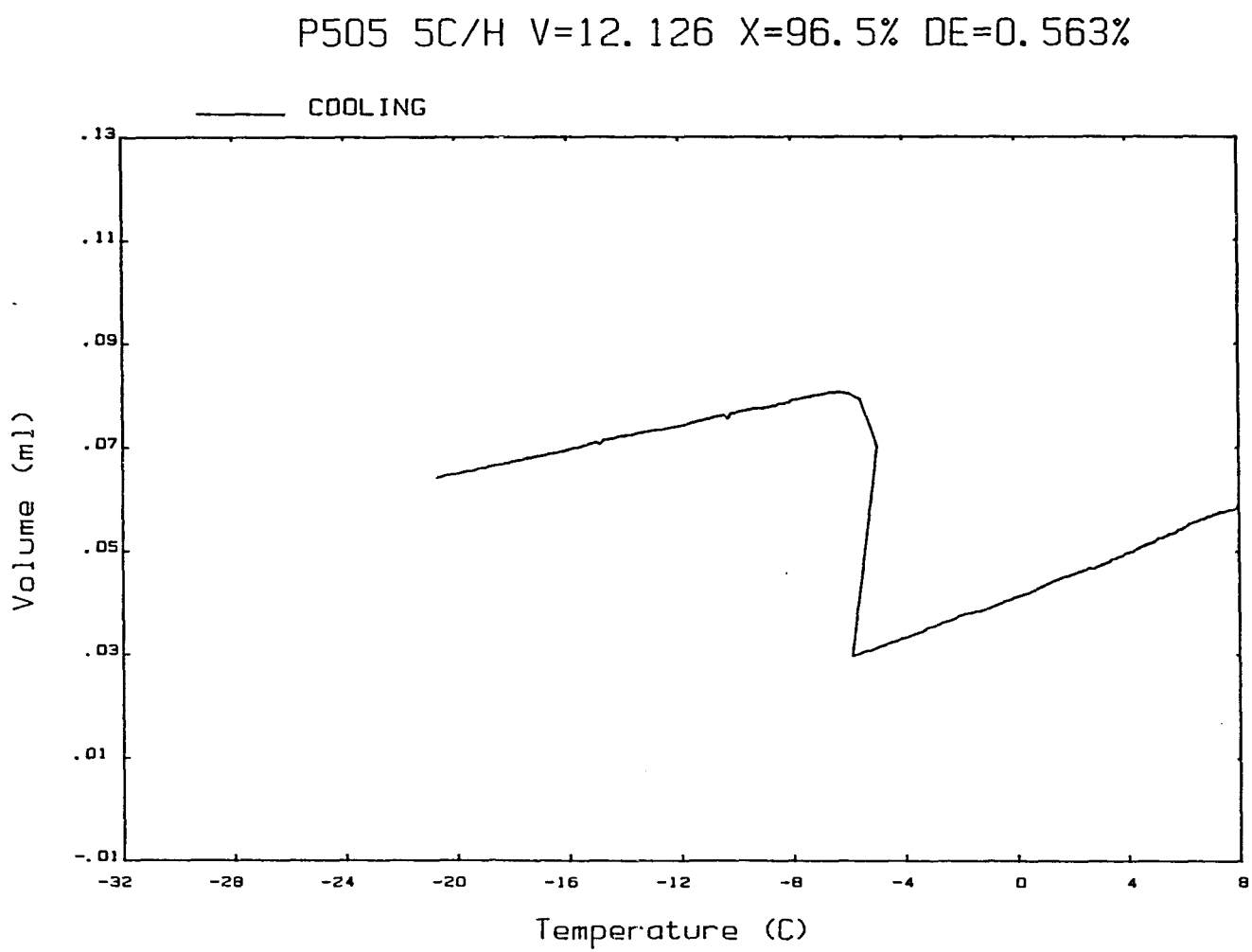
P505 5C/H V=12.126 X=96.5% DE=0.563%
COOLING
.13
.11
.09
.07
.05
.03
.01
-.01
Volume (ml)
-32
-28
-24
-20
-16
-12
-8
-4
0
4
8
Temperature (C)

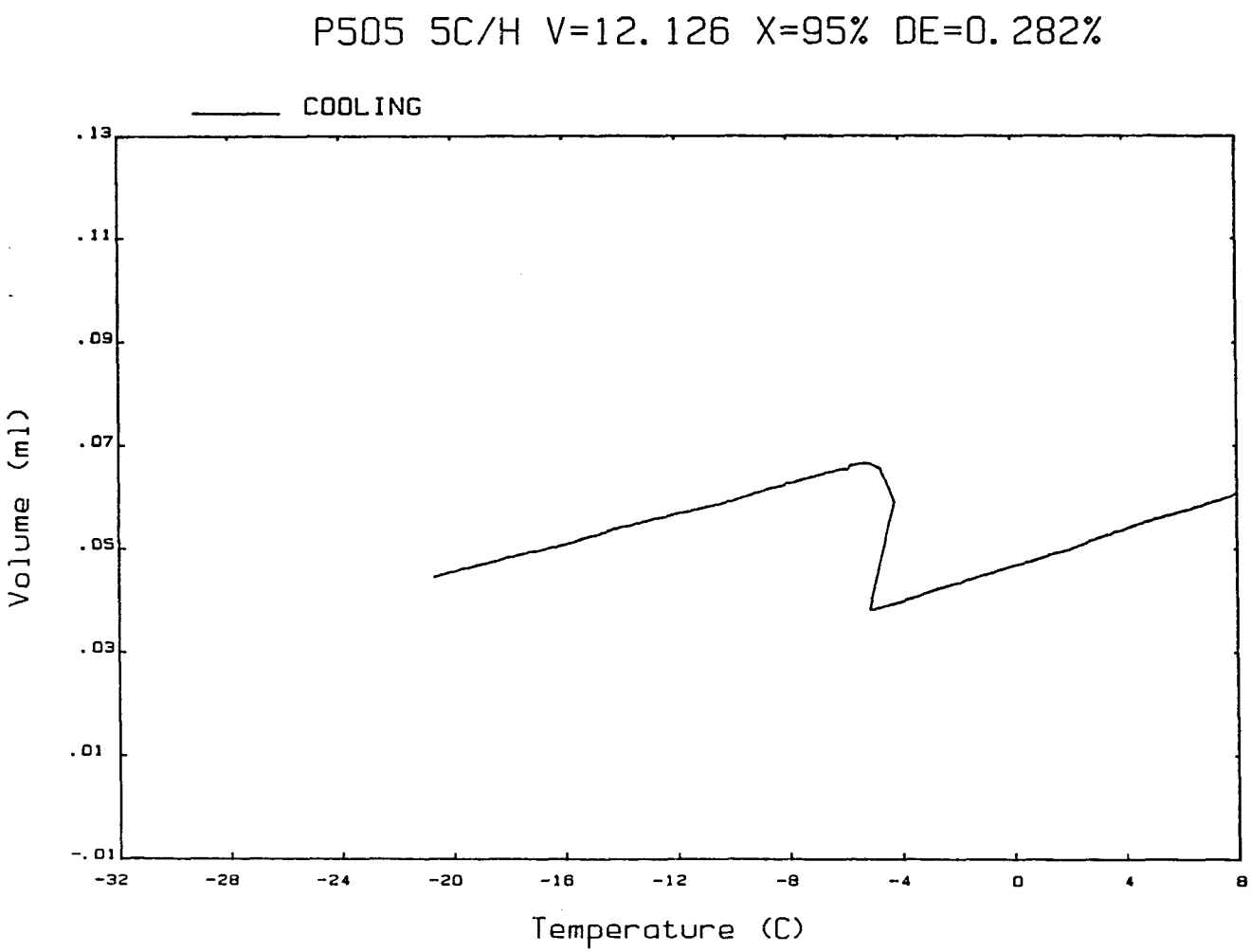
P505 5C/H V=12.126 X=95% DE=0.282%
COOLING
.13
.11
.09
.07
.05
.03
.01
-.01
Volume (ml)
-32
-28
-24
-20
-16
-12
-8
-4
0
4
8
Temperature (C)

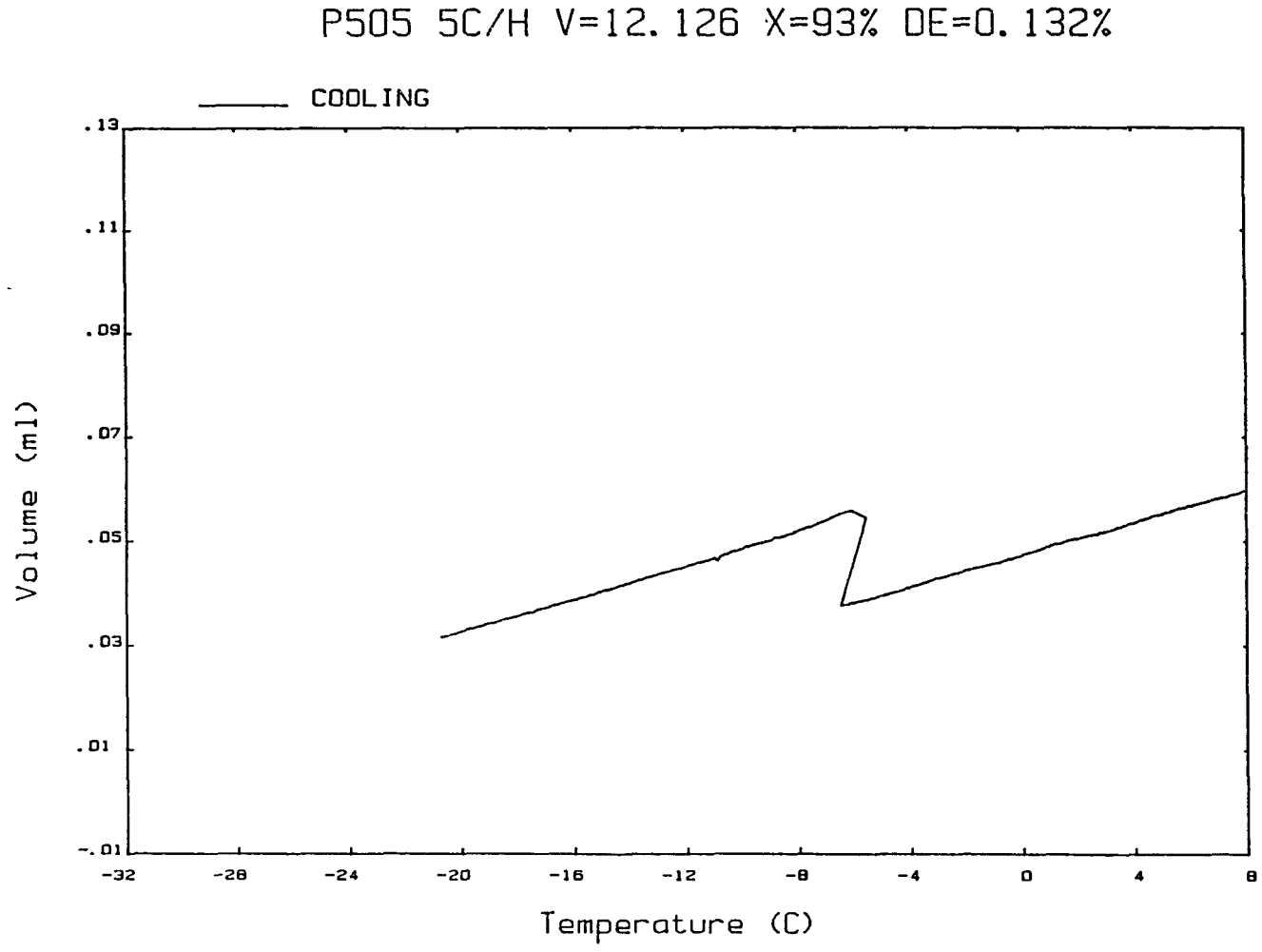
P505 5C/H V=12.126 X=93% DE=0.132%
COOLING
.13
.11
.09
.07
.05
.03
.01
-.01
Volume (ml)
-32
-28
-24
-20
-16
-12
-8
-4
0
4
8
Temperature (C)

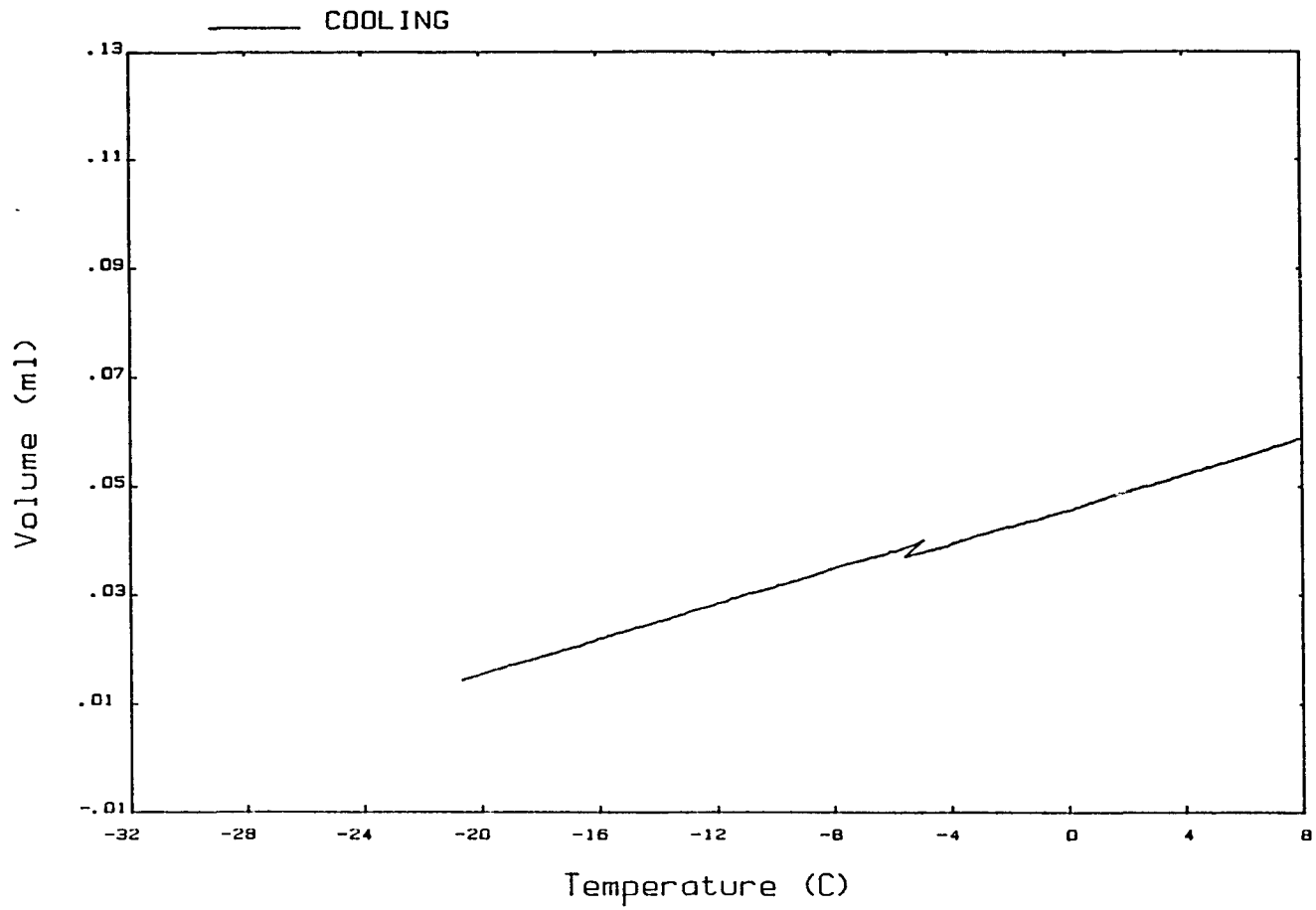
P505 5C/H V=12.126 X=91% DE=0.020%
COOLING
.13
.11
.09
.07
.05
.03
.01
-.01
Volume (ml)
-32
-28
-24
-20
-16
-12
-8
-4
0
4
8
Temperature (C)

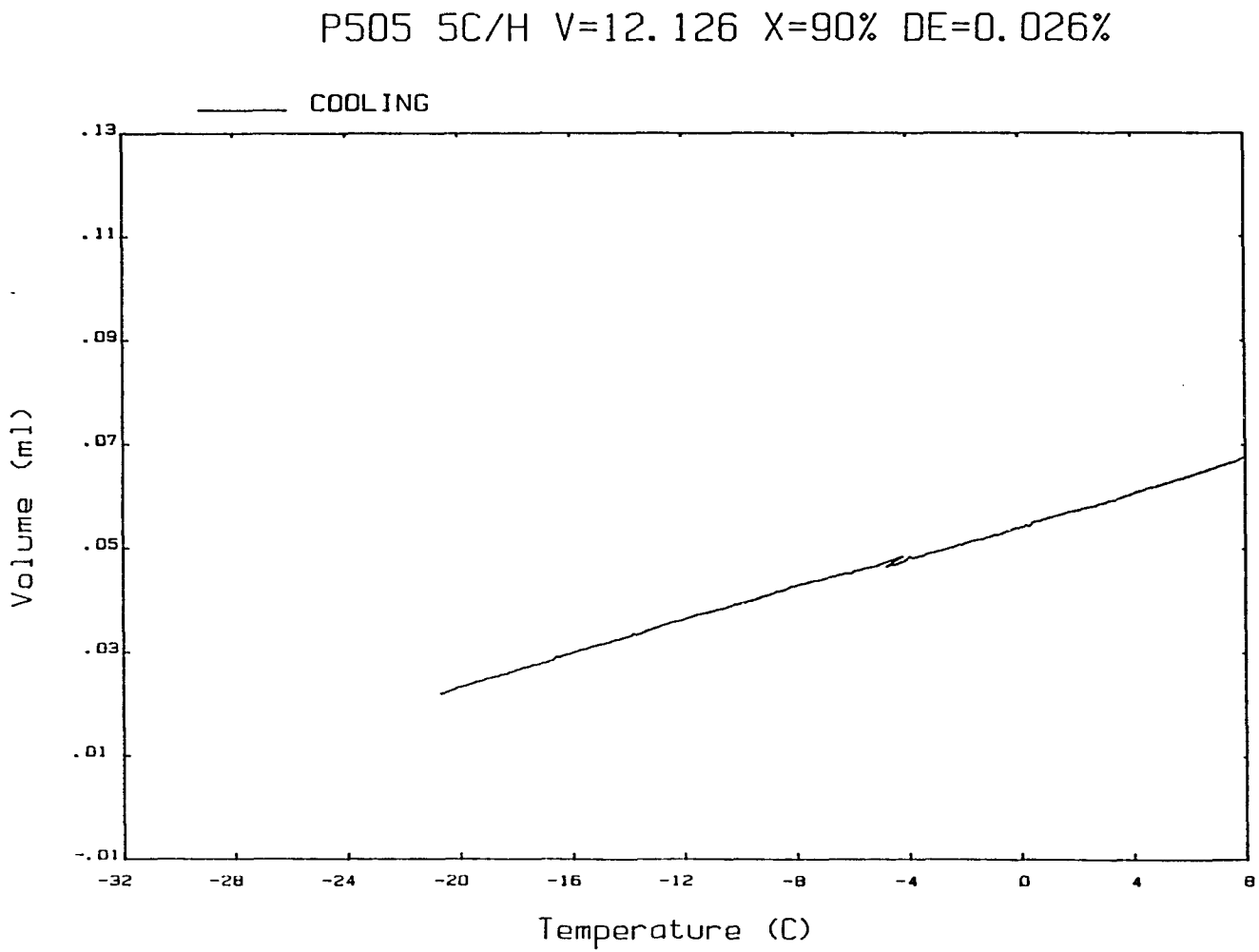
P505 5C/H V=12.126 X=90% DE=0.026%
COOLING
.13
.11
.09
.07
.05
.03
.01
-.01
Volume (ml)
-32
-28
-24
-20
-16
-12
-8
-4
0
4
8
Temperature (C)

APPENDIX E

PORE SIZE DISTRIBUTION OF MORTAR AND AGGREGATE SAMPLES

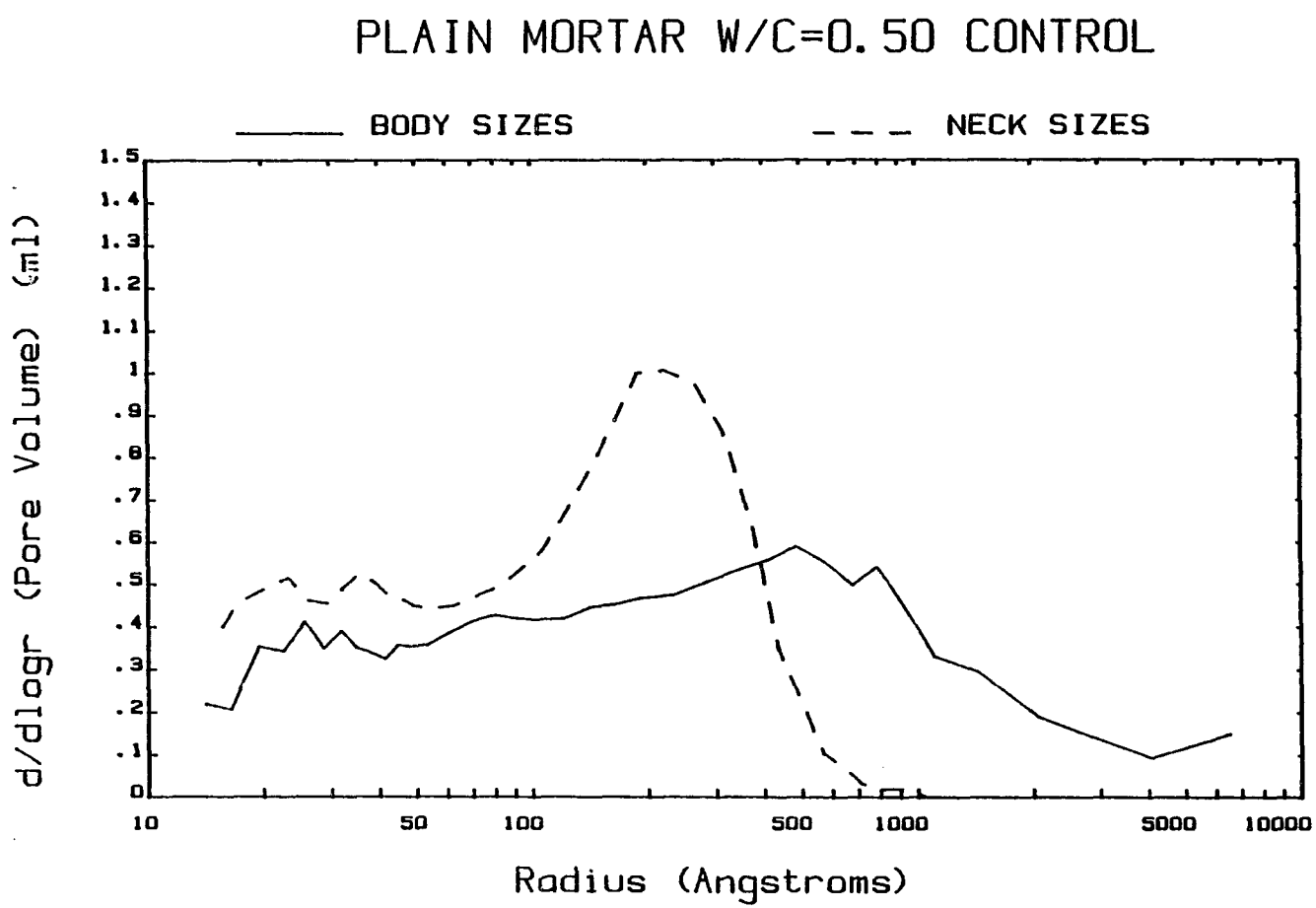
PLAIN MORTAR W/C=0.50 CONTROL
BODY SIZES
NECK SIZES
d/dlogr (Pore Volume) (ml)
1.5
1.4
1.3
1.2
1.1
1
.9
.8
.7
.6
.5
.4
.3
.2
.1
0
10
50
100
500
1000
5000
10000
Radius (Angstroms)

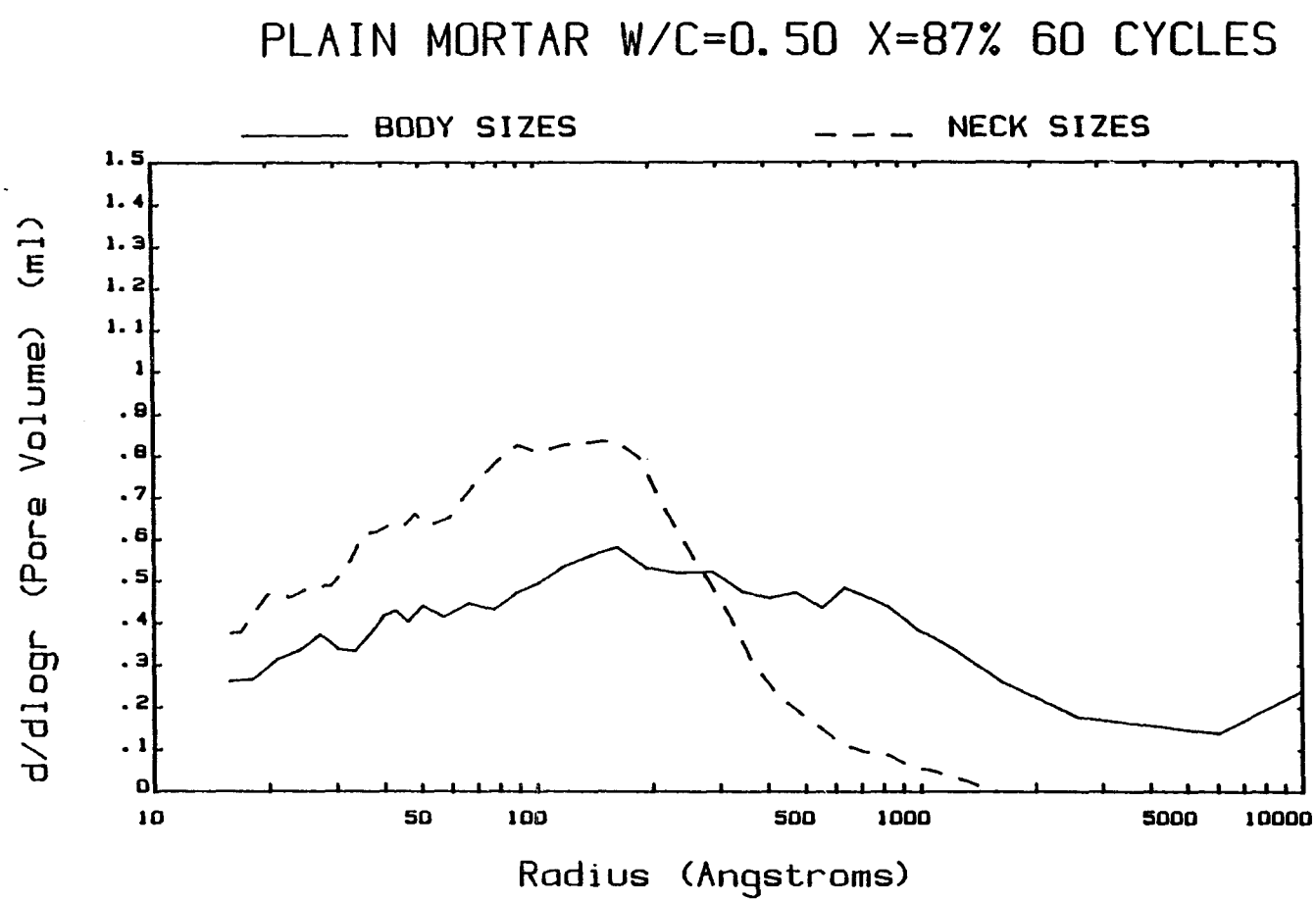
PLAIN MORTAR W/C=0.50 X=87% 60 CYCLES
BODY SIZES
NECK SIZES
d/dlogr (Pore Volume) (ml)
1.5
1.4
1.3
1.2
1.1
1
.9
.8
.7
.6
.5
.4
.3
.2
.1
0
10
50
100
500
1000
5000
10000
Radius (Angstroms)

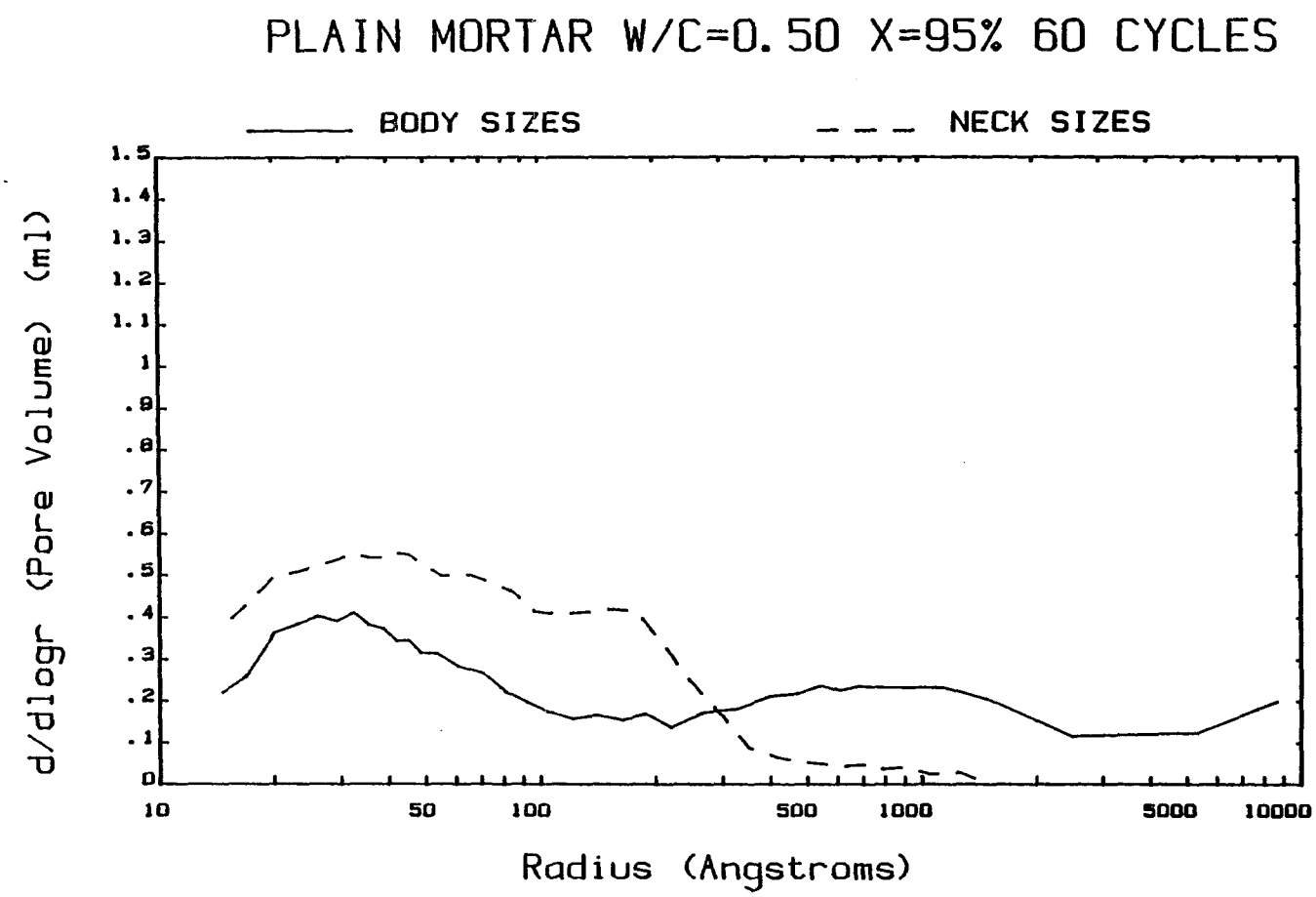
PLAIN MORTAR W/C=0.50 X=95% 60 CYCLES
BODY SIZES
NECK SIZES
d/dlogr (Pore Volume) (ml)
1.5
1.4
1.3
1.2
1.1
1
.9
.8
.7
.6
.5
.4
.3
.2
.1
0
10
50
100
500
1000
5000
10000
Radius (Angstroms)

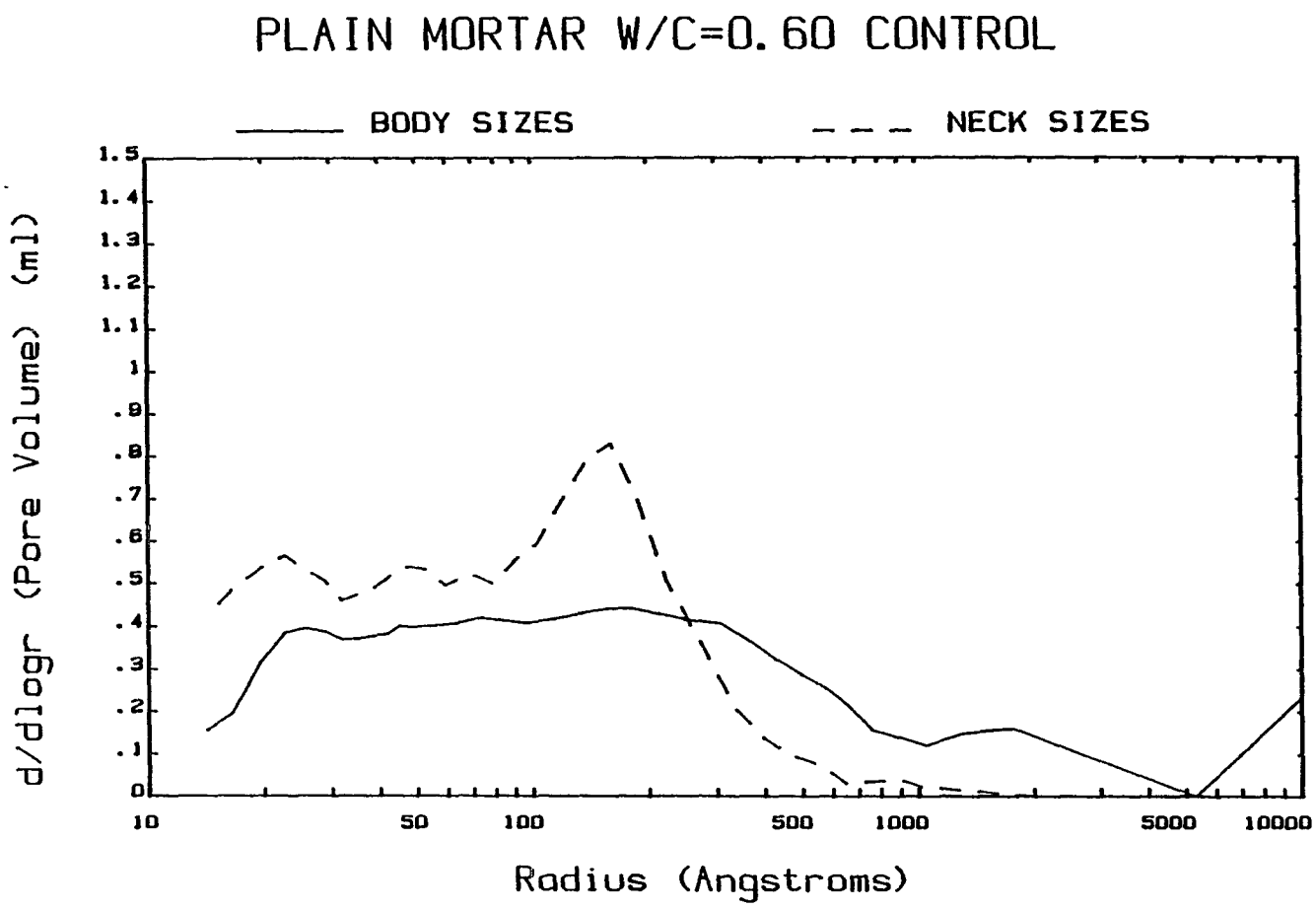
PLAIN MORTAR W/C=0.60 CONTROL
BODY SIZES
NECK SIZES
d/dlogr (Pore Volume) (ml)
1.5
1.4
1.3
1.2
1.1
1
.9
.8
.7
.6
.5
.4
.3
.2
.1
0
10
50
100
500
1000
5000
10000
Radius (Angstroms)

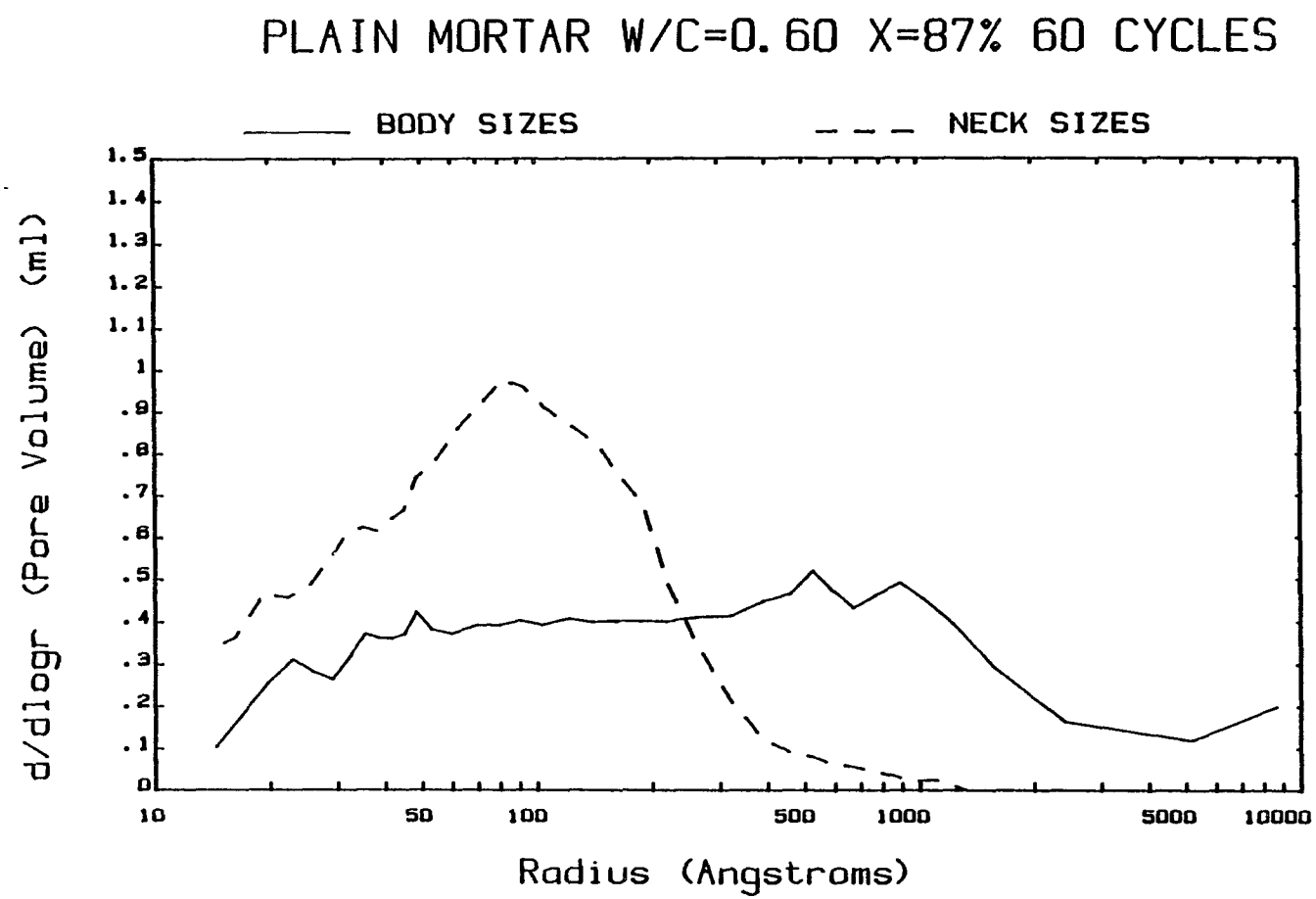
PLAIN MORTAR W/C=0.60 X=87% 60 CYCLES
BODY SIZES
NECK SIZES
d/dlogr (Pore Volume) (ml)
1.5
1.4
1.3
1.2
1.1
1
.9
.8
.7
.6
.5
.4
.3
.2
.1
0
10
50
100
500
1000
5000
10000
Radius (Angstroms)

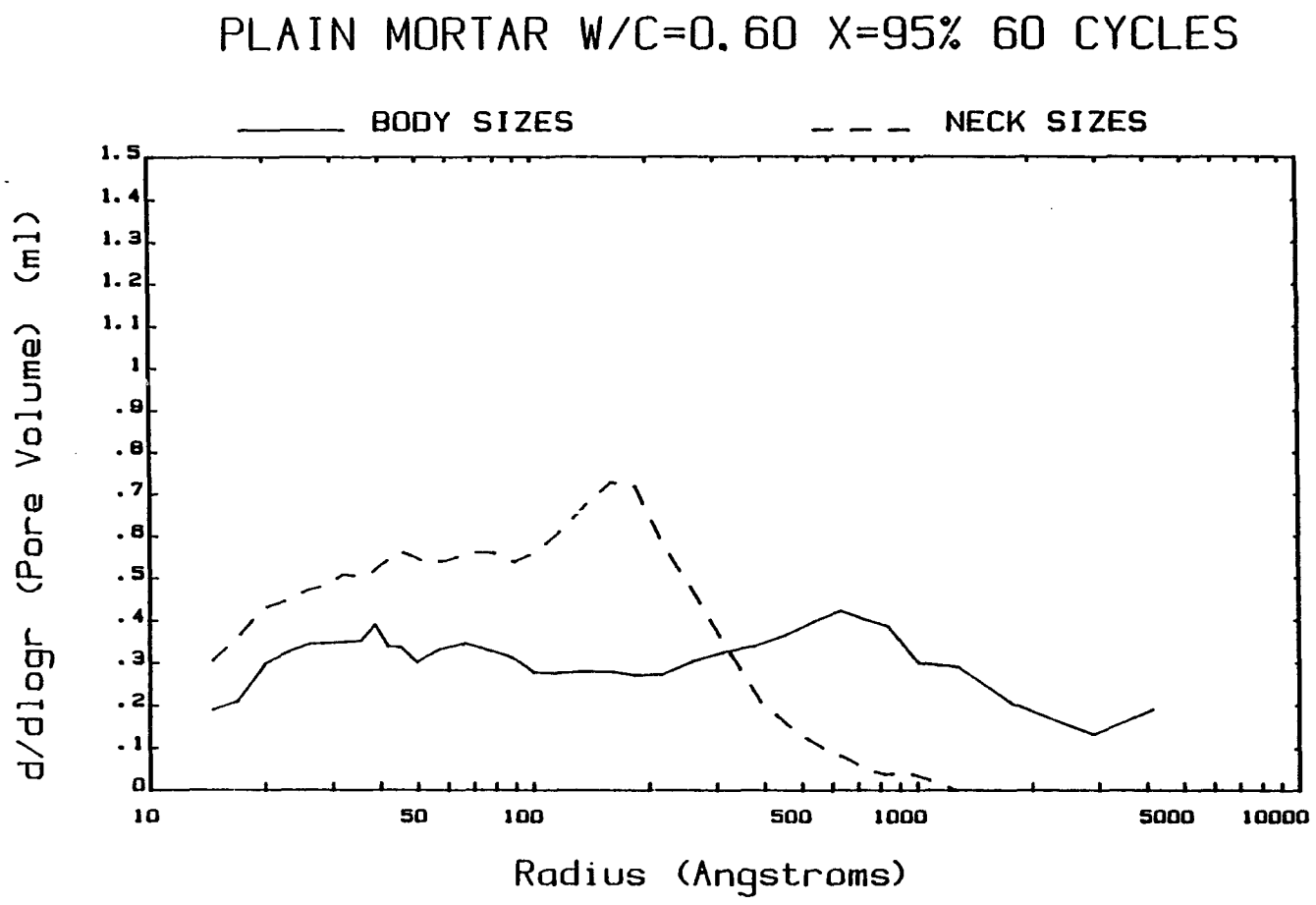
PLAIN MORTAR W/C=0.60 X=95% 60 CYCLES
BODY SIZES
NECK SIZES
d/dlogr (Pore Volume) (ml)
1.5
1.4
1.3
1.2
1.1
1
.9
.8
.7
.6
.5
.4
.3
.2
.1
0
10
50
100
500
1000
5000
10000
Radius (Angstroms)

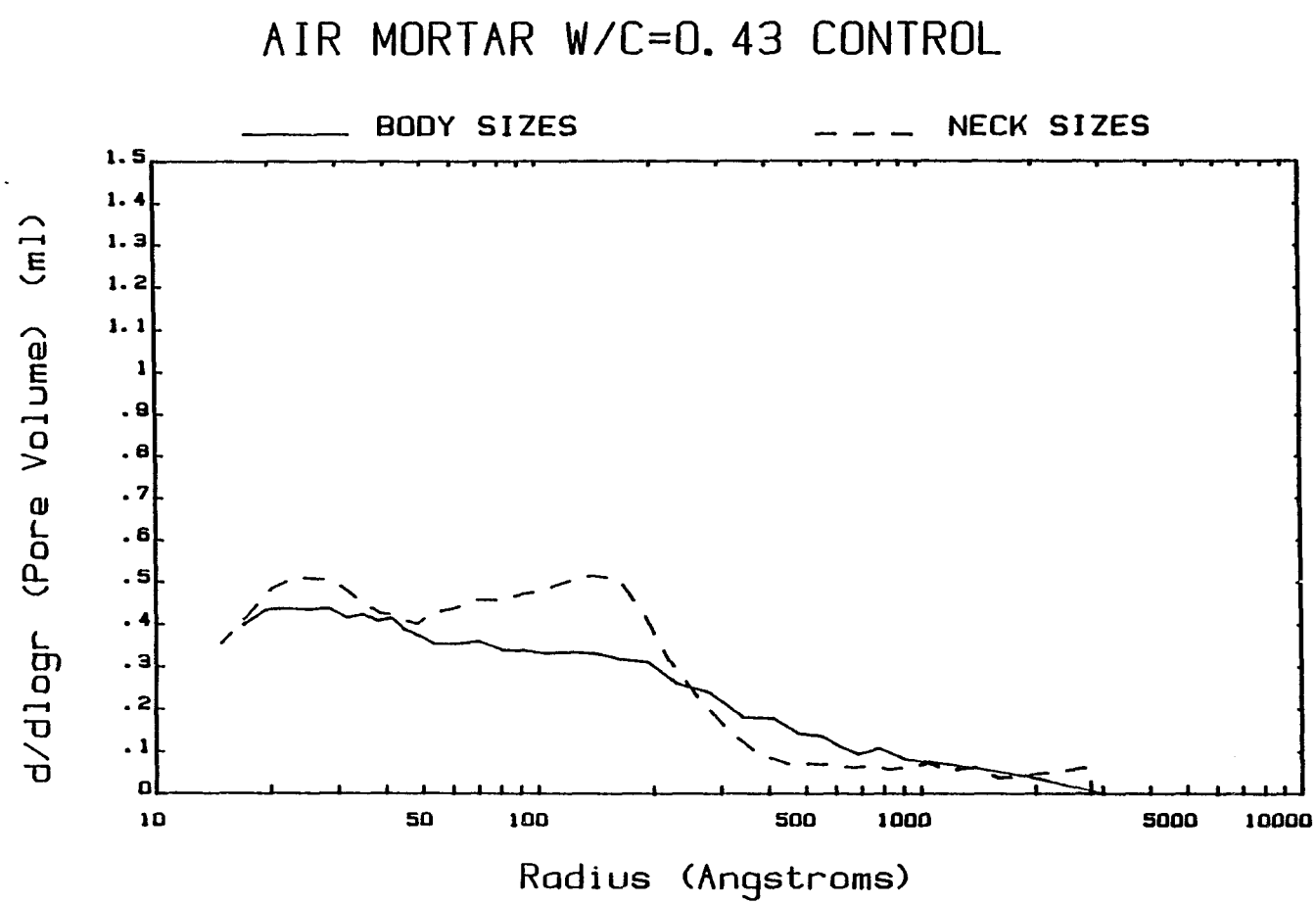
AIR MORTAR W/C=0.43 CONTROL
BODY SIZES
NECK SIZES
d/dlogr (Pore Volume) (ml)
1.5
1.4
1.3
1.2
1.1
1
.9
.8
.7
.6
.5
.4
.3
.2
.1
0
10
50
100
500
1000
5000
10000
Radius (Angstroms)

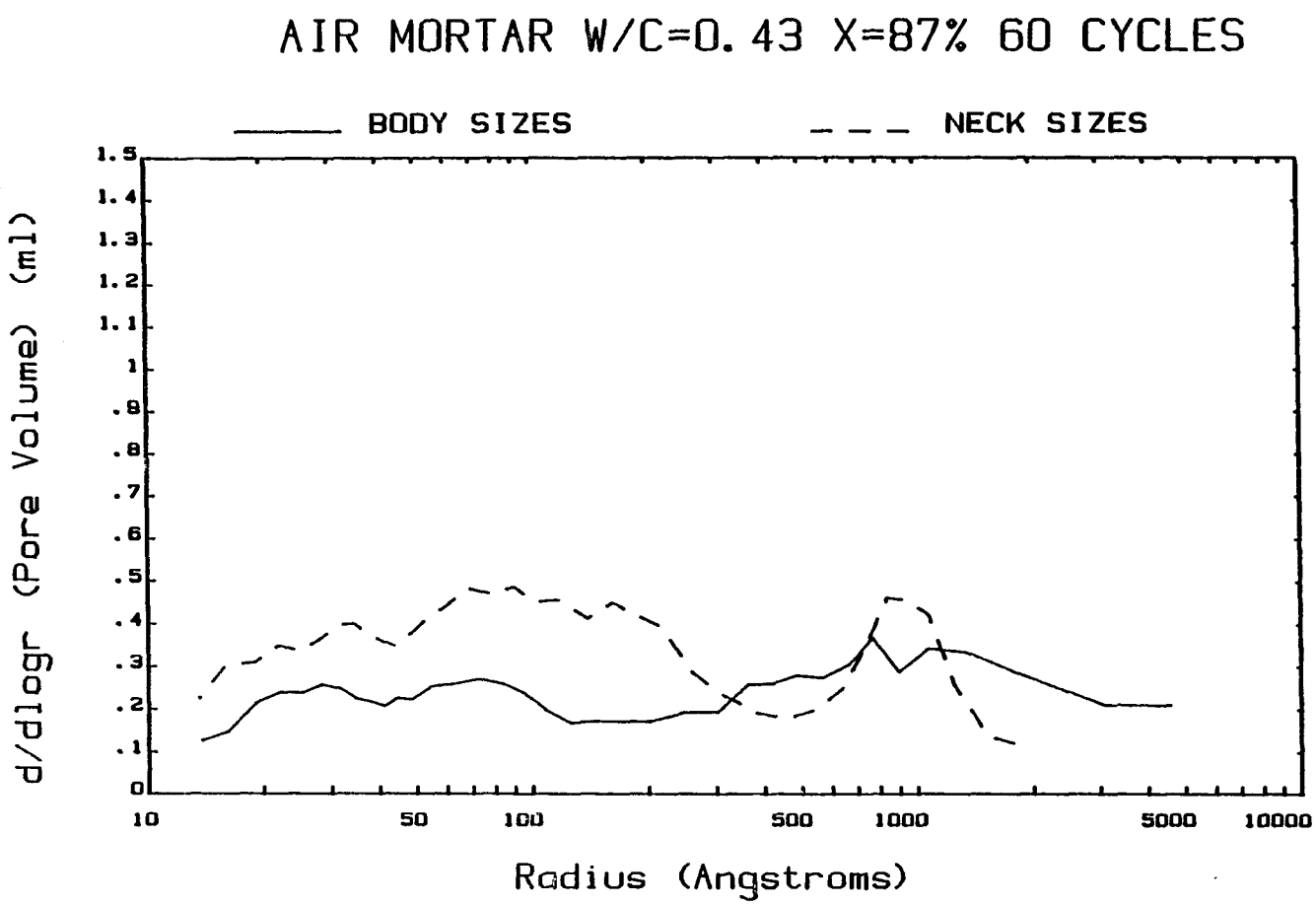
AIR MORTAR W/C=0.43 X=87% 60 CYCLES
BODY SIZES
NECK SIZES
d/dlogr (Pore Volume) (ml)
1.5
1.4
1.3
1.2
1.1
1
.9
.8
.7
.6
.5
.4
.3
.2
.1
0
10
50
100
500
1000
5000
10000
Radius (Angstroms)

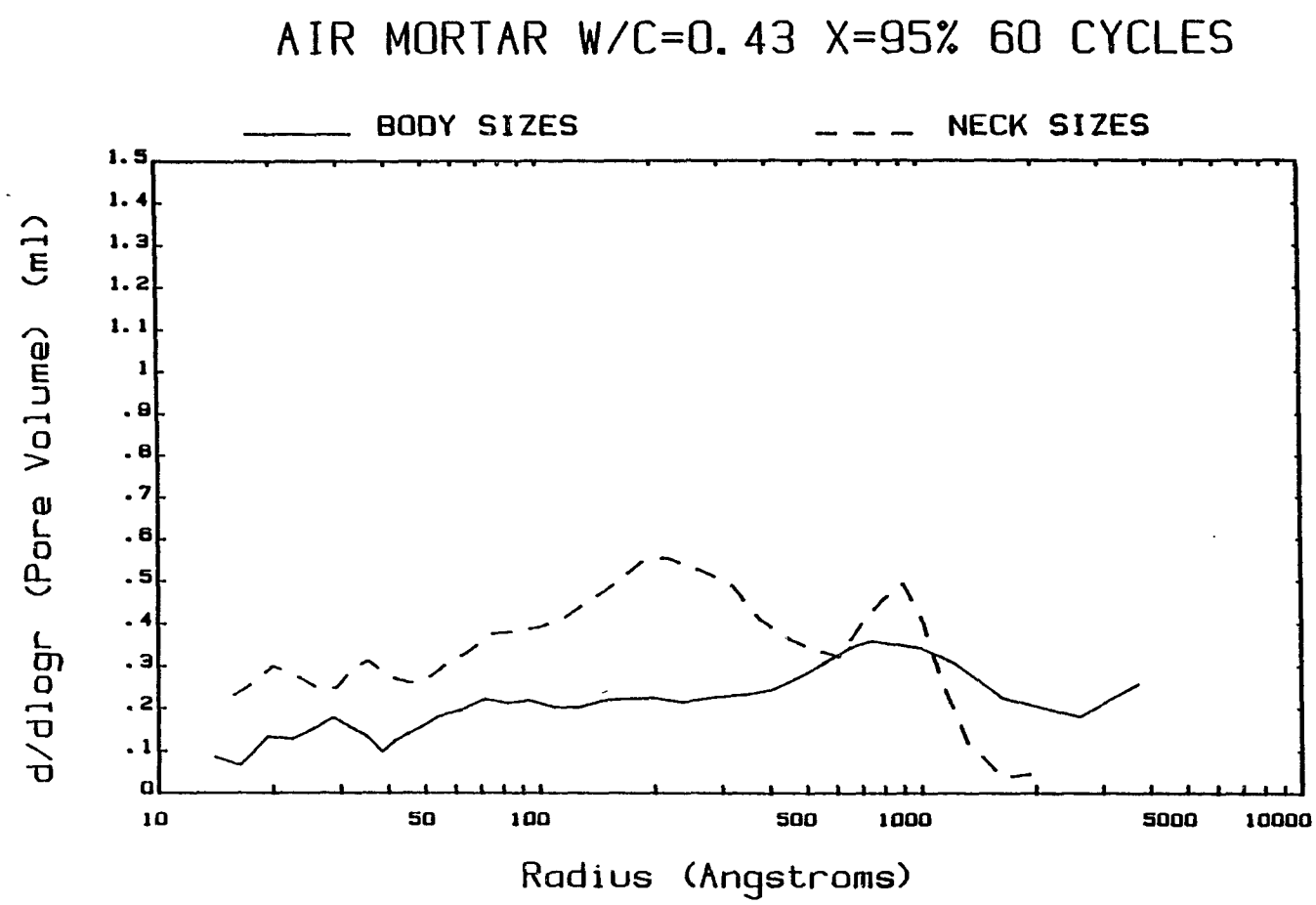
AIR MORTAR W/C=0.43 X=95% 60 CYCLES
BODY SIZES
NECK SIZES
d/dlogr (Pore Volume) (ml)
1.5
1.4
1.3
1.2
1.1
1
.9
.8
.7
.6
.5
.4
.3
.2
.1
0
10
50
100
500
1000
5000
10000
Radius (Angstroms)

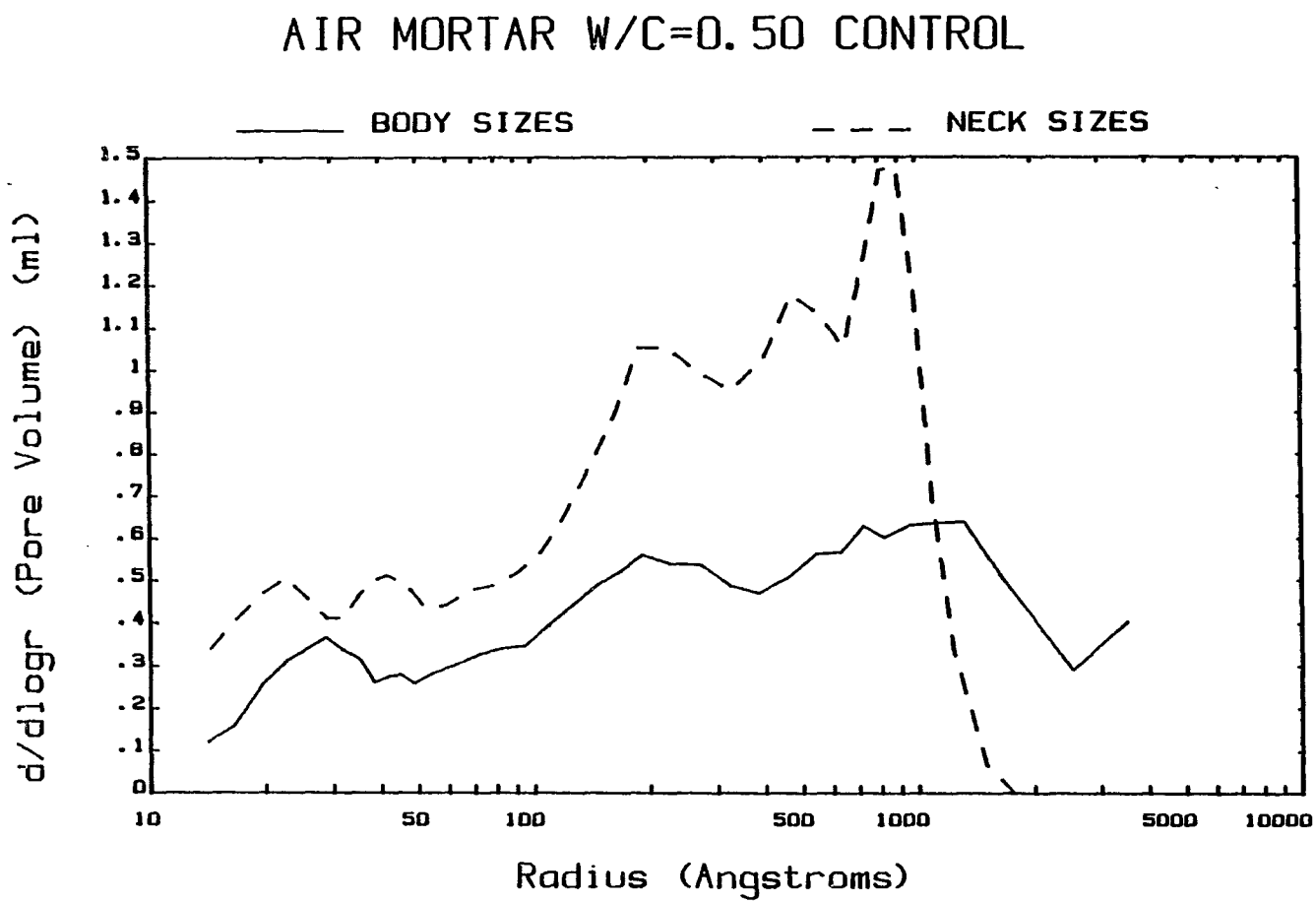
AIR MORTAR W/C=0.50 CONTROL
BODY SIZES
NECK SIZES
d/dlogr (Pore Volume) (ml)
1.5
1.4
1.3
1.2
1.1
1
.9
.8
.7
.6
.5
.4
.3
.2
.1
0
10
50
100
500
1000
5000
10000
Radius (Angstroms)

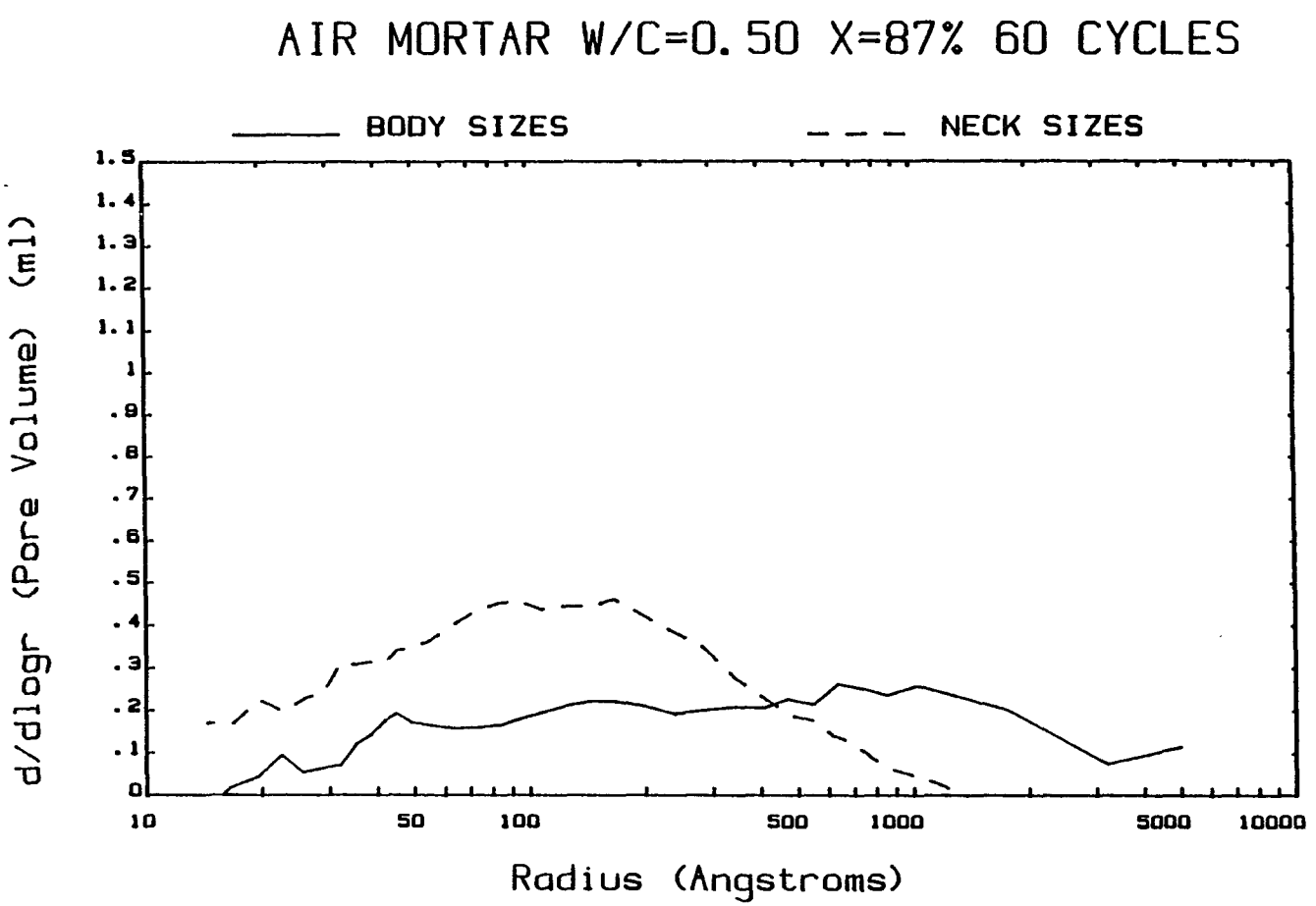
AIR MORTAR W/C=0.50 X=87% 60 CYCLES
BODY SIZES
NECK SIZES
d/dlogr (Pore Volume) (ml)
1.5
1.4
1.3
1.2
1.1
1
.9
.8
.7
.6
.5
.4
.3
.2
.1
0
10
50
100
500
1000
5000
10000
Radius (Angstroms)

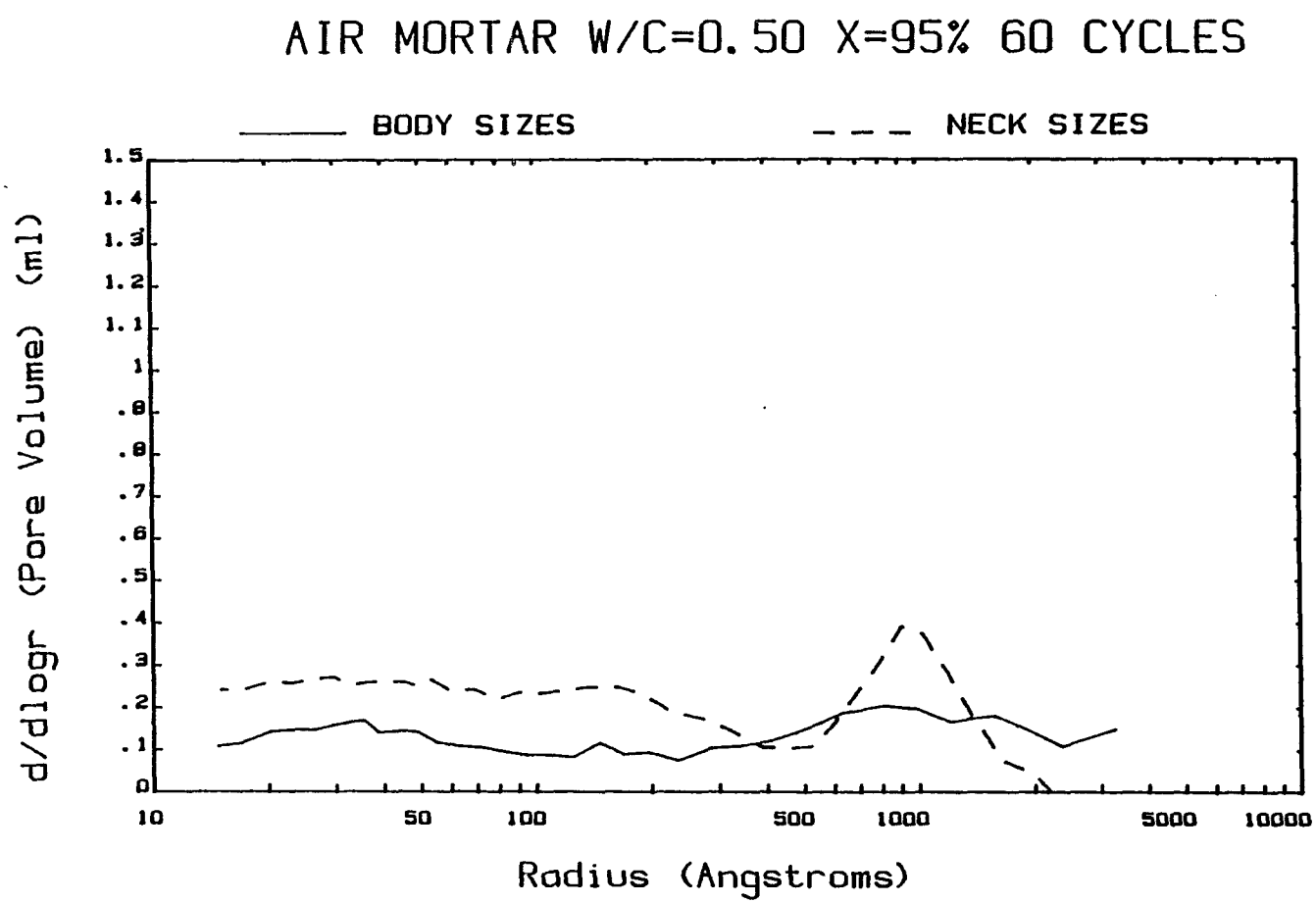
AIR MORTAR W/C=0.50 X=95% 60 CYCLES
BODY SIZES
NECK SIZES
d/dlogr (Pore Volume) (ml)
1.5
1.4
1.3
1.2
1.1
1
.9
.8
.7
.6
.5
.4
.3
.2
.1
0
10
50
100
500
1000
5000
10000
Radius (Angstroms)

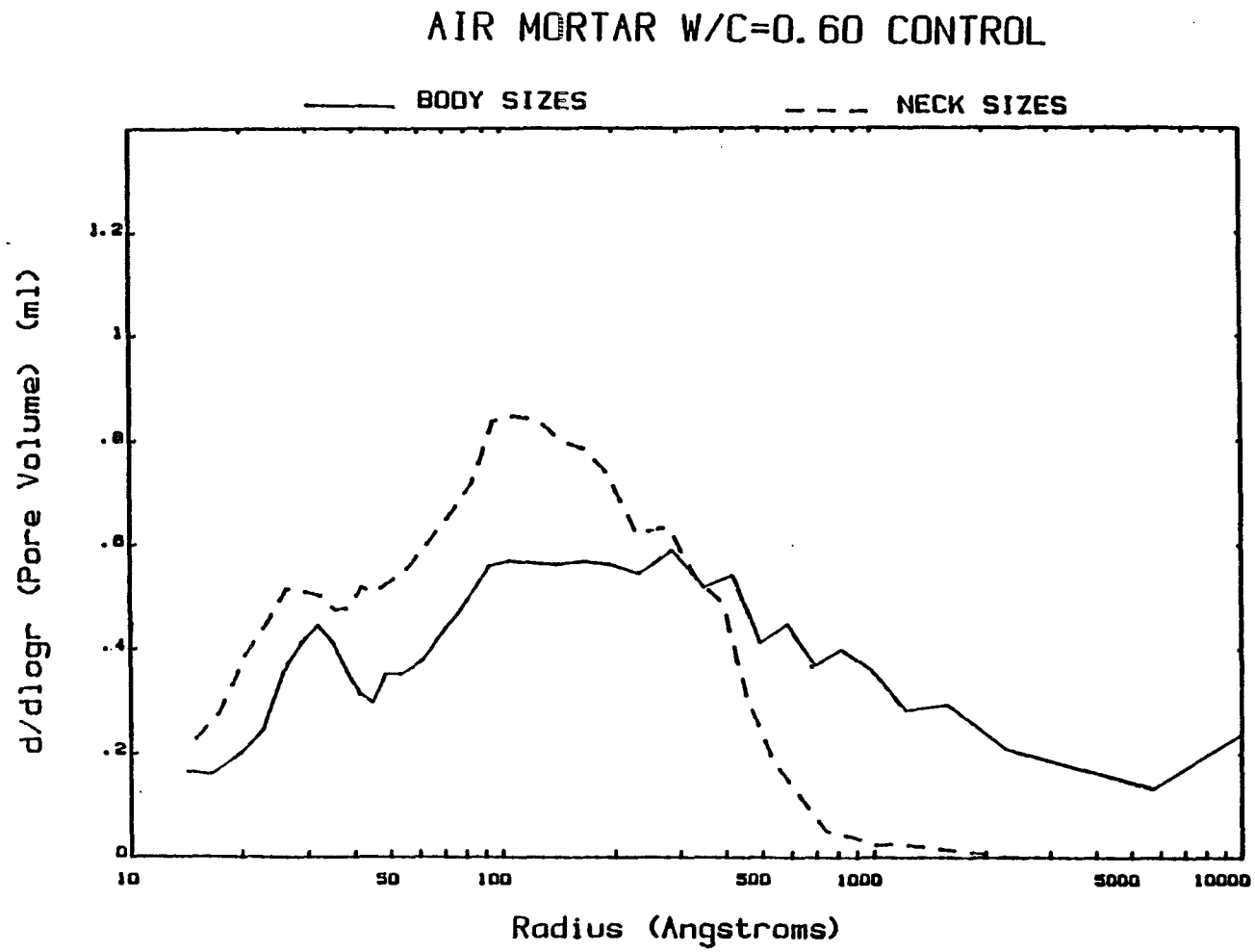
AIR MORTAR W/C=0.60 CONTROL
BODY SIZES
NECK SIZES
d/dlogr (Pore Volume) (ml)
1.2
1
.8
.6
.4
.2
0
10
50
100
500
1000
5000
10000
Radius (Angstroms)

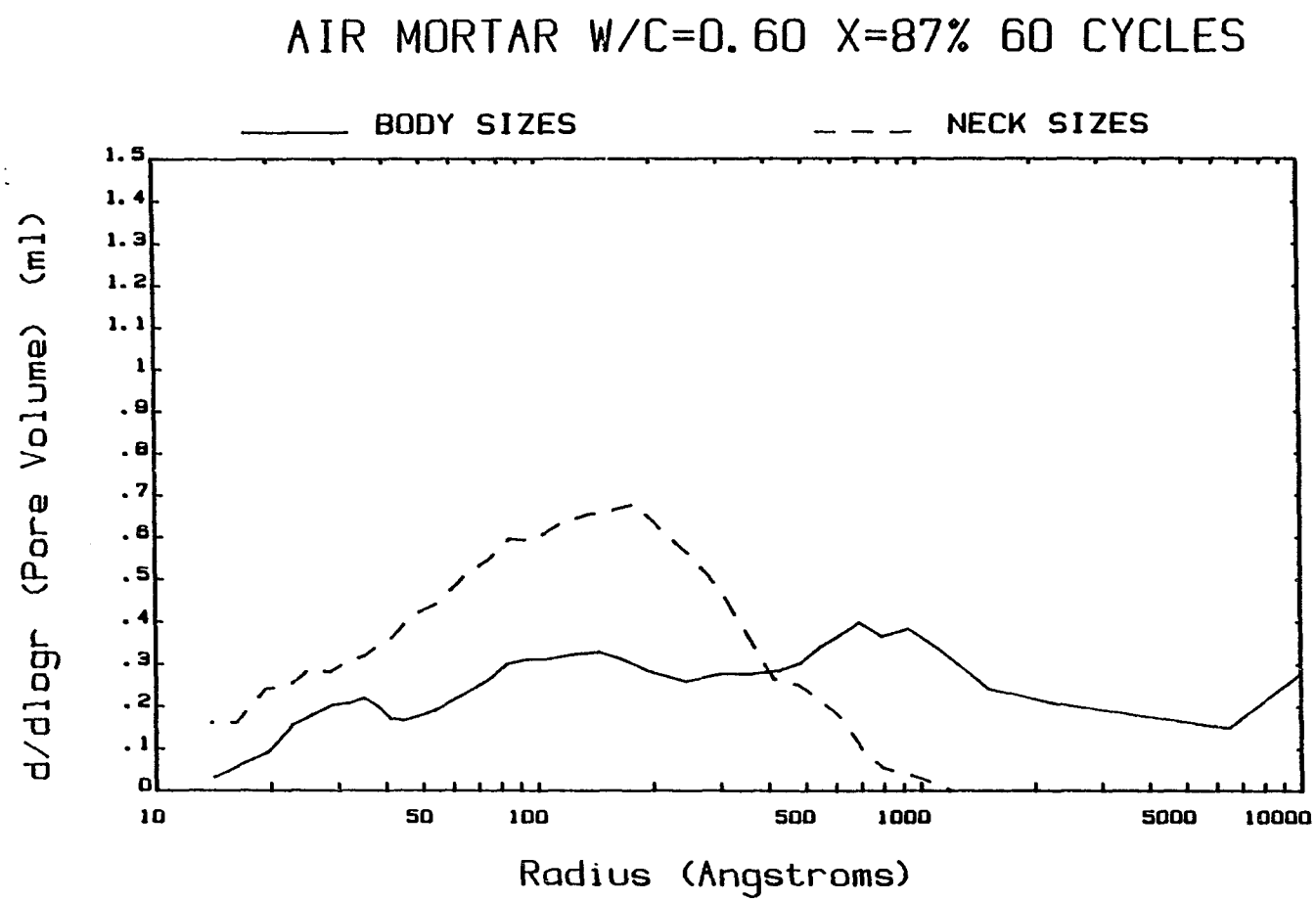
AIR MORTAR W/C=0.60 X=87% 60 CYCLES
BODY SIZES
NECK SIZES
d/dlogr (Pore Volume) (ml)
1.5
1.4
1.3
1.2
1.1
1
.9
.8
.7
.6
.5
.4
.3
.2
.1
0
10
50
100
500
1000
5000
10000
Radius (Angstroms)

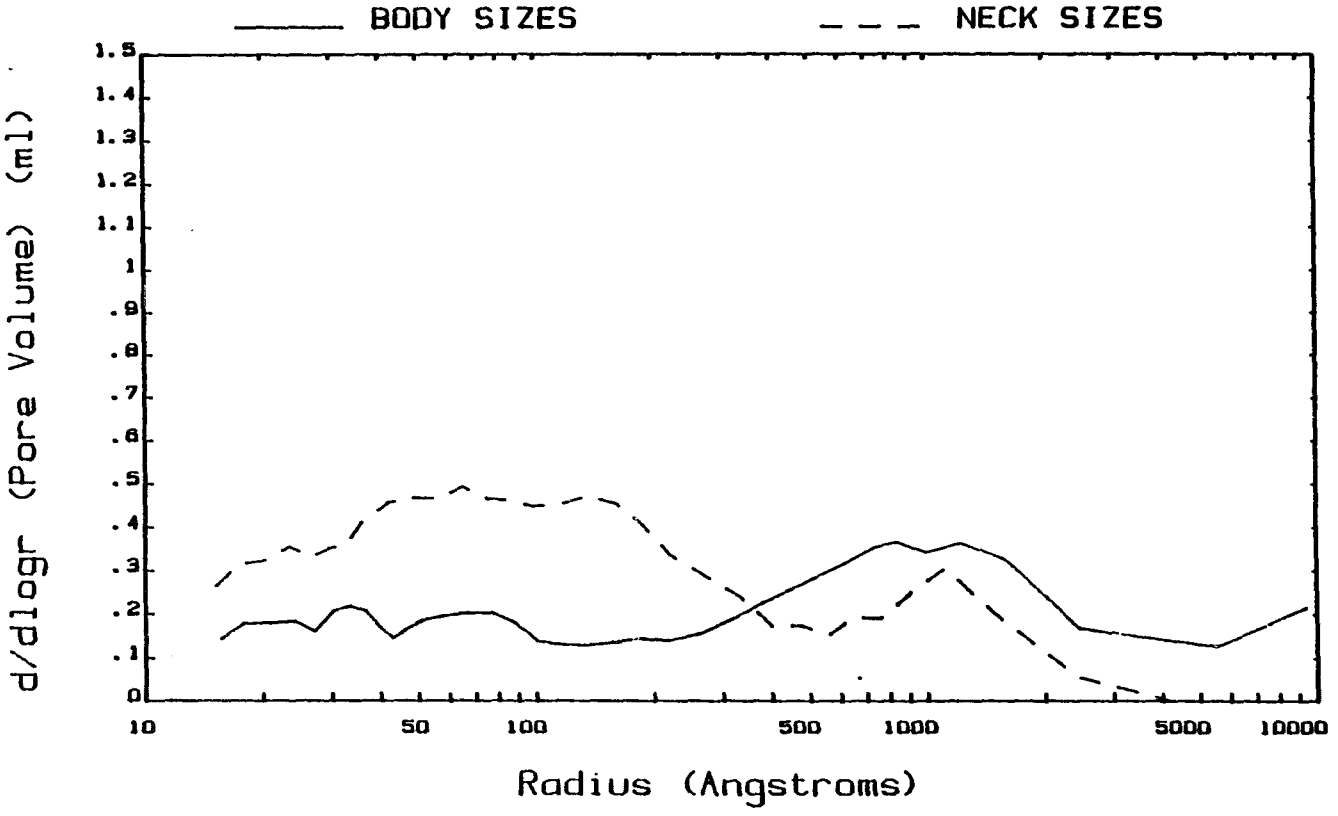
AIR MORTAR W/C=0.60 X=95% 60 CYCLES
BODY SIZES
NECK SIZES
d/dlogr (Pore Volume) (ml)
1.5
1.4
1.3
1.2
1.1
1
.9
.8
.7
.6
.5
.4
.3
.2
.1
0
10
50
100
500
1000
5000
10000
Radius (Angstroms)

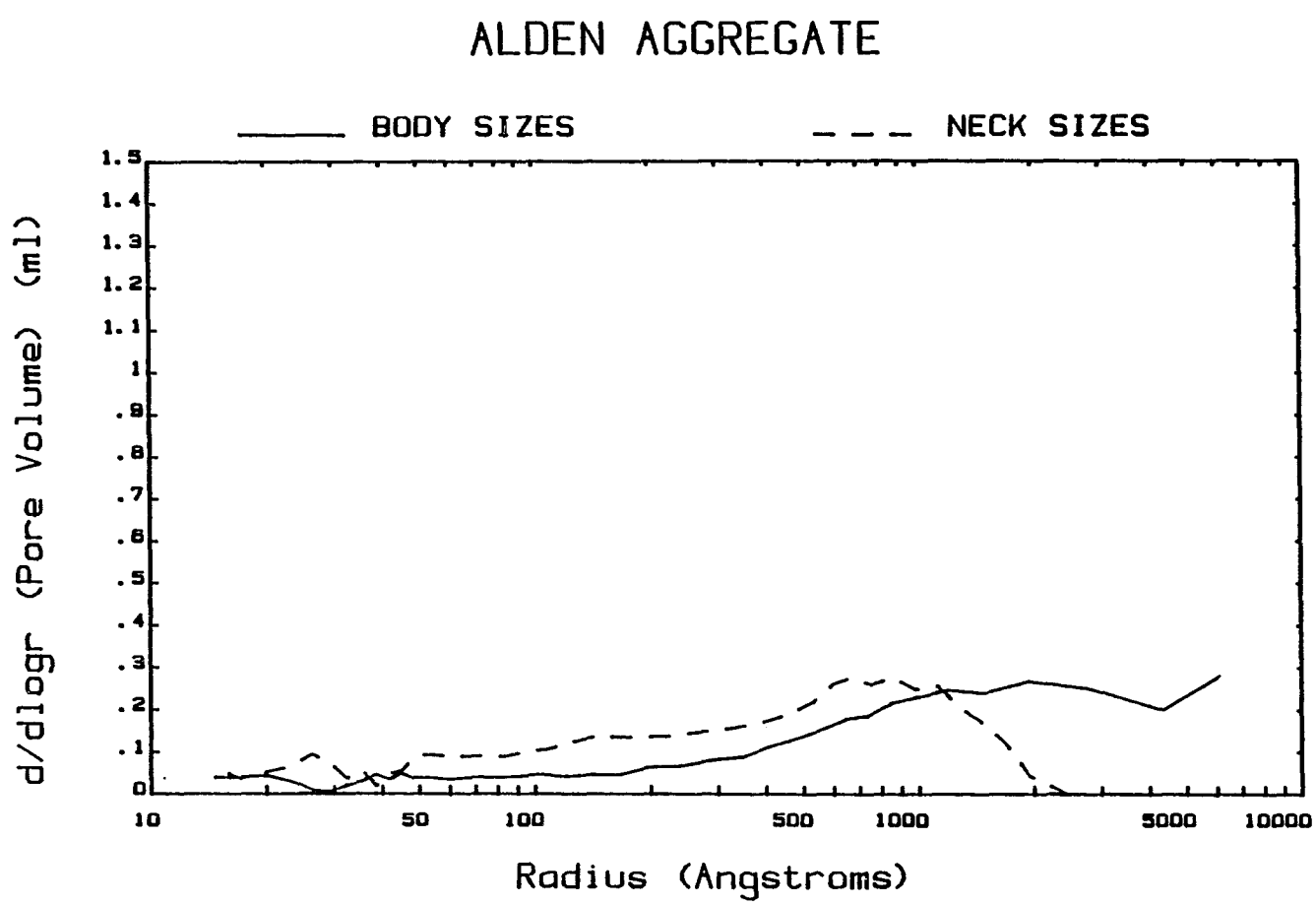
ALDEN AGGREGATE
BODY SIZES
NECK SIZES
d/dlogr (Pore Volume) (ml)
1.5
1.4
1.3
1.2
1.1
1
.9
.8
.7
.6
.5
.4
.3
.2
.1
0
10
50
100
500
1000
5000
10000
Radius (Angstroms)

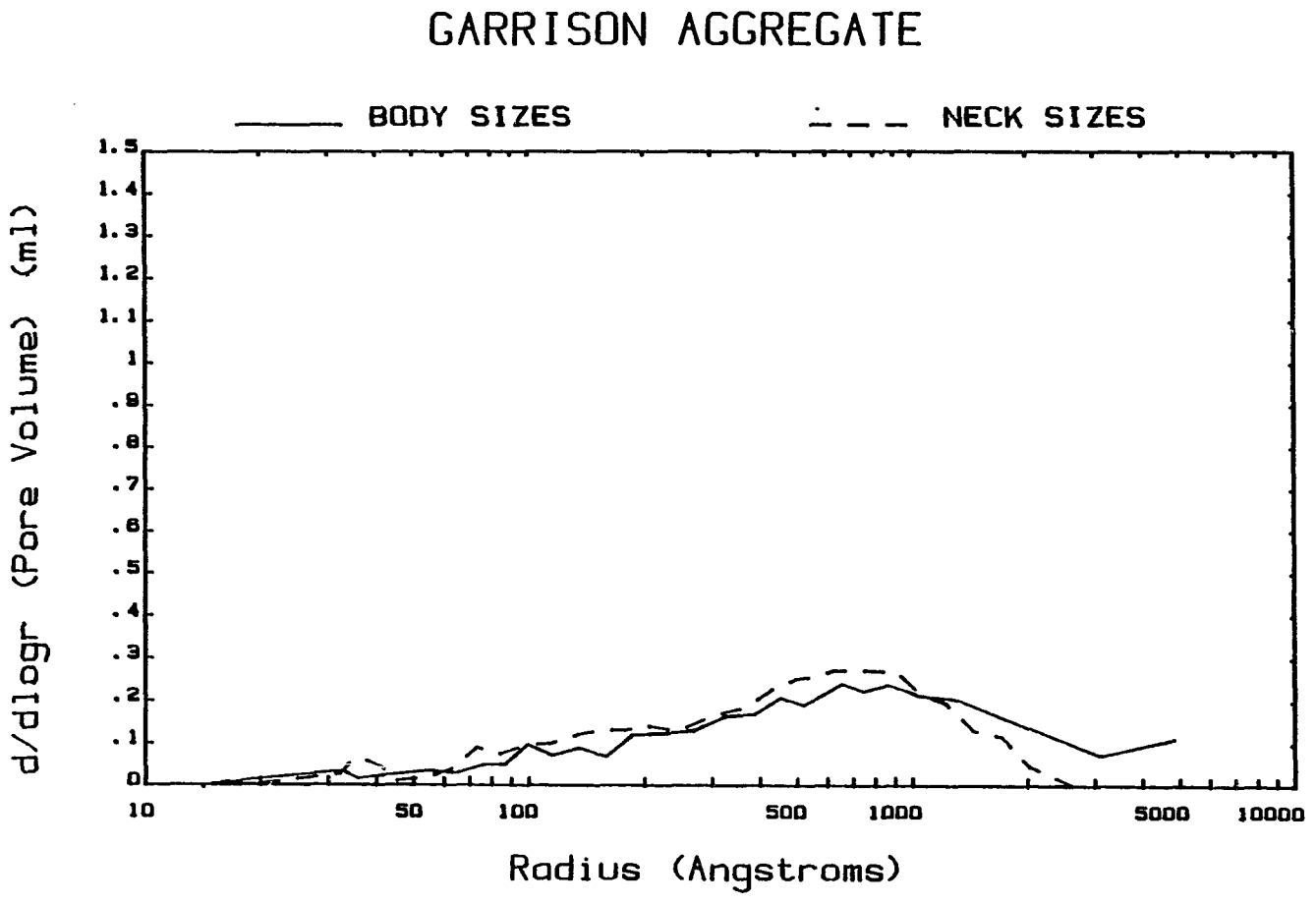
GARRISON AGGREGATE
BODY SIZES
NECK SIZES
d/dlogr (Pore Volume) (ml)
1.5
1.4
1.3
1.2
1.1
1
.9
.8
.7
.6
.5
.4
.3
.2
.1
0
10
50
100
500
1000
5000
10000
Radius (Angstroms)

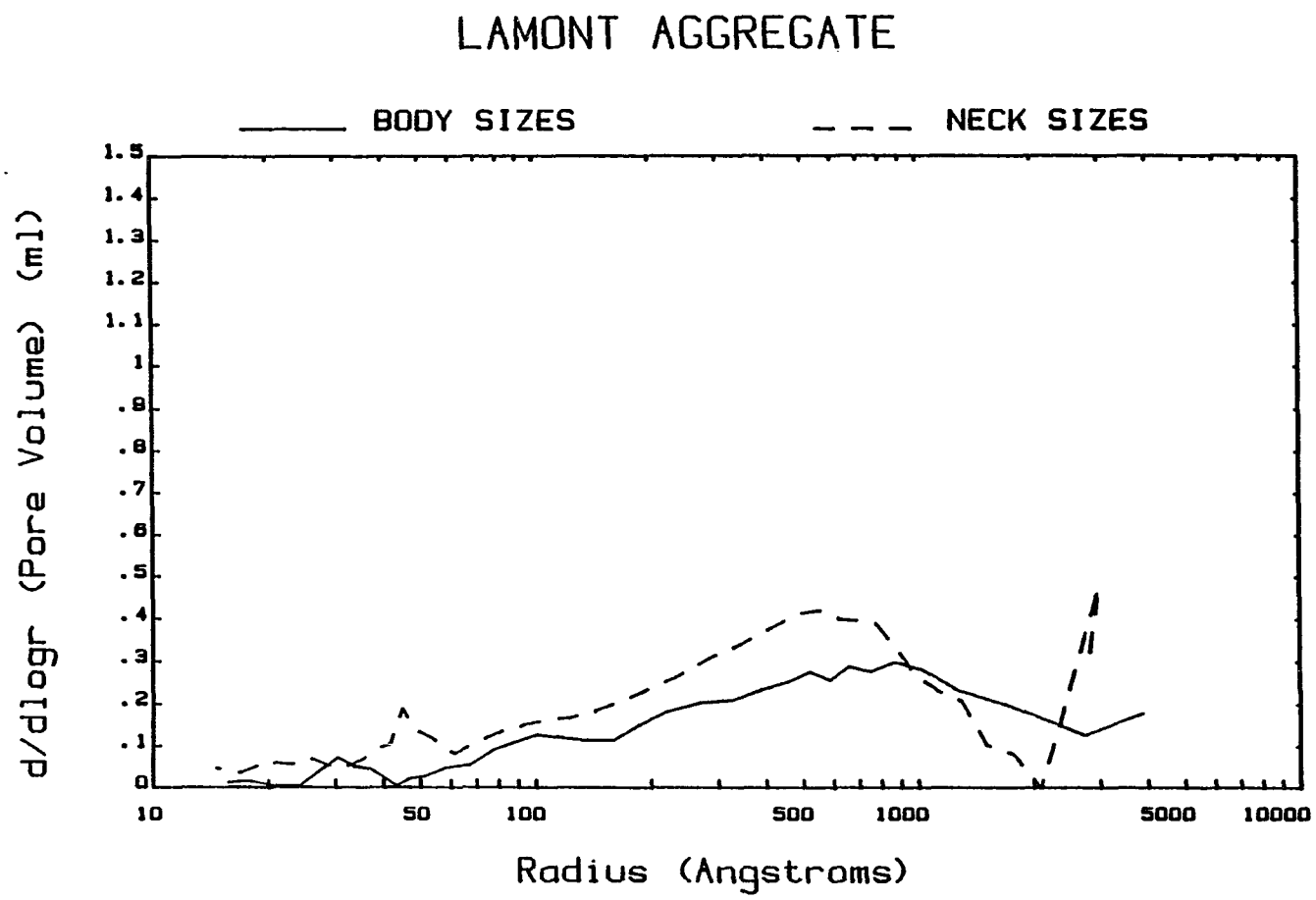
LAMONT AGGREGATE
BODY SIZES
NECK SIZES
d/dlogr (Pore Volume) (ml)
1.5
1.4
1.3
1.2
1.1
1
.9
.8
.7
.6
.5
.4
.3
.2
.1
0
10
50
100
500
1000
5000
10000
Radius (Angstroms)

APPENDIX F

SELECTING REPRESENTATIVE SAMPLES

Obviously, the smaller size of samples used in the experiments is not considered representative of actual field concrete. Although this drawback cannot be completely eliminated, this research suggests selecting representative samples from about 12 cores by finding the "average" samples based on porosity measurement. The following presents an example on how average samples can be selected.

A total of 12 core samples were prepared. Their dry densities were determined. The average dry density and standard deviation was also calculated. Samples with dry density within one standard deviation are considered acceptable. In the example shown below, all samples are considered acceptable except sample number 8.

Sample number	Dry density (g/cm^3)
1	2.25
2	2.27
3	2.27
4	2.27
5	2.25
6	2.24
7	2.26
8	2.23
9	2.25
10	2.26
11	2.27
12	2.27

Average density = 2.257
Standard deviation = 0.013